STAT3 AND SMAD SIGNALING IN MOUSE MODELS OF ONCOSTATIN M-INDUCED LUNG EXTRACELLULAR MATRIX REMODELING

STAT3 AND SMAD SIGNALING IN MOUSE MODELS OF ONCOSTATIN M-INDUCED LUNG EXTRACELLULAR MATRIX REMODELING

By STEVEN WONG, B.H.Sc Honours (McMaster University)

A Thesis Submitted to the School of Graduate Studies in Partial Fulfillment of the Requirements for the Degree Masters of Science

McMaster University © Copyright by Steven Wong, August 2013

MASTERS OF SCIENCE (2013) McMaster University, Hamilton Ontario

(Medical Sciences: Infection and Immunology)

TITLE: STAT3 and SMAD Signaling in Mouse Models of Oncostatin M-induced Lung Extracellular Matrix Remodeling

AUTHOR: Steven Wong, B.H.Sc Hons. (McMaster University)

SUPERVISOR: Dr. Carl Richards, BSc., MSc., Ph.D.

NUMBER OF PAGES: xi, 164

ABSTRACT

IPF is a respiratory condition of unknown etiology that has poor survival prognosis. The stiffening of the lung associated with this condition is attributed to the irreversible turnover of healthy lung tissue into scar tissue, which affects gas exchange and can eventually lead to organ failure. Numerous studies have implicated the pro-fibrogenic growth factor TGF-β, through activation of the SMAD2/3 pathway, as a central mediator in the pathology of this condition. However, other cytokines, including members of the IL-6/gp130 family such as OSM, and other signaling pathways may be implicated in ECM accumulation in certain conditions. In particular, STAT3 activation and an impairment of the BMP-SMAD1 signaling axis is thought to contribute to lung ECM accumulation. Based on the finding that transient pulmonary overexpression of OSM induces lung ECM accumulation in C57Bl/6 mice, it was hypothesized that OSM-induced ECM remodeling would be associated with STAT3 activation and suppression of the BMP-SMAD1-signaling axis.

Findings in this thesis revealed that transient pulmonary overexpression of OSM induces ECM remodeling in both BALB/c and C57Bl/6 mice after seven days, despite a dichotomous response in other experimental models of ECM remodeling. However, parenchyma, but not airway, pathology resolved after 28 days in AdOSM-treated BALB/c mice. Furthermore, OSM-induced ECM remodeling occurred independently of IL-6-associated inflammation as well as TGF-β/SMAD3 signaling. MLF cultures treated with OSM did not directly regulate gene expression of ECM-related genes, suggesting that other cells may be responsible for OSM-induced ECM accumulation *in vivo*. OSM

overexpression *in vivo* was associated with STAT3 activation and SMAD1 suppression, and an assessment of STAT3 and SMAD signaling *in vitro* showed that OSM activated the STAT3 pathway in MLF cultures, mouse type two pneumocytes, and human airway cells, while OSM suppressed the SMAD1 pathway in mouse type two pneumocytes, and human airway cells. Collectively, this thesis shows that OSM induces novel pathways in models of lung ECM remodeling, and this may have implications for IPF pathogenesis.

ACKNOWLEDGEMENTS

With the completion of this thesis, I am considerably indebted to many people, all of whom have aided in my self-growth and maturation and made this experience enjoyable over the past two years. First and foremost, I would like to extend my gratitude to my supervisor and mentor, Dr. Carl Richards. Your contagious enthusiasm and passion for your work has motivated me to tackle each of life's endeavors with a positive and critical mindset. I would also like to thank my committee members, Dr. Jack Gauldie and Dr. Martin Kolb for providing me with excellent scientific guidance throughout my Master's degree and challenging my knowledge in the least painful way possible.

To my colleagues, both past and present, it was a pleasure working alongside each of you. In particular, Sean Lauber, as grandmaster of the intubation method, thank you for all your technical support with the *in vivo* experiments. David Schnittker, I enjoyed all the sports discussions we have, and I hope we both continue to dominate fantasy sports for years to come. Laura Izakalian and Karen Kwofie, you both came into the lab just in time to become good friends and I look forward to sticking around in the near future. To Jessica Guerette, Rebecca Rodrigues, Christine Demers, Jane Ann Smith, Katherine Liu, Tamanna Chibber, and other MIRC members, you have all made this an enjoyable place to complete my degree. I sincerely wish everyone the best of luck in your future endeavors, and hope our paths will cross in the future.

To my parents and sister, thank you for all of your unconditional love and hard work. I am fortunate to have you there to celebrate my highs, and support me during my lows. Lastly, thank you Shirley Ma for all your love and support. I am blessed to have you in my life, as you brighten each of my days. I know you will go on to do great things, and I look forward to being with you every step of the way.

TABLE OF CONTENTS

CHAPTER 1: Introduction **1**
1.1 Idiopathic pulmonary fibrosis **1**
1.2 Normal Wound Repair of the Lung **2**
1.3 Aberrant and Chronic Wound Healing **4**
1.4 Fibroblasts and Myofibroblasts **5**
1.5 Epithelial Cells **8**
1.6 Animal Models to Study Pulmonary Fibrosis **9**
1.7 Role of Inflammation and Immunology in Pulmonary Fibrosis **11**
1.8 Transforming Growth Factor Beta (TGF-β) **13**
1.9 TGF-β and Pulmonary Fibrosis **15**
1.10 Gp130 cytokines and OSM **16**
1.11 OSM and Lung Disease **18**
1.12 Bone Morphogenetic Proteins (BMP) **19**
1.13 BMP and Pulmonary Fibrosis **21**
1.15 Aims and Hypotheses **24**

CHAPTER 2: Materials and Methods **25**
2.0 Intubation of mice with adenovirus and subsequent sample collection **25**
2.1 Histology and Immunohistochemistry **25**
2.2 Histology Imaging and Quantification **26**
2.3 Lung crushing **26**
2.4 Lung homogenization for protein and RNA analysis **27**
2.5 Hydroxyproline Assay **27**
2.6 Cell Culture **28**
2.7 Cell Lysates **29**
2.8 Running of lung homogenates and cell lysates on immunoblots **30**
2.9 RNA Extraction and purification from cell culture **31**
2.10 Quantification using Taqman **32**
2.11 Analysis of BALF using Enzyme-linked immunosorbent assay (ELISA) **33**
2.12 Statistical Analysis **33**

CHAPTER 3: Results of Aim 1 ..... **34**

CHAPTER 4: Results of Aim 2 ..... **61**

CHAPTER 5: Results of Aim 3 ..... **84**

CHAPTER 6: Discussion **128**

CHAPTER 7: Conclusions **147**

CHAPTER 8: References **149**

LIST OF FIGURES

Figure 1: PSR stained lung sections of AdOSM-treated C57Bl/6 and BALB/c mice (Day 7)…….42

Figure 2: Masson's Trichrome and PSR stained lung sections of AdOSM-treated C57Bl/6 and BALB/c mice (Day 7)……..45

Figure 3: Lung collagen assessment of AdOSM-treated C57Bl/6 and BALB/c mice (Day 7).……47

Figure 4: BALF cytokine analysis of AdOSM-treated C57Bl/6 and BALB/c mice (Day 7)……..……...……49

Figure 5: qRT-PCR analysis of AdOSM-treated C57Bl/6 and BALB/c mice (Day 7)….51

Figure 6: H&E stained lung sections of AdOSM-treated BALB/c mice (Day 28)……...53

Figure 7: BALF analysis of AdOSM-treated BALB/c mice (Day 28)……..……55

Figure 8: qRT-PCR analysis of C57Bl/6 MLF cultures……..……..57

Figure 9: qRT-PCR analysis of BALB/c MLF cultures.……..…….59

Figure 10: H&E stained lung sections of AdOSM-treated IL-6 -/- mice (Day 14)…..….66

Figure 11: Masson's Trichrome and PSR stained lung sections of AdOSM-treated IL-6 -/- mice (Day 14).……68

Figure 12: Lung collagen assessment of AdOSM-treated IL-6 -/- mice (Day 14)……70

Figure 13: BALF cell counts of AdOSM-treated IL-6 -/- mice (Day 7)……..…….72

Figure 14: BALF cytokine analysis of AdOSM-treated IL-6 -/- mice (Day 7)…….……74

Figure 15: Histological analysis of AdOSM-treated SMAD3 -/- mice (Day 7)……76

Figure 16: Lung collagen assessment of AdOSM-treated SMAD3 -/- mice (Day 7)…...78

Figure 17: BALF cell counts of AdOSM-treated SMAD3 -/- mice (Day 7)……..…80

Figure 18: BALF cytokine analysis of AdOSM-treated SMAD3 -/- mice (Day 7).…….82

Figure 19: Immunoblots of AdOSM-treated C57Bl/6 and BALB/c lung homogenates (Day 7)……...….....94

Figure 20: Immunoblots of AdOSM-treated BALB/c lung homogenates (Day 2)…….,.96

Figure 21: IHC for pSMAD1/5/8 on AdOSM-treated C57Bl/6 and BALB/c lung sections (Day 7)…….……...98

Figure 22: IHC for pSMAD1/5/8 on AdOSM-treated BALB/c lung sections (Day 2)...103

Figure 23: IHC for pSMAD2 on AdOSM-treated C57Bl/6 and BALB/c lung sections (Day 7)…….….105

Figure 24: Immunoblots of C57Bl/6 MLF cultures after time course stimulation……..108

Figure 25: Immunoblots of BALB/c MLF cultures after time course stimulation……..110

Figure 26: Immunoblots of C57Bl/6 MLF cultures after 1 and 3 day stimulation……..112

Figure 27: Immunoblots of BALB/c MLF cultures after 1 and 3 day stimulation……..114

Figure 28: Immunoblots of Beas 2B cells after 1 hour stimulation……....116

Figure 29: Immunoblots of Beas 2B cells after 1 day stimulation……..118

Figure 30: Immunoblots of A549 cells after 1 hour stimulation…….120

Figure 31: Immunoblots of A549 cells after 1 day stimulation……...122

Figure 32: Immunoblots of C10 type two pneumocytes after 1 hour stimulation……...124

Figure 33: Immunoblots of C10 type two pneumocytes after 1 and 3 day stimulation..126

LIST OF ABBREVIATIONS

AdDl70 – Adenovirus encoding empty vector

AdOSM – Adenovirus vector encoding Oncostatin M

AEC – Alveolar epithelial cells

α-SMA – Alpha smooth muscle actin

BALF – Bronchioalveolar lavage fluid

BMP – Bone morphogenetic protein

BSA – Bovine serum albumin

CO_2 – Carbon dioxide

Co-SMAD – Common SMAD

CTGF – Connective tissue growth factor

CD – Cluster of differentiation

DNA – Deoxyribonucleic acid

DTT – Dithiothreitol

ECM – Extracellular matrix

ELISA – Enzyme linked immunosorbent assay

EMT – Epithelial-to-mesenchymal transition

EndoMT – Endothelial-to-mesenchymal transition

FPAH – Familial pulmonary arterial hypertension

FBS – Fetal bovine serum

Gp130 – Glycoprotein 130

H&E – Hematoxylin and Eosin

HRCT – High resolution computed tomography

HRP – Horse-radish peroxidase

IHC – Immunohistochemistry

IL – Interleukin

IPF – Idiopathic pulmonary fibrosis

I-SMAD – Inhibitory SMAD

JAK – Janus kinase

KC - Keratinocyte chemoattractant

LAP – Latency-associated peptide

LIF – Leukemia inhibiting factor

LTBP – Latent TGF-β binding protein

MAPK – Mitogen activated protein kinase

MCP – Monocyte chemoattractant protein

MH – Mad homology

MIP – Macrophage inflammatory protein

MLF – Mouse lung fibroblast

MMP – Matrix metalloproteinase

mRNA – Messenger ribonucleic acid

OSM – Oncostatin M

PAGE – Polyacrylamide gel electrophoresis

PI3K – Phosphatidylinositol 3-kinase

PSR – Picrosirius Red

qRT-PCR - Quantitative reverse transcriptase polymerase chain reaction

RNA – Ribonucleic acid

R-SMAD – Receptor SMAD

SDF – Stromal cell-derived factor

SDS – Sodium dodecyl sulfate

SHH – Sonic hedgehog

SOCS – Suppressors of cytokine signaling

STAT – Signal Transducer and Activation of Transcription

TBS – Tris-buffered saline

TGF-β – Transforming growth factor beta

TIMP – Tissue inhibitor of metalloproteinase

TNF-α – Tumor necrosis factor alpha

CHAPTER 1: Introduction

1.1 Idiopathic pulmonary fibrosis

Pulmonary fibrosis is a debilitating disease that affects more than 20,000 Canadians[1]. Although it is a heterogeneous condition with respect to clinical features and progression rate, pulmonary fibrosis is characterized by dyspnea, impaired lung function, and the accumulative and irreversible turnover of healthy lung tissue into unhealthy scar tissue[2–4]. When patients with pulmonary fibrosis are examined using X-ray or high resolution computed tomography (HRCT), the scar tissue in the lungs can take on a honeycomb-like phenotype[4,5]. This buildup of scar formation leads to difficulties with breathing due to lung stiffness, disruption of gas exchange due to loss of alveolar surface area, and ultimately death due to lung failure[6]. Pulmonary fibrosis primarily affects the lung parenchyma, which is the functional portion of the lung involved in gas exchange[2]. This condition is categorized into several subtypes, reflective of the numerous environmental and genetic factors associated with this disease. Pulmonary fibrosis can arise from exposure to environmental agents such as asbestos and cigarette smoke[7,8]. It is also a potential consequence of bleomycin treatment, a side effect that was noticed in initial human trials for this drug back in the 1970s[9]. In certain connective tissue disorders such as scleroderma and rheumatoid arthritis, patients have a higher risk of developing pulmonary fibrosis[10,11]. However, a definitive cause for pulmonary fibrosis is unidentifiable in many cases[7,8,12]. These cases of unknown etiology are termed idiopathic pulmonary fibrosis (IPF)[12,13]. While IPF typically affects middle-aged adults, it can occur in a wide age range, with documented cases in children and infants[5]. IPF has a poor

prognosis, with a mean survival of two to six years from the time of diagnosis[14]. While 5,000 Canadians are annually diagnosed with pulmonary fibrosis, 4,000 Canadians die annually from this disease[1]. To put this statistic into perspective, the number of deaths due to prostate cancer in Canada for 2011 was approximately 4,100[15]. To further emphasize the severity of IPF, there is currently no proven treatment or cure besides lung transplantation in North America[16]. Although lung transplantation can improve the longevity and quality of life in some IPF patients, accessibility to lung transplants is limited, lung transplantation is a highly invasive procedure, and patients often require immunosuppressant drugs post-surgery, which can give rise to other complications[17]. Corticosteroids such as prednisone, which have been shown to be beneficial in other chronic diseases of the lung such as asthma, does not appear to halt the progression of IPF, and it remains debatable whether they have a beneficial effect[18,19]. Currently, IPF patients are given oxygen therapy to manage their symptoms of coughing and dyspnea[12].

1.2 Normal Wound Repair of the Lung

Repair of damaged tissues in kidney, liver, and lung, due to injury is a crucial mechanism for maintaining the integrity and homeostasis of tissues and organs[20]. The process of wound repair, also referred to as fibrogenesis, is activated upon damage to the endothelial and/or epithelial barrier[21,22]. The goal of this process is to repair wounds and to return the tissue to its original state. With regards to the lungs, which act as an interface between the body and the environment, damage to the alveolar epithelial cells (AECs) can result from, but is not limited to, bacterial and viral infections, cancer, inflammation, and allergic reactions[21,22]. AECs, also known as pneumocytes, have been shown to be

damaged in clinical cases of IPF[23]. These cells are categorized into type 1 and type 2 pneumocytes[14]. Type 1 pneumocytes are flat, elongated cells that comprise 8% of the total cell population found in the lung[23]. Despite this, type 1 pneumocytes cover 95% of the alveolar surface[23]. This large surface area allows type 1 pneumocytes to have an integral role in gas exchange between the air and the blood of the alveolar capillary bed[23]. Conversely, type 2 pneumocytes have multiple functions, including ion transport, alveolar repair in response to injury, and production of surfactant, a compound that prevents the collapse of the alveoli upon exhalation by decreasing surface tension[23,24]. Although type 2 pneumocytes cover 5% of the total alveoli area, they represent a higher population of cells found in the lung compared to type 1 pneumocytes[23]. One further difference between these two cell types is that type 1 pneumocytes are a quiescent cell type, while type 2 pneumocytes have the potential to proliferate and differentiate into type 1 pneumocytes[23].

Along with damage to the epithelium, one of the hallmark characteristics of tissue repair and fibrogenesis is the recruitment and activation of fibroblasts and myofibroblasts to the injury site[20,25,26]. In their activated state, these cells are responsible for establishing and maintaining a provisional framework for tissue remodeling[27]. This provisional framework is called the extracellular matrix (ECM), which consists of water, polysaccharides, and noncellular proteoglycans and fibrous proteins such as fibronectin and type 1 collagen[20,25,26]. Fibroblasts and myofibroblasts are also responsible for secreting factors that will attract epithelial cells to the injury site for subsequent re-epithelialization[20]. While fibroblasts and myofibroblasts are producing collagen at the injury site, collagenases such as matrix metalloproteinase (MMP)-1 and MMP-8 are

simultaneously degrading the collagen matrix[28,29]. Concomitantly, tissue inhibitors of metalloproteinases (TIMP) proteins are present at the matrix to regulate the activity of MMPs[28]. At the beginning of fibrogenesis, collagen production exceeds collagen catabolism resulting in an accumulation of collagen at the injury site[30,31]. However, once enough collagen is laid down to close the wound, collagen production reaches equilibrium with collagen degradation[30,31]. This signals for the fibroblasts to undergo apoptosis in order to halt ECM remodeling[20,25,32]. The final stage in wound repair is the process of re-epithelialization, a process that is not well understood but has been shown to involve both bronchial epithelial cells and AECs[33].

1.3 Aberrant and Chronic Wound Healing

When fibrogenesis becomes dysfunctional or tissue injury is chronic, excess accumulation of ECM causes scar formation, stiffness and thickening of the lung tissue, and impairment of lung function leading to organ failure[20,34]. It is currently thought that pulmonary fibrosis is caused by an imbalance of two processes: fibroblast proliferation versus apoptosis, and ECM accumulation versus degradation[35]. Clinical cases and some experimental models of pulmonary fibrosis have shown exaggerated proliferation of fibroblasts and myofibroblasts in clusters called fibroblast foci, as well as a lack of fibroblast apoptosis[36,37]. Other studies have shown an increase in ECM remodeling through increased collagen content, increased fibronectin expression, and elevated levels of MMP and TIMP proteins[38–40]. Another key observation in IPF patients is changes to the morphology of the alveoli such as the thickening of the alveolar walls[36,37]. These features are used to assess the severity of fibrosis through the Ashcroft score[41,42]. Other

changes to the lung environment include a decrease in nitric oxide, platelet aggregation, and tissue hypoxia[20,43]. Lastly, chronic wounding induces the inflammatory response, which is characterized at an early stage by neutrophil infiltration[44]. While neutrophils are necessary as the initial line of defense against bacteria, neutrophils also release inflammatory mediators such as IL-1 and TNF-α, which have been shown to stimulate fibroblasts and epithelial cells[45,46]. Furthermore, neutrophils are short-lived cells that release their contents upon their death, causing tissue damage as well as prolonging the inflammatory phase[47]. Thus, pathology of the lung arises when the normally homeostatic mechanism of fibrogenesis becomes constitutively active and unregulated.

1.4 Fibroblasts and Myofibroblasts

The ECM is the non-cellular component present in all tissues and organs[48]. It is comprised of water, polysaccharides, proteoglycans, and fibrous proteins such as collagen[48]. The ECM has various roles, providing mechanical and structural support for tissue, and orchestrating cellular activity, including intercellular communication and cell differentiation[48,49]. The numerous syndromes that arise from abnormalities in the composition and composition of the ECM demonstrate the importance of the ECM in tissue homeostasis[48,50]. Regulation of the ECM is determined by dynamic interactions between various cell types such as fibroblasts, epithelial cells, and endothelial cells[48].

Fibroblasts, which are a cell type derived from primitive mesenchyme, are the most abundant cell type found in connective tissues such as skin, lung, and heart[34,51]. The fibroblast's primary function is to maintain the structural integrity of organs and tissue by secreting factors that contribute to ECM remodeling, including collagen and fibronectin.

It has been shown that upon stimulation with interleukin (IL)-4 *in vitro*, fibroblasts increase collagen production, an effect abolished using a neutralizing antibody to interleukin IL-4[52]. Collagen production has destructive effects on the lung architecture when fibroblast activity is unregulated, as is the case in fibrotic diseases[34]. There is a growing body of evidence suggesting that fibroblast populations, not only from different organs, but within same organ, are heterogeneous and display different phenotypes and properties. For instance, human lung fibroblasts derived from the lung parenchyma have enhanced TGF-β signaling and alpha smooth-muscle actin (α-SMA) expression compared to fibroblasts derived from the proximal bronchi[53]. Furthermore, fibroblasts from IPF patients display a heterogeneous phenotype as well as properties that differ from normal lung fibroblasts[23]. For instance, several studies have shown that fibroblasts from IPF patients proliferate at a faster rate than control patients[36,37,54].

One histological feature that distinguishes normal lung from the lungs of an IPF patient is the presence of myofibroblasts in fibrotic lesions[55,56]. Myofibroblasts are a modified phenotype of fibroblasts with smooth muscle-like features such as α-SMA and type 1 collagen that are not present on normal lung fibroblasts[57]. However, myofibroblasts also retain fibroblast cell surface markers such as vimentin[57]. Myofibroblasts can originate from several sources. Resident fibroblasts are able to transform from a quiescent state to a proliferative contractile myofibroblast phenotype[58]. Myofibroblasts can also be derived from AEC through a process called epithelial-to-mesenchymal transition (EMT)[55,56]. In this process, epithelial cells lose cell surface markers such as E-Cadherin but gain mesenchymal cell surface markers such as

vimentin[59]. More recently is the suggestion that myofibroblasts can be derived from endothelial cells through endothelial-to-mesenchymal transition (EndoMT)[60]. Lastly, it has been suggested that fibrocytes contribute to the myofibroblast population[61]. Fibrocytes are a bone-marrow derived cell type positive for cluster of differentiation (CD) 45 and type 1 collagen, and have been detected at elevated levels in the BALF fluid of IPF patients[61,62]. Chemotactic factors historically implicated in fibrocyte recruitment from the bone marrow include stromal cell-derived factor (SDF)-1 and MCP-5[63,64].

It has been shown that myofibroblasts are associated with fibrogenesis and fibrosis since they are localized to sites of wound healing[65]. Like fibroblasts, myofibroblasts synthesize components of the ECM such as collagen types 1 and 3 to aid in the formation of a provisional framework as part of the tissue remodeling process[66]. The presence of α-SMA is necessary for myofibroblast contractile motions and mobility, which enables the physical remodeling of the matrix[67]. Myofibroblasts undergo apoptosis when wound healing is terminated, but are present during chronic ECM remodeling and can contribute to pathogenesis[68]. Along with producing excessive collagen and other components of the ECM, myofibroblasts have also been shown *in vitro* to have an invasive phenotype akin to metastatic cancer cells, a characteristic that may contribute to progressive fibrosis[69]. Transgenic mice with targeted overexpression of hyaluronan synthase in in α-SMA+ cells exhibited exacerbated responses to bleomycin compared to wildtype mice[69]. The authors of this paper attributed this to the invasiveness of myofibroblasts, as fibroblasts cultured *in vitro* from these transgenic mice were capable of invading a composite matrix with basement membrane constituents[69]. The increased

proliferation of fibroblasts and the presence of myofibroblasts in IPF patients suggest an important role for this cell type in IPF pathogenesis.

1.5 Epithelial Cells

While fibroblasts are the most abundant cell type found in lung connective tissue and contribute to the maintenance of the ECM, the role of epithelial cells in pulmonary fibrosis pathogenesis should not be understated. In fact, pulmonary fibrosis in some individuals is attributed to a mutation encoding surfactant type C, which is produced by type 2 pneumcoytes[70,71]. Furthermore, a histological examination of the lungs of IPF patients shows numerous hyperplastic and hypertrophic pneumocytes with abundant cytoplasm and large hyperchromatic nuclei[72]. These regions are adjacent to the fibroblast foci, which suggest a possible interaction between epithelial cells and fibroblasts[72]. Lastly, a prominent pathological finding in IPF patients is that bronchial epithelial cells and peumocytes contribute to the re-epithelialization of damaged alveoli[33]. Abnormalities in both the morphology of pneumocytes and bronchial epithelial cells in IPF patients suggest a potential role of these cells in the disease process.

As previously mentioned, injury to the AECs is known to trigger fibrogenesis. Evidence for this claim comes from the work of Sisson and coworkers, who used transgenic mice that expressed diphtheria toxin receptor on type 2 pneumocytes[73]. Upon exposure to diphtheria toxin, these transgenic mice developed pulmonary fibrosis concomitantly to lung epithelium damage in the interstitial space[73]. Moreover, type 2 pneumocyte injury has been linked to spontaneous IPF in felines[74]. It is thought that continuous injury to pneumocytes recruit and differentiate fibroblasts into a myofibroblast

phenotype. Pneumocytes undergoing EMT also contribute to the myofibroblast population, a process that is stimulated by TGF-β. The EMT of pneumocytes is modulated by the ECM, as Kim and colleagues in 2006 showed that primary pneumocyes grown on fibronectin undergo EMT upon stimulation with TGF-β, but pneumocytes grown on a collagen/laminin mixture undergo apoptosis upon TGF-β stimulation[56]. These activated fibroblasts can induce further pneumocyte cell death, thus creating a vicious cycle of microwounding. While type 1 pneumocytes are vulnerable to injury, type 2 pneumocytes are more more resistant, and thus serve as a progenitor population during lung repair. Type 2 pneumocytes also synthesize numerous enzymes and growth factors in response to injury such as TNF-α, TGF-β, and MCP-1. It is now believed that pneumocytes are responsible for the secretion of some of the cytokines commonly associated with inflammatory cells such as alveolar macrophages. Thus, epithelial cells may play a prominent role in IPF pathogenesis, possibly through interactions with the fibroblasts in the underlying ECM and this warrants further investigation.

1.6 Animal Models to Study Pulmonary Fibrosis

To date, various animal models have been used to study the pathogenesis of pulmonary fibrosis. Such models include, but are not limited to, exposure of rodents to asbestos, silica, bleomycin, and radiation[18,75–77]. Other models include the overexpression of specific cytokines, such as TGF-β, using an adenovirus vector[78]. However, there are several limitations to these animal models. One of the major criticisms when trying to draw conclusions about IPF from experimental models is the fact that known agents such as bleomycin are being administered to these animals, whereas the causative agent is

unknown in IPF. In fact, some scientists argue that more is known regarding bleomycin-induced fibrosis in rodents than about IPF. Further contrasting animal models from pulmonary fibrosis in humans is the timeline of disease progression. ECM remodeling in rodents is induced over several weeks, whereas it develops over several decades in the human condition. In some animal models, such as exposure of rodents to either bleomycin or silica, fibrosis spontaneously resolves, a feature not seen in the human condition. This resolution process remains poorly characterized but may be important to investigate in terms of potential therapeutics. Lastly, administration of an adenovirus to overexpress a particular cytokine creates an artificial environment where cytokine levels are typically higher than physiological levels. While animal models are a useful method of studying IPF pathogenesis, the limitations of each model need to be acknowledged.

The bleomycin model of pulmonary fibrosis in rodents remains the most frequently used model for studying fibrosis[79]. A single dosage of bleomycin can be administrated into the airways through the intranasal or endotracheal route, or systemically through subcutaneous, intraperitoneal or intravenous injections[79]. The bleomycin model is often utilized to determine the efficacy of prospective drugs prior to use in human clinical trials[18]. Bleomycin-treated mice and rats have impaired lung function and increased ECM remodeling compared to control mice by 21 days[79]. Bleomycin induces the expression of myofibroblasts and increased collagen in the lung parenchyma, as seen by increased α-SMA and picrosirius red (PSR) staining. A hydroxyproline assay that measures total lung collagen content showed that mice treated with bleomycin have increased collagen content compared to saline-treated mice.

Interestingly enough, bleomycin is able to induce ECM remodeling in C57Bl/6 strain of mice, but less so in BALB/C mice[80]. Studies have suggested that BALB/c mice are more resistant than C57Bl/6 mice due to higher levels of bleomycin hydrolase, which inactivates the bleomycin drug[81]. Differences also exist in the bronchioalveolar lavage fluid (BALF) constituents of bleomycin-treated C57Bl/6 mice relative to saline-treated mice, with increased cell numbers, increased neutrophils, as well as increased lymphocytes[82]. In more recent years, there has been a push to refine the bleomycin model from a single administration of the drug to an eight biweekly dosing regiment[83]. Although mortality is higher using this model, this dosing regiment results in persistent fibrosis that is maintained 70 days after the last bleomycin administration[83]. Furthermore, mouse lungs have more phenotypic similarities with the human condition, with the abundance of prominent type 2 pneumocyte hyperplasia as well as the presence of fibroblast foci that is absent in the original bleomycin model[83].

1.7 Role of Inflammation and Immunology in Pulmonary Fibrosis

Injury to the pneumocytes activates apoptotic pathways, resulting in the presentation of damaged associated molecular patterns to the innate immune system[20]. This induces an inflammatory response characterized by the release of cytokines, which are small glycoproteins that mediate intercellular communication[47]. Cytokines found in the bronchioalveolar lavage fluid (BALF) of IPF patients but not in control patients include monocyte chemoattractant protein (MCP)-1, macrophage inflammatory protein (MIP)-1, and IL-8[20,26]. These cytokines attract immune cells such as neutrophils and monocytes to the injury site where they subsequently release a number of growth factors

and chemotactic factors such as transforming growth factor beta (TGF-β) and connective tissue growth factor (CTGF)[20]. This ensuing inflammatory response results in the release of numerous soluble factors from the fibroblasts, epithelial cells, endothelial cells, macrophages, and the underlying matrix such as TGF-β and TNF-α[20].

While TGF-β has been implicated in IPF pathogenesis, the role of immunity and inflammation remains controversial and splits the opinions of scientists. On one hand, certain indicators of immunity and inflammation such as T cells, IL-6, IL-17A, are found at higher levels in the BAL fluid of IPF patients compared to control patients[84]. This suggests a role for inflammation in IPF pathogenesis. However, a major argument against the involvement of inflammation and immunity is that most IPF patients do not positively respond to immunosuppressive and anti-inflammatory treatments such as corticosteroids[84].

With regards to T cells, T cell infiltration into the lungs occurs in most IPF patients, and this observation is also seen in animal models of pulmonary fibrosis[85]. Marchal-Sommé and coworkers showed that 80% of the activated T cells found in lung biopsies taken from IPF patients were positive for CD45RO[86]. The presence of CD45RO+ T-cells, associated with a memory T cell phenotype, suggests that T cells persist in the lung and contribute to chronic fibrosis. However, contradictory evidence supports the notion that T cells are not involved in fibrosis. Transgenic mice lacking T cells respond to bleomycin comparably to their wild type counterparts[87]. These same conclusions were made using an alternative approach where T cells were systemically

depleted from mice prior to bleomycin administration[88]. Therefore, the evidence surrounding the role of T cells in IPF pathogenesis remains unclear.

There are several hypotheses that attempt to fit inflammation into the pathogenesis of pulmonary fibrosis. One possibility is that inflammation plays an integral role in driving the initial phase of IPF pathogenesis, but is not involved in the late phases of fibrosis[85]. Another possibility is that fibrosis and inflammation are two simultaneously occurring processes that can influence one another[85]. The last possibility is that fibrosis and inflammation are two processes occurring simultaneously, but do not influence one another[85]. Research remains to be done to elucidate the role of inflammation and immunity in IPF pathogenesis.

1.8 Transforming Growth Factor Beta (TGF-β)

TGF-β is a cytokine involved in numerous cellular processes such as cell proliferation, differentiation, and matrix synthesis[2]. It is associated with oncogenesis, embryogenesis, as well as mediating wound repair[2]. The functional diversity of TGF-β is attributed to the existence of three TGF-β isoforms, several isoforms of a TGF-β binding partner that keeps TGF-β in its latent form, different mechanisms by which TGF-β is released from its binding partner to become activated, and the induction of multiple downstream cell signaling pathways[89]. It is thought that TGF-β plays a role in IPF pathogenesis as levels of active TGF-β1 are elevated in the BALF of IPF patients[13,90]. Furthermore, targeting TGF-β1 using monoclonal antibodies and inhibitors have been efficacious in animal models of pulmonary fibrosis[91–93].

TGF-β is initially inactive upon translation, with activation occurring after a series of steps[89]. Pro-TGF-β residing within the cell forms homodimers that bind to latency-associated peptide (LAP) to form the small latent complex (SLC)[89]. This complex remains in the cell until the SLC binds to latent TGF-β binding protein (LTBP) to form the large latent complex (LLC)[89]. The LLC is capable of leaving the cell, where it becomes sequestered at the ECM[89]. TGF-β activation requires the dissociation of the LLC complex, which occurs through either proteolytic degradation of the LLC complex or mechanical stretching, a process that involves integrin proteins found on the ECM[89].

Activated TGF-β binds to membrane bound TGF-βR2, which causes the recruitment of TGF-βR1[94]. Upon recruitment, TGF-βR1 becomes phosphorylated and acts as a receptor kinase[95]. In terms of the canonical pathway, this results in the phosphorylation of cytoplasmic signaling molecules termed Receptor Mothers Against Decapentaplegic Homolog (R-SMAD) proteins[95]. In the case of the TGF-β pathway, SMAD2/3 become serine phosphorylated[95]. SMAD2/3 form a heteromeric complex with a common SMAD (Co-SMAD) protein called SMAD4[89]. This heteromeric complex acts as a transcription factor to affect gene regulation in the nucleus. In terms of regulating the SMAD pathway, a family of SMAD proteins called inhibitory SMADs (I-SMAD) compete with binding of pSMAD2/3 to SMAD4[95]. In particular, SMAD7 has been shown to act as an I-SMAD for the TGF-β pathway[96]. With regards to noncanonical pathways, TGF-β has been shown to activate both the mitogen activated protein kinase (MAPK) as well as Rho kinase pathways, the latter of which is involved in actin fiber polymerization.

1.9 TGF-β and Pulmonary Fibrosis

Since TGF-β has been shown to modulate lung fibroblast and epithelial cell function, it has been thought that TGF-β is a key regulator of the fibrotic response. Emphasizing the role of TGF-β in the fibrotic response are studies that conclude that transient over-expression of TGF-β induces symptoms in rodents similar to that of IPF[78,97]. Activation of TGF-β is necessary for modulation of the ECM, as mice null of integrin-β6, implicated in the binding and activation of TGF-β, are resistant to bleomycin-induced pulmonary fibrosis[98]. Inhibition of the canonical TGF-β pathway through transient overexpression of SMAD7 has been shown to prevent bleomycin-induced pulmonary fibrosis in mice[99]. Lastly, it has been shown that myofibroblast contraction is capable of activating latent TGF-β from the ECM[100].

TGF-β regulates the cellular activity of many cell types in the lung parenchyma. TGF-β has been known to induce EMT in epithelial cells, providing one source for the myofibroblast population found in IPF patients[55,56]. TGF-β also induces the recruitment and differentiation of fibroblasts and myofibroblasts, which express TGF-β receptors on the cell surface[101]. TGF-β also stimulates lung fibroblasts to produce fibronectin and type 1 collagen[102]. *In vitro s*tudies have shown that TGF-β plays a role in ECM remodeling, fibroblast activation, as well as cell death[103]. Lastly, TGF-β directly induces the production of platelet-derived growth factor (PDGF) by alveolar macrophages as well as myofibroblasts[104]. PDGF is responsible for the expansion of the myofibroblast population through cell proliferation and migration[6,105]. These findings support the current paradigm that TGF-β plays a major role in the induction of IPF.

Despite evidence to support the importance of TGF-β in the pathology of pulmonary fibrosis, to date clinical trials based on targeting TGF-β have not reported success in alleviating symptoms of pulmonary fibrosis. Hence, this raises the possibility that TGF-β independent mechanisms may be involved in the pathogenesis of IPF.

1.10 Gp130 cytokines and OSM

Gp130 cytokines are a family of cytokines involved in inflammatory processes, hematopoiesis, cardiovascular action, and neuronal survival[106–108]. These cytokines are classified together based on the requirement that these cytokines engage a receptor complex consisting of at least one gp130 receptor subunit found on the cell surface[108]. The various receptor complex combinations that gp130 receptors bind to allows these cytokines to be involved in many cellular mechanisms, but the presence of gp130 gives it several hallmark characteristics[109]. These characteristics include the induction of the signal transducer and activation of transcription (STAT) pathway, MAPK pathway, and the PI3K pathway[109]. Examples of gp130 cytokines include IL-6, leukemia inhibiting factor (LIF), IL-11, IL-31, and Oncostatin M (OSM)[109]. Gp130 cytokines have been suggested to play a potential role in fibrotic diseases[110]. For instance, overexpression of IL-11 *in vivo* results in peribronchiolar mononuclear cell inflammation, type 1 collagen deposition, and increase in number of myofibroblasts in the lungs of mice[110]. IL-6 is another gp130 cytokine is elevated in the BALF of IPF patients[111]. IL-6 has been shown to mediate many inflammatory processes in the lung. For instance, mice lacking IL-6 have attenuated immune cell infiltration into the lungs upon antigen challenge[112]. In terms of fibrosis and ECM remodeling, the work of Saito and coworkers showed that

bleomycin-induced pulmonary fibrosis was attenuated in IL-6 knockout mice compared to wildtype mice, suggesting a role for IL-6 in ECM remodeling[112].

OSM is another member of the gp130 cytokine family. Upon recruitment to the site of inflammation, macrophages, T cells, and granulocytes produce OSM. OSM is a pleiotropic cytokine that binds to a specific receptor complex comprised of gp130 and OSMRβ in the murine system[113,114]. However, human OSM can bind either to the OSMRβ/gp130 receptor complex or to the LIF/gp130 receptor complex in cells of human origin, thus eliciting responses through both receptor complexes. Binding of OSM to the OSMRβ or LIFR complex recruits cytoplasmic Janus kinases (JAKs) [115]. These proteins are responsible for phosphorylating specific tyrosine residues on the gp130 receptor subunit, which allows for the subsequent binding of the protein phosphatase SHP2 as well as STAT proteins[115]. With regards to the former, SHP2 is involved in the activation of the MAPK pathway through the involvement of the adaptor protein GRB2[115]. In contrast, members of the STAT family bind to other intracellular phosphorylated tyrosine sites found on the gp130 receptor subunit. Once phosphorylated, STAT proteins such as STAT3 translocate to the nucleus to affect gene expression. STAT proteins are negatively regulated in several ways. Suppressors of cytokine signaling (SOCS) proteins are able to inhibit STAT protein phosphorylation by interacting with the catalytic domain of JAK proteins[116]. SHP2 is also able to regulate phosphorylation of STAT proteins by acting as a tyrosine phosphatase. Along with cell signaling pathways, OSM stimulates the release of IL-6 in lung fibroblasts, lung epithelial cells, and airway smooth muscle cells, the latter which has been shown to occur in a dose and time dependent fashion[117].

OSM is of major interest in our laboratory since it is a pleiotropic cytokine. OSM receptor chains are expressed in many cell types and hence has a potential involvement in many biological processes and diseases including asthma[118]. OSM has been implicated in a variety of conditions that involve ECM remodeling, such as rheumatoid arthritis, atherosclerosis, and bone remodeling[119–121]. With regards to the latter process, OSM has been shown to enhance BMP-2 induced alkaline phosphatase activity in C2C12 cells[121].

1.11 OSM and Lung Disease

OSM may have a prominent role in certain lung diseases, as levels of OSM are elevated in the BALF of patients suffering from scleroderma-associated interstitial lung disease, IPF, and severe asthma[122,123]. It is well established that OSM is involved in the regulation of MMP and TIMP proteins[124,125]. Transient ECM remodeling can also be induced in C57Bl/6 mice using an adenovirus encoding for OSM (AdOSM)[126]. One of the characteristics of this model is that OSM overexpression induces airway eosinophilia in C57Bl/6 mice, a feature seen in asthmatic patients[126]. OSM overexpression also results in the STAT-6 dependent regulation of IL-4, IL-13, chemokines, MMP-1, but also the STAT-6 independent regulation of total collagen production and α-SMA[126]. IL-4 and IL-13 are two T-helper (Th)-2 cytokines that stimulate fibroblast proliferation and ECM production *in vitro*[127,128]. With regards to *in vitro* studies, OSM has also been shown to stimulate cellular proliferation, induce collagen production, and inhibit apoptosis in human lung fibroblasts, all of which were mitigated in the presence of a MAPK inhibitor[129]. In asthma, another lung disease that involves ECM remodeling around the major airways, patients with severe airway obstruction had elevated levels of OSM in

their sputum samples[123]. Thus, there is growing evidence to support the involvement of OSM in the pathogenesis of certain lung diseases.

It is imperative to continue to characterize the model involving the overexpression of OSM to induce transient ECM remodeling of the lung. A better understanding of the mechanisms involved in this model may be beneficial in looking for alternative TGF-β-independent therapeutics for this disease.

1.12 Bone Morphogenetic Proteins (BMP)

BMPs are part of the TGF-β superfamily, which also comprises the activin family of proteins[130]. To date, more than 20 BMPs have been identified[130]. Although the name bone morphogenetic protein originated when BMPs were initially discovered to be involved in bone formation and development, studies have implicated BMPs in other processes, including lung development and regulation of neural induction[96,131]. Such is their involvement in a multitude of other cellular processes that some have proposed that the term BMP should be renamed to body morphogenetic protein[132]. *In vivo* studies show that BMPs are quintessential in neonate bone formation, and that knocking out these genes causes prenatal death[133,134]. BMPs are also a potent inducer of osteoinduction, and thus are currently being used to treat single-level lumbar degenerative disc disease[135]. Recombinant human BMP2 has also recently been approved by the FDA for use in treating intervertebral disk regeneration by facilitating spinal fusion[135]. BMPs may also play a role in diseases of the lung, and therefore modulation of BMP pathways may show some therapeutic promise in disrupting pulmonary fibrosis pathogenesis.

The canonical signaling pathway by which BMP induces effects on cells involves SMAD1/5/8 signaling proteins[130]. The canonical BMP pathway is analogous but distinct from the canonical TGF-β pathway, which utilizes SMAD2/3 as intracellular signaling proteins. SMAD proteins comprise of a mad homology 1 (MH1) and MH2 domain, which are linked together by a linker region[130]. The MH1 domain represents the N-terminus of the protein whereas the MH2 domain represents the C-terminus of the protein[130]. Both of these domains are highly conserved between SMAD species[130]. BMPs bind to a cell membrane-bound tetrameric receptor complex comprising of two BMP receptor (BMPR) 1 chains and two BMPR2 chains[130]. Three BMPR1 have been identified to date: Alk2 or AVGR1, Alk3 or BMPR1a, and Alk6 or BMPR1b[130]. In the SMAD1/5/8 pathway, BMP ligands bind to BMPR2, causing the recruitment and serine phosphorylation of BMPR1[130]. This serine/threonine kinase receptor subsequently causes the serine phosphorylation of R-SMAD proteins SMAD1/5/8 at the MH2 domain[130]. These bind together with the co-SMAD SMAD4 to form an oligomeric complex[130]. This oligomeric complex acts as a transcription factor in the nucleus, affecting genes implicated in cell differentiation, apoptosis, and collagen deposition/mineralization such as RUNX2, osterix, and Id1[130]. As a negative feedback system to turn off SMAD1/5/8 signaling, SMAD6/7 are I-SMAD proteins that dissociate the SMAD1/5/8 oligomeric complex from SMAD4, thus rendering it unable to act as a transcription factor[130]. In addition, endogenous BMP antagonists exist to prevent the binding of BMP ligands to their receptors[136]. Gremlin acts as an antagonist of BMP2, 4, and 7 by heterodimerizing to the BMP ligands[136].

BMP is also able to activate noncanonical pathways such as MAPK, Rho-like GTPases, and phosphatidylinositol 3-kinase (PI3K)/Akt, all of which have significance in pathology[137]. For instance, Rho-like GTPases have been shown to play a major role in EMT-induced by TGF-β[138]. Furthermore, PI3K pathway is responsible for BMP-induced cell migration[139]. It has also been shown that noncanonical cell signaling of the BMP pathway results in the upregulation of genes such as Cox2 and Msk1 in primary murine bone marrow mesenchymal stem cells[137].

When unregulated, the canonical BMP pathway is associated with pathology. Excessive SMAD1/5/8 cell signaling, as well as an absence of it, causes mouse death at mid-gestatation[140]. A mutation to BMPR2 results in increased susceptibility of endothelial cells to apoptosis, and this is considered crucial in the pathogenesis of pulmonary hypertension[141]. In another example, a mutation to Alk2 causes constitutively active BMP cell signaling, and this is has been associated with the disease fibrodysplasia ossificans progressiva[142]. Inhibiting the BMP cell signaling pathway using the pharmacological BMP inhibitor LDN193189 was able to attenuate the effects of this mutation[142].

1.13 BMP and Pulmonary Fibrosis

Tissue repair of the lung as a result of injury draws parallels to embryonic lung development, a process that BMPs play an important role in. In terms of embryonic lung development, BMP pathways have been shown to be activated in mice during the pseudoglandular stages (between embryonic day 12 and day 16.5), at which time branching morphogenesis of the lung occurs[143]. SMAD1 and SMAD5 KO mice have been shown to die mid-gestation, further illustrating the significance of the canonical

BMP pathway in embryogenesis[140,144,145]. While BMP pathway involvement has been characterized in embryogenesis, less is known about the role of the BMP pathways in postnatal processes. It has been shown that BMPR2 is highly expressed on the vascular endothelium of pulmonary arteries, though it has been detected at lower levels in fibroblasts as well pulmonary arterial smooth muscle cells[141]. The current paradigm with regards to IPF pathogenesis is that in the context of TGF-β/BMP signaling, TGF-β pathways are activated whereas BMP pathways are suppressed[136]. Clinical data from IFP patients show that patients have an increased expression of gremlin, an antagonist of BMP2, 4, and 7 cell signaling[136]. Furthermore, overexpressing gremlin *in vivo* has shown to induce the proliferation of fibroblasts and myofibroblasts, and collagen deposition in the lungs of rats[146]. However, only recently has it been shown that the canonical BMP pathway is activated upon injury to the lungs in some experimental models of lung ECM remodeling[143]. In a C57Bl/6 mouse model where binding of the pSMAD1/5/8 oligocomplex to the Id1 promoter region causes GFP expression, bleomycin administration to C57Bl/6 mice induced the canonical BMP pathway in type two pneumocytes by Day 4 compared to control treated animals[143]. Naphthalene, another fibrosis-inducing agent, was able to activate the canonical BMP pathway in bronchial epithelial cells by day 2[143]. This data suggests that while the BMP pathway may be suppressed at later stages of fibrosis, perhaps the BMP pathway is immediately activated following injury as a repair mechanism. Therefore, the role of BMPs in the context of pulmonary fibrosis and tissue injury must be further investigated. Utilizing the OSM overexpression model as the basis to study the role of BMPs presents a novel approach to

addressing this question. To date, there has been no report of a cross-talk between the OSM and BMP cell signaling pathway in the literature with regards to the lung environment. However, given the fact that OSM is expressed in many disease states such as atherosclerosis, rheumatoid arthritis, and asthma, and that OSM and BMP together are able to induce phenotypic changes in certain cells, it is possible that OSM and BMP interact with one another in the context of fibrotic lung diseases. Discovery of a cross-talk between these two pathways would be important for exploring novel pathways to tissue fibrosis in lungs and potentially even other tissues.

1.14 Summary of Project

Chronic ECM remodeling of the lung drives the development of pulmonary fibrosis[35]. However, the pathogenesis of IPF, one subtype of pulmonary fibrosis, remains poorly understood. Evidence suggests that TGF-β through SMAD2/3 signaling is a principle regulator of ECM remodeling, as it stimulates the production of CTGF, differentiates epithelial cells and fibroblasts into α-SMA+ myofibroblasts, and stimulates collagen production in lung fibroblasts[101,102,104]. Nonetheless, therapeutics for IPF targeting TGF-β alone has not at present shown clinical efficacy and other pathways may drive fibrosis in certain conditions. Thus, the scope of this project was to examine the effects of another ECM-remodeling cytokine, OSM, and its mechanisms involved in lung ECM remodeling in animal models. To address this task *in vivo*, C57Bl/6, BALB/c, IL-6 -/-, and SMAD3 -/- mice were endotracheally administered an adenovirus encoding the pleiotropic cytokine OSM, and lung tissue was examined after two and seven days. Responses of MLF cultures, human airway epithelial cells, human A549 cells, and mouse

C10 pneumocytes to OSM were also examined *in vitro*. In particular, potential OSM regulation of the STAT3 and SMAD1 signaling pathways were explored, as these pathways have been implicated in other models of lung ECM remodeling. By exposing tissue and cells to OSM, it was hypothesized that STAT3 activation would be elevated and the BMP-SMAD1 signaling axis would be suppressed, leading to a loss in lung homeostasis and an accumulation of the ECM.

1.15 Aims and Hypotheses

Main Goal: To examine STAT and SMAD signaling in a model of OSM-induced lung ECM remodeling

Hypotheses: OSM-induced ECM remodeling involves STAT3 activation and BMP-signaling dysregulation

Aim 1: To compare responses to OSM overexpression in the lung of fibrosis-prone C57Bl/6 mice to fibrosis-resistant BALB/c mice, and responses of MLF cultures derived from these strains

Aim 2: To determine if OSM-induced ECM remodeling required IL-6 or SMAD3 signaling utilizing knockout mice.

Aim 3: To determine the activation of STAT3, SMAD1/5/8, and SMAD2/3 cell signaling pathways associated with OSM-induced effects *in vivo* and *in vitro*.

CHAPTER 2: Materials and Methods

2.0 Intubation of mice with adenovirus and subsequent sample collection

Mice from C57Bl/6 and BALB/c background were intubated with $5x10^7$ pfu of adenovirus vector encoding OSM (AdOSM) to induce transient pulmonary OSM overexpression, or $5x10^7$ pfu of adenovirus containing an empty vector (AdDl70) as a control. At days 2, 7, 12, 14, and 28 mice were culled and lungs were excised from the thoracic cavity. Lungs were initially perfused with 1xPBS to collect BALF and inflammatory cells residing in the lungs. This lavage fluid was spun down at 12,000 rpm for 2 minutes, and the supernatant/BALF was stored at -80°C until further use. The remaining cell pellet was resuspended in 1xPBS in order to perform total cell counts, and cell differentials through Wright-Giemsa staining of cytocentrifuge smears. Lung tissue was collected for histology, RNA and protein analysis, as well as hydroxyproline assay. For histology preparation, lungs were perfused with 10% formalin, stored in 10% formalin for 48 hours, before being transferred into 70% ethanol. Lungs were then cut and paraffin embedded. For lungs being used for RNA and protein analysis, as well as the hydroxyproline assay, lungs were immediately snap frozen in liquid nitrogen and stored at -80°C until further use.

2.1 Histology and Immunohistochemistry

5 μm sections of paraffin-embedded lungs were put on slides and stained for H&E, Masson's Trichrome, and PSR by MIRC Core Histology. For IHC, 5 μm unstained sections of paraffin-embedded lungs were prepared. An IHC protocol was followed in order to stain for pSTAT3, pSMAD2, pSMAD1/5/8, and α-SMA. Slides were

deparafinized at 60°C for 45 minutes before being washed with xylene, alcohol, and water. Antigen retrieval was performed using proteinase K (Dako, Burlington, Ontario) for five minutes, and sections were blocked using 5% normal goat serum for 15 minutes. The sections were then stained with 1:100 dilution of the pSMAD2 and pSMAD1/5/8 antibody for one hour at room temperature, or a 1:100 dilution of the pSTAT3 antibody overnight at room temperature. Slides were then washed and developed using Envision Rabbit detection system (Dako, Burlington, Ontario). The sections were counterstained with Mayer's hematoxylin and mounted in glycerin.

2.2 Histology Imaging and Quantification

Photomicrographs of histology slides were taken with OpenLab software (version 3.0.3; Improvision, Guelph, Canada) using a Leica camera and microscope (Leica MicroSystems, Richmond Hill, Canada). For quantification of parenchymal collagen, a modified version of the Ashcroft score was used. Multiple photomicrographs of PSR-stained slides visualized under polarized light were taken at 5x objective lens to cover the entire lung section. Pictures were then rated by four blind assessors from a score of 0-8 based on amount of positive staining in the lung parenchyma. Scores for each lung section were averaged and compared to control lung section (AdDl70) whenever possible.

2.3 Lung crushing

Lung crushing was performed to optimize the analysis of mouse lung. This procedure allowed for the collection of lung samples for protein analysis via SDS-PAGE and subsequent Western blot, gene expression analysis via Taqman, and collagen content analysis via hydroxyproline assay. Frozen lungs were kept cool on liquid nitrogen or dry

ice during the entire process to prevent thawing. Lungs were transferred into a pre-chilled metal pestle and mortar apparatus, and crushed and mixed into fine powder by hammering the pestle. Afterwards, approximately one third of the crushed lung powder was placed into Trizol for RNA analysis, while the rest of the crushed lung powder was kept in radioimmunoprecipitation (RIPA) lysis buffer containing 1% Igepal CA-630, 0.5% sodium deoxycholate, 0.1% sodium dodecyl sulfate (SDS) diluted in 1xPBS, and protease inhibitors 1mM sodium orthovanadate, 0.1 mg/mL phenylmethylsulfonylflouride (PMSF), 5 μg/mL aprotinin, and 1 mM dithiothreitol (DTT) for protein analysis as well as the hydroxyproline assay. Samples were stored at -20°C until further use.

2.4 Lung homogenization for protein and RNA analysis

Crushed lung powder stored in either Trizol or RIPA buffer containing protease inhibitors was homogenized using a Brinkmann Homogenizer Polytron PT 3000. RNA was extracted from Trizol according to manufacturer's instructions, and stored at -80°C until further use. For protein analysis and hydroxyproline assay, homogenized tissue was spun for 30 minutes at 2,000 rpm. The supernatant was collected and stored at -80°C until further use. Lung homogenates were resuspended in 1xPBS and stored at -20°C until hydroxyproline determination.

2.5 Hydroxyproline Assay

Lung hydroxyproline content was determined using a colorimetric assay with a hydroxyl-L-proline standard. Briefly, lung homogenates in 1xPBS were dried overnight using a freeze dry lyophilizer to obtain dry-weight tissue. This tissue was weighed, and subsequently incubated overnight at 110°C in 6 N HCl. Samples were then adjusted to pH

7.0 using NaOH. Chloramine T was added to these samples to induce oxidation, and this reaction was stopped using 70% perchloric acid. Ehrlich's reagent was added to the samples, which were incubated at 60°C to induce a color change. Finally, spectrophotometer readings at 557 nm were obtained and computed into a hydroxyproline concentration (μg of hydroxyproline per mg of dry tissue weight) using Microsoft Excel.

2.6 Cell Culture

C75Bl/6 and BALB/c mouse lung fibroblasts (MLF) cultures were generated from mouse lung explants. Briefly, mice were culled and lungs were excised from the thoracic cavity. Lungs were subsequently washed in 1xPBS and minced using forceps and scissors. The lung extracts were then transferred to a T25 supplemented with MEM-F15 media containing 10% heat inactivated FBS, 1% penicillin streptomycin, 1% L-glutamine, and 0.1% fungizone (Life Technologies, Carlsbad, CA) and cultured at 37°C in 5% CO_2. After 4 days, lung explants were removed and the adherent cell population was left to expand. Experiments were performed on these cells until passage 10, and split at a 1:4 ratio in tissue culture treated flasks and dishes.

Human A549 pneumocytes were received as a generous gift from the lab of Dr. Jack Gauldie (McMaster University). A549 cells were cultured in α-MEM media containing 10% heat inactivated FBS, 1% penicillin streptomycin, 1% L-glutamine, and 0.1% fungizone (Life Technologies, Carlsbad, CA) and cultured at 37°C in 5% CO_2. These cells were split at a 1:7 ratio in T150 flasks and plated at 14000 cells/cm^2 on tissue culture treated dishes for experimentation the following day.

Beas 2B bronchial epithelial cells were received as a generous gift from the lab of Dr. Mark Larché (McMaster University). Beas 2B cells were cultured in LHC-9 media, containing 10% heat inactivated FBS, 1% penicillin streptomycin, 1% L-glutamine, and 0.1% fungizone (Life Technologies, Carlsbad, CA) and cultured at 37°C in 5% CO_2. These cells were grown on cell-cultured flasks and dishes pre-coated with LHC Basal Media (Gibco-Invitrogen Corporation) containing 0.03 mg/mL PureCol (Cohesion), 0.01 mg/mL fibronectin bovine (MP Biomedicals Inc.), and 0.01 mg/mL BSA Fraction V. These cells were split at a 1:8 ratio in T150 flasks. Experiments were performed on these cells between passages 5 and 7, with cells being plated at 14000 cells/cm^2 on pre-coated tissue culture treated dishes for experimentation the following day.

Mouse C10 type two pneumocytes were received as a generous gift from the lab of Dr. Chris Migliaccio (University of Montana). C10 cells were cultured in RPMI media, containing 10% heat inactivated FBS, 1% penicillin streptomycin, 1% L-glutamine, and 0.1% fungizone (Life Technologies, Carlsbad, CA) and cultured at 37°C in 5% CO_2. These cells were split at a 1:8 ratio in T150 flasks. Experiments were performed on these cells earlier than passage 5, with cells being plated at 14000 cells/cm^2 on pre-coated tissue culture treated dishes for experimentation the following day.

2.7 Cell Lysates

On the experimentation day, cells were stimulated with media containing 10% FBS and recombinant OSM, recombinant BMP2, recombinant TGF-β, or combinations of these cytokines. Cells were stimulated for one hour, one day, three day, or over a six hour time course. Following stimulation for the allotted time, whole cell lysates were generated

using RIPA lysis buffer containing protease inhibitors, as previously described. Briefly, cells were washed twice with 1xPBS before being incubated on ice with RIPA lysis buffer. After two minutes, cells were scraped off the bottom of the well using cell scrapers, and were collected and incubated on ice for one hour. Samples were sheared with a 21 gauge needle attached to a 1 mL syringe, and centrifuged for 10 minutes at 4°C and 12,000 rpm. Lastly, cell lysates were stored at -80°C until further use.

2.8 Running of lung homogenates and cell lysates on immunoblots

The protein concentration of cell lysates from *in vitro* experiments and lung homogenates from *in vivo* experiments was quantified using a Bradford Assay, with samples being run in triplicate. Using a BSA protein standard as a comparison, samples were diluted 1/32 in distilled water and 20% Bio-Rad Protein Assay Dye Reagent Concentrate (Bio Rad, Hercules, CA). The optical density at 595 nm of the standard and each sample was measured using a plate reader. Microsoft Excel was then used to quantify the protein concentration in each sample based on the optical density readings.

5-15 μg of protein was subsequently run on a 6 or 8% SDS-PAGE gel alongside a molecular weight ladder at 120 V for 60 minutes. The SDS-PAGE gel was subsequently transferred onto a nitrocellulose membrane (Pall Corp., Port Washington, NY) by electrical transfer using a BioRad Mini-Protean II equipment (Bio Rad) at 400 mA for 60 minutes. Membranes with transferred proteins were blocked using 5% skim milk powder (Nestle Carnation, Vevey, Switzerland) in 1x tris buffered saline (TBS) containing 0.15% Tween 20 (Sigma Aldrich Corp.) for 1 hour at room temperature. The membranes were then probed while rocking overnight at 4°C using antibodies diluted at 1:1000 in either

5% BSA or 5% skim milk powder in 1x (TBS) containing 0.15% Tween 20. Antibodies targeting pSTAT-3, STAT-3, pSMAD1/5, SMAD1, pSMAD2, BMPR2 were purchased from Cell Signaling Technology (Danvers, MA). The antibody targeting pSMAD1/5/8 was purchased from Millipore. The antibody targeting BMPR1A and total actin were purchased from Santa Cruz Biotechnology Inc. Blots were washed the following day three times using 1xTBS containing 0.15% Tween 20 for 8 minutes at room temperature. Blots were then incubated with a secondary antibody diluted at 1:2500 that was conjugated to horseradish peroxidase (either mouse anti-goat IgG-HRP or goat anti-rabbit IgG-HRP, Santa Cruz Biotechnology Inc.) Membranes were then washed two times for 8 minutes each at room temperature with 1x TBS containing 0.15% Tween 20, and two times for 8 minutes each at room temperature with 1x TBS. The membranes were then incubated with Pierce ECL 2 Western Blotting Kit (ThermoFisher Scientific, Waltham, MA) reagents according to manufacturer's instructions for 5 minutes, taken to the dark room, and exposed to CL-X Posure Film (ThermoFisher Scientific, Waltham, MA).

Nitrocellulose membranes already probed for a particular protein were also stripped in order to probe for other proteins. Membranes were washed thrice in 1xTBS containing 0.15% Tween 20 for 8 minutes, washed four times in 55°C-preheated glacial acetic acid (diluted 1:175) for 15 minutes, before finally washed thrice in 1xTBS containing 0.15% Tween 20 for 8 minutes.

2.9 RNA Extraction and purification from cell culture

On the experimentation day, cells were stimulated with media containing 10% FBS and recombinant OSM, recombinant BMP2, recombinant TGF-β, or combinations of

these cytokines. Cells were stimulated for six hour or one day. Following stimulation for the allotted time, RNA was extracted from cells using Pure Link RNA mini kit (Life Technologies, Carlsbad, CA) following the manufacturers protocol. RNA was stored at -80°C until further use.

2.10 Quantification using Taqman

The RNA concentration of the samples was determined using the NanoVue Spectrophotometer (GE Healthcare, Little Chalfont, UK). Genomic DNA was removed from the sample using Ambion DNA-free kit (Life Technologies, Carlsbad, CA) according to the manufacturer's instructions. RNA was reverse transcribed to complementary DNA using SuperScript II RT (Life Technologies) following the manufacturer's protocol and stored at -20°C until future use.

Expression of mouse IL-6, collagen 1A1, collagen 1A2, fibronectin, Id1, and α-SMA was determined by Taqman using predeveloped assay reagents purchased from Ambion (Life Technologies). In a MicroAmp Optical 96 well reaction plate (Life Technologies), 10 ng of cDNA was added to TaqMan Universal Master Mix (Life Technologies), along with the predeveloped assay reagent targeting a specific gene. The reaction plate was then placed into a 7900HT Fast RealTime PCR System (Life Technologies), which was operated by Sequence Detection System Software version 2.4 (Life Technologies). mRNA expression levels for each sample were calculated using the ΔΔCT method using 18S expression levels as a housekeeping gene. Gene expression for a particular sample was expressed relative to control (media alone) values.

2.11 Analysis of BALF using Enzyme-linked immunosorbent assay (ELISA)

BALF from mice were analyzed for mouse IL-6, keratinocyte chemoattractant (KC), vascular endothelial growth factor (VEGF), and eotaxin-2 using DuoSet kits purchased from R&D. These ELISAs were performed according to the manufacturer's instructions. An in-house mouse OSM ELISA developed by Sean Lauber and Dr. Carl Richards was used to measure OSM levels in the BALF. GlaxoSmithKline Inc provided the reagents for this ELISA. With all ELISAs, color change was measured at an optical density of 450 nm using the Bio-Tek EL 800 (BioTek, Winooski, VT).

2.12 Statistical Analysis

Statistical tests were performed using GraphPad Prism 5 software (GraphPad Software Inc., San Diego, USA). Student's t-test and Mann Whitney U tests were primarily used to determine statistical significance. A p-value less than 0.05 was considered statistically significant. A Bonferroni's post-test was applied in all cases. All error bars indicate the mean standard error.

CHAPTER 3: Results of Aim 1

The phenotype of OSM-induced lung ECM remodeling in both C57Bl/6 and BALB/c mice will be described in this chapter. This collection of work includes examining changes in histopathology, BALF constituents, and gene expression of lung homogenates. Changes in gene expression of both C57Bl/6 and BALB/c MLF cultures treated with OSM will also be examined, and compared to MLF cultures treated with BMP2 or TGF-β.

3.1 Pathology of OSM-overexpression Model in C57Bl/6 and BALB/c Mice

To assess the pathology of OSM-induced ECM remodeling in C57Bl/6 and BALB/c mice, mice from both strains were administered $5x10^7$ pfu of AdOSM or AdDl70 through the endotracheal route. After seven (both mice strains) or 28 days (BALB/c mice only), mice were culled, and lungs were extracted. The left lung was assessed using histology whereas the right lung was used for hydroxyproline assay and mRNA analysis via qRT-PCR. BALF was also collected for cytokine analysis by ELISA.

3.1.1 H&E staining of lung sections from AdOSM-treated C57Bl/6 and BALB/c mice

H&E sections of AdOSM-treated mouse lung from both strains showed pathology in the airways and the parenchyma compared to AdDl70-treated mice. Although the lung pathology was heterogeneous, with some areas of the lungs being more affected than others, AdOSM-treated mice consistently showed more dense accumulation in the peribronchial and perivascular areas compared to AdDl70-treated mice (**Fig. 1A**). Furthermore, the airway epithelial cells were hyperplastic, while the alveolar septa were thicker in AdOSM-treated than in AdDl70-treated mice (**Fig. 1B**). These observations

showed some similarities to the human condition of pulmonary fibrosis, where the lungs of IPF patients showed pathology in some regions of the lungs but not others.

AdOSM-treated BALB/c mice displayed abnormal pathology relative to AdDl70-treated BALB/c mice 28 days after endotracheal administration of AdOSM. While pathology appeared to resolve in the lung parenchyma, with no visible differences in alveolar structure between AdOSM and AdDl70-treated BALB/c mice, the airway epithelial cells of AdOSM-treated BALB/c mice appeared to remain hyperplastic (**Fig. 6**). Furthermore, there were increased total cell numbers in the BALF of AdOSM-treated mice after 28 days intubation (**Fig. 7A**). Cell differentials identified that the increased in total cells is attributed to increased macrophages as well as lymphocytes (**Fig. 7B**).

3.1.2 Collagen assessment in lungs of AdOSM-treated C57Bl/6 and BALB/c mice

To assess collagen content, sections of AdOSM-treated mice from both strains were stained with Masson's Trichrome as well as PSR. A microscopic examination of Masson's Trichrome slides showed disruption of the alveolar and airway epithelium (**Fig. 2A**) that was also seen in the H&E-stained slides (**Fig. 1A**). From a qualitative perspective, Masson's Trichrome-stained slides of AdOSM-treated mouse lung showed more intermittent areas in the lung parenchyma that stain blue, which was indicative of collagen accumulation. This observation was verified using PSR-stained slides, where cross-linked collagen can be seen when observing slides under polarized light (**Fig. 2B**).

Quantitative observations regarding changes in collagen accumulation in the lung were accomplished using two separate analyses. Using one approach, four assessors blinded to the animal identification examined and rated microscopic pictures taken of

PSR-stained slides under polarized light to assess parenchymal collagen. This technique is a modification of the Ashcroft scoring methodology that examines changes in alveolar phenotype. The results showed that there was increased amount of parenchymal collagen in AdOSM-treated mice of both strains compared to AdDl70-treated mice (**Fig. 3A**). Interestingly, increases in parenchymal PSR staining were similar in both AdOSM-treated BALB/c mice and AdOSM-treated C57Bl/6 mice compared to control mice (**Fig. 3A**).

Total lung collagen was also quantified by hydroxyproline assay. The hydroxyproline assay results were consistent with the modified Ashcroft scoring methodology, with elevated levels of collagen in AdOSM-treated mice (**Fig. 3B**). Furthermore, there was a comparable fold increase in both strains of AdOSM-treated mice (**Fig. 3B**). However, unlike the modified Ashcroft score approach, the hydroxyproline assay results were not statistically significant.

3.1.3 Cytokine analyses of BALF from AdOSM-treated C57Bl/6 and BALB/c mice

BALF was assessed for OSM using an in house mouse OSM ELISA to confirm elevation of OSM protein levels in AdOSM-treated mice. AdOSM-treated mice from both strains had significantly elevated levels of OSM in the BALF compared to AdDl70-treated mice, in which OSM was not detectable (**Fig. 4A**). However, AdOSM-treated C57Bl/6 mice had significantly elevated levels of OSM in BALF compared to AdOSM-treated BALB/c mice (average 15000 pg/mL vs. 3000 pg/mL, respectively) (**Fig. 4A**). Variation in virus preparation and intubation method were ruled out as all mice were intubated on the same day using the same adenovirus vector batch. Furthermore, mice were all culled on the same day, with no changes in methodology for collecting BALF.

Lastly, samples were run on the same plate to eliminate variations in ELISA results. OSM was not detected in the BALF of AdOSM-treated BALB/c mice at Day 28 (**Fig. 7C**)

BALF was next analyzed for IL-6 and KC, two pro-inflammatory cytokines that have been shown to be elevated in IPF patients. AdOSM-treated C57Bl/6 and BALB/c mice had detectable IL-6 in the BALF at day seven, (average 1500 pg/mL and. 250 pg/mL, respectively) (**Fig. 4B**). However, IL-6 was undetectable in BALF of AdOSM-treated BALB/c mice after Day 28 (**Fig. 7D**). Overexpression of OSM also induced KC levels in both AdOSM-treated C57Bl/6 and BALB/c mice at day seven (**Fig. 4C**). BALF levels of KC were slightly higher in AdOSM-treated C57Bl/6 mice compared to AdOSM-treated BALB/c mice (average 225 pg/mL vs 180 pg/mL) (**Fig. 4C**). However, KC was detected in AdDl70-treated BALB/c but not AdDl70-treated C57Bl/6 mice (**Fig. 4C**).

BALF was analyzed for VEGF to determine if angiogenesis was occurring concomitantly to ECM remodeling. VEGF was not detected in C57Bl/6 mice, and was not regulated in BALB/c mice (**Fig. 4D**).

MCP-5 was measured in the BALF of both C57Bl/6 and BALB/c mice. Previous work from the Richards laboratory has shown that OSM overexpression causes a recruitment of CD45+Col1+ fibrocytes into the lungs, but that SDF-1 was not elevated in the lungs concomitantly with the recruitment process (unpublished data). ELISA analysis of BALF showed that there are elevated levels of MCP-5 in the BALF of AdOSM-treated C57Bl/6 mice (450 pg/mL), but not in BALB/c mice (**Fig. 4E**).

3.1.4 Gene expression of AdOSM-treated C57Bl/6 and BALB/c mouse lung homogenates

qRT-PCR was performed to analyze changes in gene expression of AdOSM-treated mouse lungs after seven days. α-SMA was analyzed to confirm previous *in vivo* data showing that OSM overexpression causes an accumulation of α-SMA+ cells in the lung parenchyma. Unexpectedly, steady state mRNA levels of α-SMA were downregulated in both AdOSM-treated C57Bl/6 and BALB/c mice at day seven (**Fig. 5A**). As a comparator, steady state mRNA levels of TIMP-1 was analyzed, as previous unpublished data showed that AdOSM-treated C57Bl/6 and BALB/c mice have elevated levels of TIMP-1 steady state mRNA five days post-intubation. The qRT-PCR analyses indicated that AdOSM-treated mouse lungs had elevated levels of TIMP-1 mRNA, though there was more of an increase in AdOSM-treated C57Bl/6 mice than in AdOSM-treated BALB/c mice (approximately 40 fold vs. 15 fold) (**Fig. 5B**).

Lastly, qRT-PCR was performed to analyze steady state mRNA levels of gremlin. Gremlin is a BMP antagonist that has been shown to be upregulated in IPF patients, and is thought to have a profibrotic role by blocking BMP-stimulated wound healing. In the OSM overexpression model, there was an increase of steady state gremlin mRNA levels in both AdOSM-treated C57Bl/6 and BALB/c mice compared to AdDl70-treated mice, though neither observation was statistically significant (**Fig. 5C**).

3.2 Responses of C57Bl/6 and BALB/c MLF cultures to OSM

Lung fibroblasts are thought to be principal regulators of the ECM, and thus responses of C57Bl/6 and BALB/c MLF cultures to OSM were examined. This work involved examining changes to gene expression of C57Bl/6 and BALB/c MLF cultures

treated with 5 ng/mL OSM after six and 24 hours stimulation, and comparing this to MLF cultures stimulated with 50 ng/mL BMP2 or 5 ng/mL TGF-β after six and 24 hours.

3.2.1 IL-6 steady state mRNA levels in C57Bl/6 and BALB/c MLF cultures

To ensure that both C57Bl/6 and BALB/c MLF cultures responded to OSM, steady state mRNA levels of IL-6 were initially assessed. As expected, OSM induced IL-6 steady state mRNA levels in both MLF cultures at both six and 24 hours (**Fig. 7A**, **Fig. 8A**). Interestingly, TGF-β was able to induce IL-6 steady state mRNA levels in BALB/c MLF cultures but not C57Bl/6. Though induction occurred at both time points, TGF-β-induced IL-6 steady state mRNA levels were more pronounced at 24 hours. BMP2 did not modulate IL-6 steady state mRNA levels in either C57Bl/6 or BALB/c MLF cultures.

3.2.2 Id1 steady state mRNA levels in C57Bl/6 and BALB/c MLF cultures

To ensure that C57Bl/6 and BALB/c MLF cultures responded to BMP2, levels of Id1 mRNA were assessed. While TGF-β had an inhibitory effect, BMP2 induced Id1 mRNA levels in both fibroblast cell lines (**Fig. 7F**, **8F**). BMP-induced Id1 mRNA production was more pronounced in C57Bl/6 MLF cultures, and after six hours of stimulation. OSM appeared to induce steady state mRNA levels of Id1 in BALB/c MLF cultures, though not in C57Bl/6 MLF cultures.

3.2.3 Steady state mRNA levels of ECM genes in C57Bl/6 and BALB/c MLF cultures

As a comparator, TGF-β-induced mRNA levels of fibronectin, collagen 1a1, collagen 1a2, and α-SMA were examined in both C57Bl/6 and BALB/c MLF cultures. As shown in **Fig. 7B-D** and **Fig. 7G**, TGF-β stimulated steady state mRNA expression of collagen 1a2 after six hours stimulation, and collagen 1a1 and α-SMA at 24 hours in

C57Bl/6 MLF cultures. However, fibronectin steady state mRNA levels were not modulated by TGF-β in C57Bl/6 MLF cultures. In contrast to C57Bl/6 MLF cultures, TGF-β did not stimulate steady state mRNA expression of collagen 1a1, collagen 1a2, fibronectin, or α-SMA in BALB/c MLF cultures (**Fig. 8B-D** and **Fig. 8G)**.

In comparison, BMP2 decreased steady state mRNA levels of collagen 1a1, collagen 1a2, fibronectin, and α-SMA after six hours of stimulation in C57Bl/6 MLF cultures, but not after 24 hours stimulation (**Fig. 7B-D** and **Fig. 7G**). In BALB/c MLF cultures, BMP decreased steady state mRNA expression of collagen 1a1, collagen 1a2, fibronectin and α-SMA after 24 hours stimulation (**Fig. 8B-D** and **Fig. 8G)**. However, after six hours stimulation, with the exception of fibronectin, there appears to be no changes in the steady state mRNA expression of collagen 1a1, collagen 1a2, and α-SMA.

OSM appeared to not modulate steady state mRNA expression of collagen 1a1, collagen 1a2, fibronectin and α-SMA after six hours stimulation in C57Bl/6 MLF cultures, but decreased steady state mRNA expression of fibronectin and α-SMA after 24 hours stimulation (**Fig. 7B-D** and **Fig. 7G**). In BALB/c MLF cultures, OSM decreased steady state mRNA expression of collagen 1a1, collagen 1a2, fibronectin and α-SMA after 24 hours stimulation (**Fig. 8B-D** and **Fig. 8G)**.

3.2.4 Steady state mRNA levels of gremlin in C57Bl/6 and BALB/c MLF cultures

MLF cultures were next examined for steady state mRNA levels of gremlin. OSM was able to induce gremlin mRNA expression in both C57Bl/6 and BALB/c MLF cultures after 24 hours of stimulation, while BMP2 was also able to induce gremlin mRNA expression after six hours stimulation in BALB/c MLF cultures (**Fig. 7E** and **8E**).

Though TGF-β has been reported to induce gremlin mRNA expression in smooth muscle and epithelial cells, the data shown using C57Bl/6 and BALB/c MLF cultures suggested that TGF-β does not modulate gremlin mRNA expression in these cell culture systems.

Figure 1: Age-matched C57Bl/6 and BALB/c mice were endotracheally administered $5x10^7$ pfu of AdOSM or control vector AdDl70 (n=5 per group). Mice were culled after seven days. The left lung of each mouse was fixed in 10% formalin and paraffin-embedded. Sections of the lung were stained with H&E. Mouse lung sections from two representative mice were examined using the 10x objective lenses (A), while mouse lung sections from one representative mouse was examined using the 40x objective lenses (B)

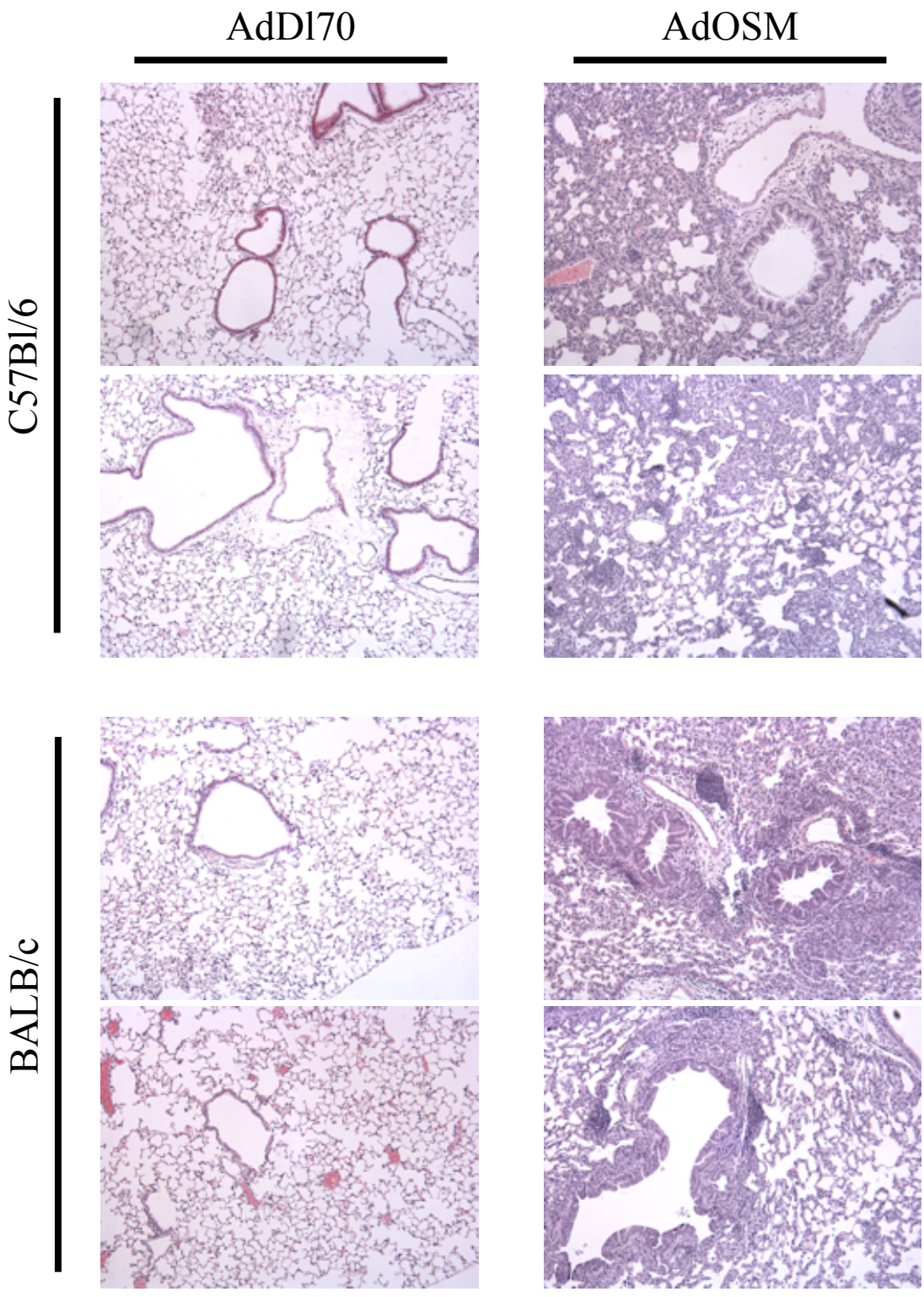

Figure 1A

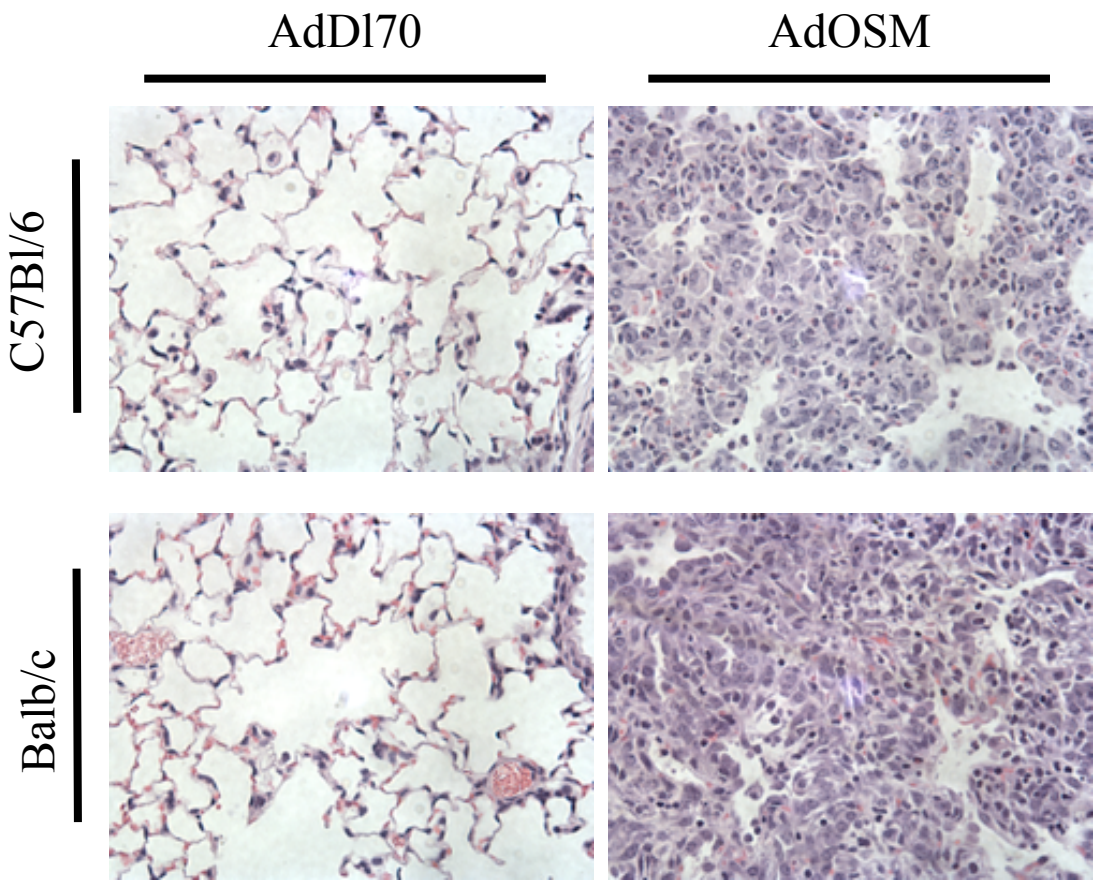

Figure 1B

Figure 2: Age-matched C57Bl/6 and BALB/c mice were endotracheally administered $5x10^7$ pfu of AdOSM or control vector AdDl70 (n=5 per group). Mice were culled after seven days. The left lung of each mouse was fixed in 10% formalin and paraffin-embedded. Sections of the lung were either stained with Masson's Trichrome and examined using the 20x objective lenses (A), or PSR and examined using the 5x objective lenses (B).

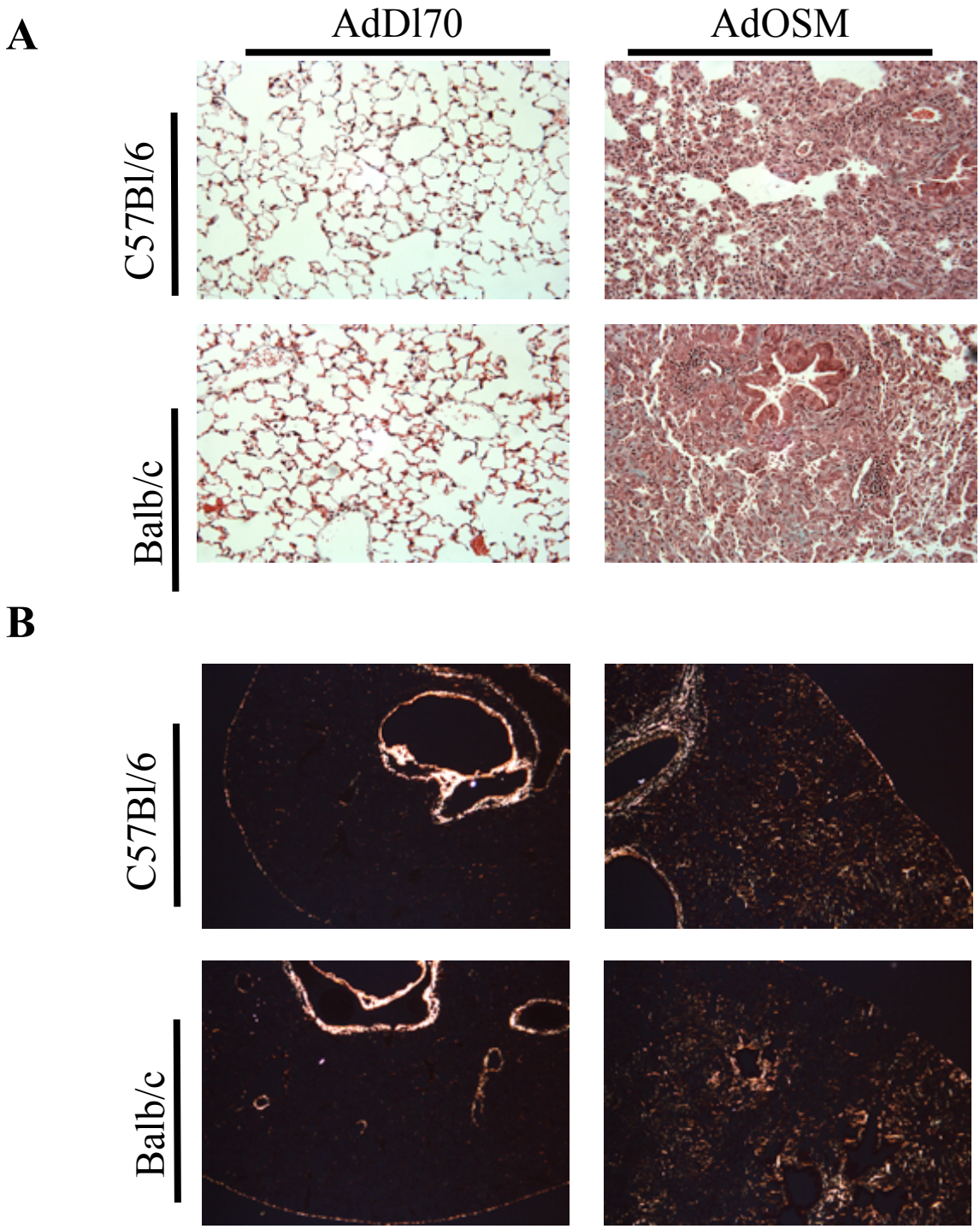

Figure 2

Figure 3: Age-matched C57Bl/6 and BALB/c mice were endotracheally administered $5x10^7$ pfu of AdOSM or control vector AdDl70 (n=5 per group). Mice were culled after seven days.

A – Quantification of parenchymal collagen in C57Bl/6 and BALB/c mouse lung using the modified Ashcroft score. 8-15 microphotographs were taken of PSR-stained lung sections viewed under polarized light using the 5x objective lenses to cover the entire lung area. Subsequently, four assessors blinded to the animal identification rated each microphotograph from a score of 0-8 for amount of parenchymal collagen staining, with 8 being the highest score. Results are displayed relative to AdDl70-treated mice of each mouse strain. Statistical significance is shown where * = $p<0.05$, ** = $p<0.001$, *** = $p<0.0001$

B – Right lung homogenates were put into a freeze dry lyophilizer to obtain dry weight tissue. Subsequently, a hydroxyproline assay was performed on dry tissue to assess total lung collagen. Results are shown relative to AdDl70-treated mice of each mouse strain. Statistical significance is shown where * = $p<0.05$, ** = $p<0.001$, *** = $p<0.0001$

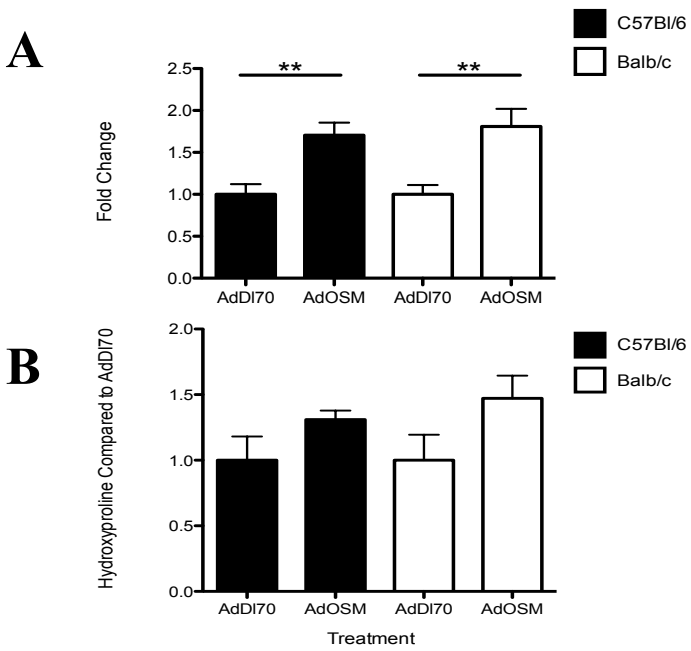
A
B
C57Bl/6
Balb/c
Fold Change
Hydroxyproline Compared to AdDl70
**
**
2.5
2.0
1.5
1.0
0.5
0.0
AdDl70
AdOSM
AdDl70
AdOSM
Treatment

Figure 3

Figure 4: Age-matched C57Bl/6 and BALB/c mice were endotracheally administered $5x10^7$ pfu of AdOSM or control vector AdDl70 (n=5 per group). Mice were culled after seven days. BALF was collected and analyzed for OSM (A), IL-6 (B), KC (C), VEGF (D), and MCP-5 (E). Inflammatory cells were collected from the BALF and counted for total cell numbers (F). Statistical significance is shown where * = $p<0.05$, ** = $p<0.001$, *** = $p<0.0001$

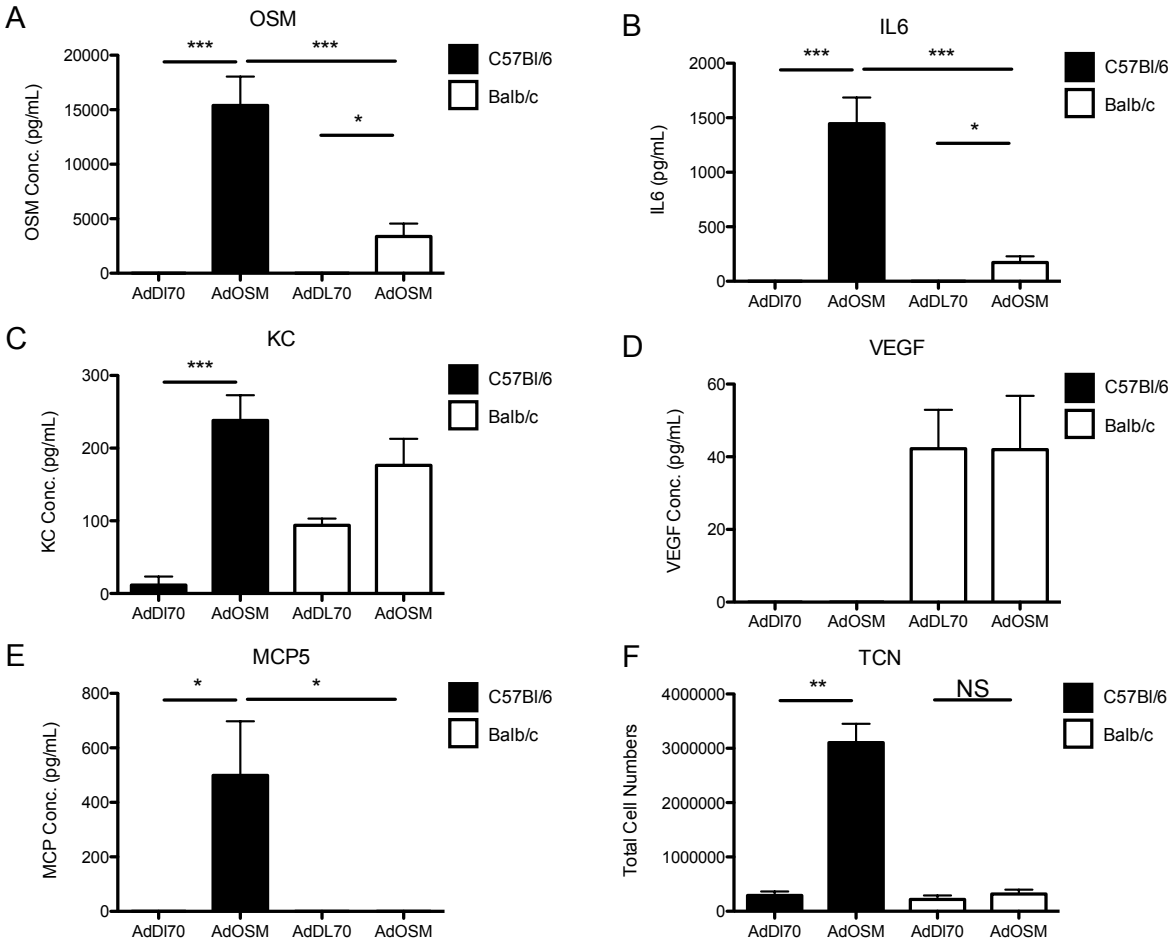
A
OSM
OSM Conc. (pg/mL)
20000
15000
10000
5000
0
***
***
*
C57Bl/6
Balb/c
AdDl70
AdOSM
AdDL70
AdOSM
B
IL6
IL6 (pg/mL)
2000
1500
1000
500
0
***
***
*
C57Bl/6
Balb/c
AdDl70
AdOSM
AdDL70
AdOSM
C
KC
KC Conc. (pg/mL)
300
200
100
0
***
C57Bl/6
Balb/c
AdDl70
AdOSM
AdDL70
AdOSM
D
VEGF
VEGF Conc. (pg/mL)
60
40
20
0
C57Bl/6
Balb/c
AdDl70
AdOSM
AdDL70
AdOSM
E
MCP5
MCP Conc. (pg/mL)
800
600
400
200
0
*
*
C57Bl/6
Balb/c
AdDl70
AdOSM
AdDL70
AdOSM
F
TCN
Total Cell Numbers
4000000
3000000
2000000
1000000
0
**
NS
C57Bl/6
Balb/c
AdDl70
AdOSM
AdDl70
AdOSM

Figure 4

Figure 5: Age-matched C57Bl/6 and BALB/c mice were endotracheally administered $5x10^7$ pfu of AdOSM or control vector AdDl70 (n=5 per group). Mice were culled after seven days. RNA was isolated from lung homogenates and analyzed via qRT-PCR for steady state mRNA levels of α-SMA (A), TIMP-1 (B), and gremlin-1 (C). Statistical significance is shown where * = $p<0.05$, ** = $p<0.001$, *** = $p<0.0001$

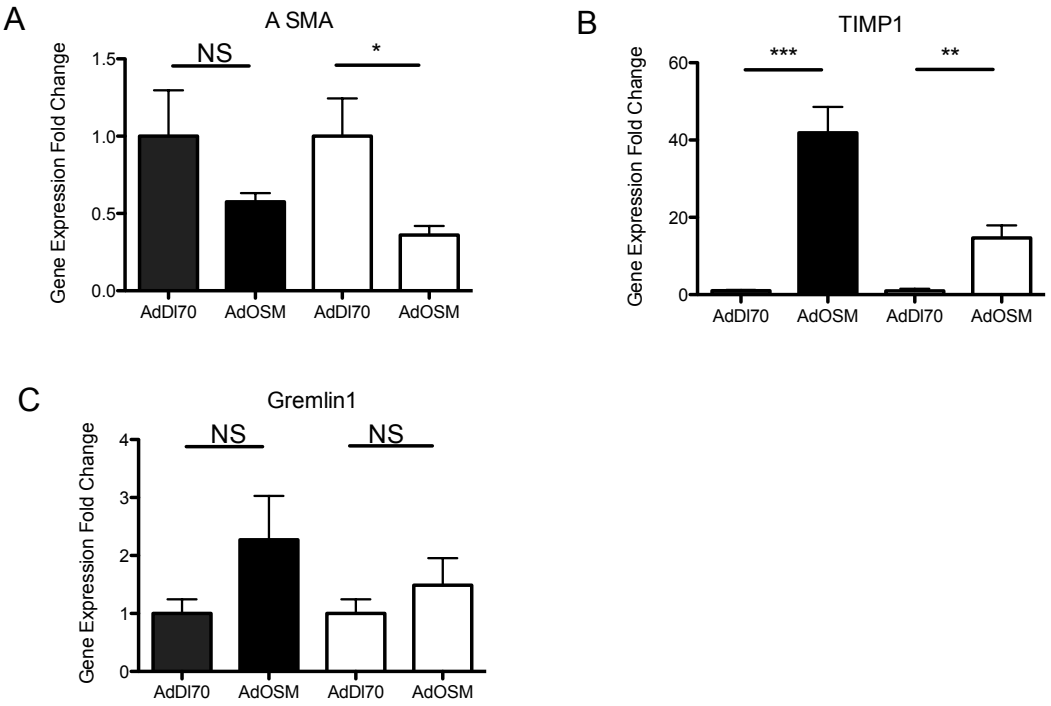
A
A SMA
NS
*
Gene Expression Fold Change
1.5
1.0
0.5
0.0
AdDl70
AdOSM
AdDl70
AdOSM
B
TIMP1
***
**
Gene Expression Fold Change
60
40
20
0
AdDl70
AdOSM
AdDl70
AdOSM
C
Gremlin1
NS
NS
Gene Expression Fold Change
4
3
2
1
0
AdDl70
AdOSM
AdDl70
AdOSM

Figure 5

Figure 6: Age-matched BALB/c mice were endotracheally administered $5x10^7$ pfu of AdOSM or control vector AdDl70 (n=5 per group). Mice were culled after 28 days. The left lung of each mouse was fixed in 10% formalin and paraffin-embedded. Sections of the lung were stained with H&E. Mouse lung sections from one representative mouse per group were examined using the 10x objective lenses as an overview. Additionally, a 40x objective lenses was used to examine both the airway and the lung parenchyma.

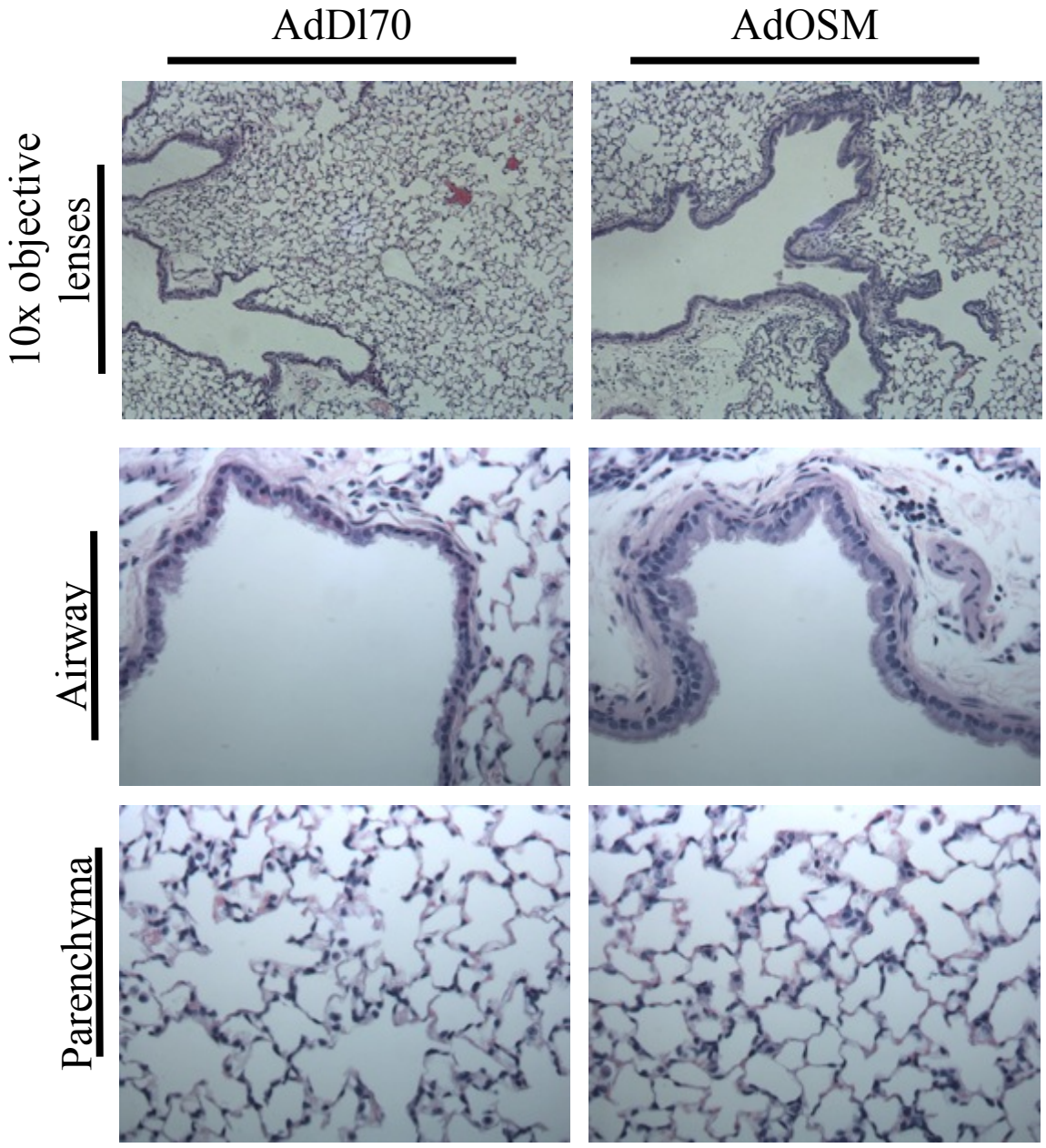

Figure 6

Figure 7: Age-matched BALB/c mice were endotracheally administered $5x10^7$ pfu of AdOSM or control vector AdDl70 (n=5 per group). Mice were culled after 28 days. BALF cells were quantified by cell counts (A) and identified by cytocentrifuge smears (B). BALF was collected and analyzed for OSM (C) and IL-6 (D). Statistical significance is shown where * = $p<0.05$, ** = $p<0.001$, *** = $p<0.0001$

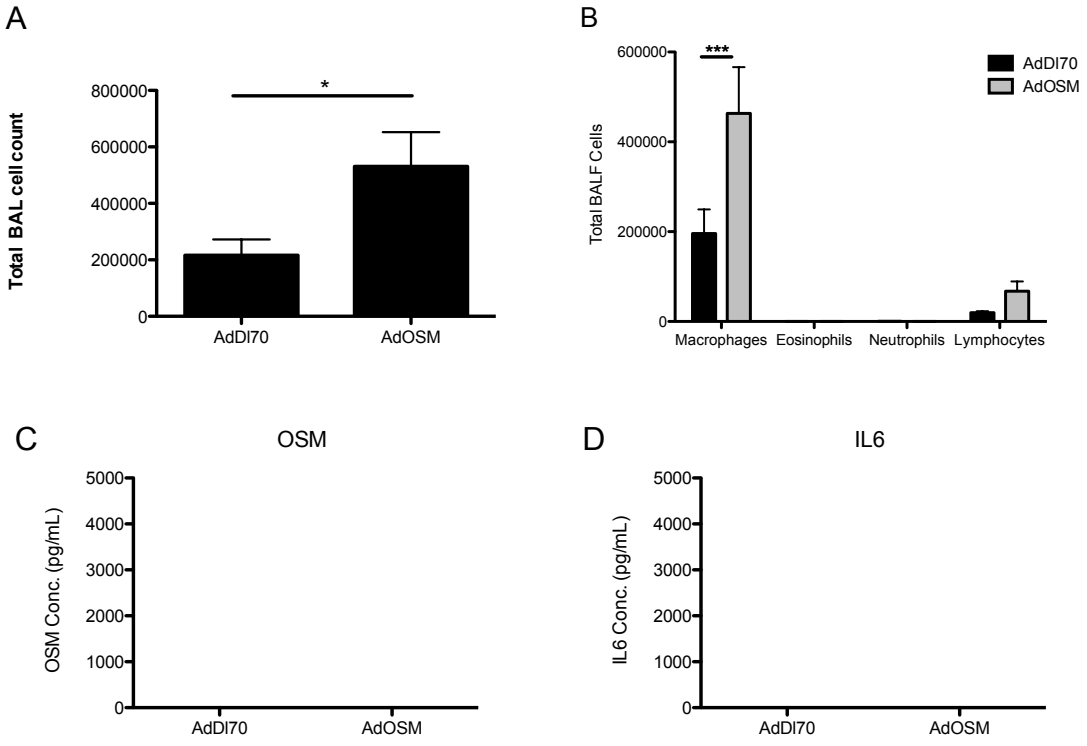
A
Total BAL cell count
800000
600000
400000
200000
0
*
AdDl70
AdOSM
B
Total BALF Cells
600000
400000
200000
0
***
AdDl70
AdOSM
Macrophages
Eosinophils
Neutrophils
Lymphocytes
C
OSM
OSM Conc. (pg/mL)
5000
4000
3000
2000
1000
0
AdDl70
AdOSM
D
IL6
IL6 Conc. (pg/mL)
5000
4000
3000
2000
1000
0
AdDl70
AdOSM

Figure 7

Figure 8: C57Bl/6 MLF cultures were treated with recombinant OSM (5 ng/mL), BMP-2 (50 ng/mL), or TGF-β (5 ng/mL) for six and 24 hours. mRNA was extracted, reversed transcribed into cDNA, and assessed for steady state mRNA levels of IL-6 (A), fibronectin (B), collagen 1a1 (C), collagen 1a2 (D), gremlin-1 (E), Id1 (F), and α-SMA (G) via qRT-PCR

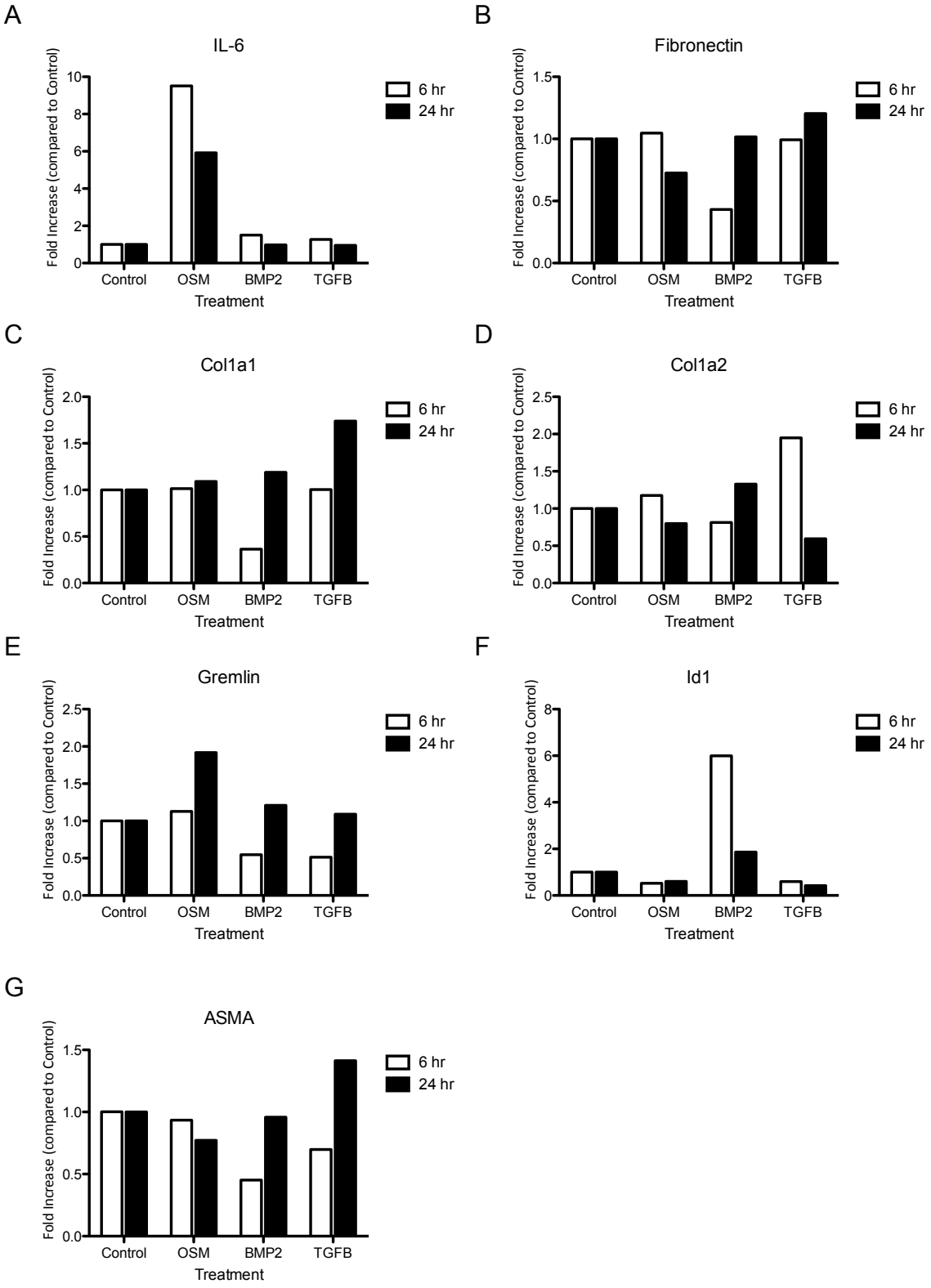
A
IL-6
Fold Increase (compared to Control)
10
8
6
4
2
0
Control
OSM
BMP2
TGFB
Treatment
6 hr
24 hr
B
Fibronectin
Fold Increase (compared to Control)
1.5
1.0
0.5
0.0
Control
OSM
BMP2
TGFB
Treatment
6 hr
24 hr
C
Col1a1
Fold Increase (compared to Control)
2.0
1.5
1.0
0.5
0.0
Control
OSM
BMP2
TGFB
Treatment
6 hr
24 hr
D
Col1a2
Fold Increase (compared to Control)
2.5
2.0
1.5
1.0
0.5
0.0
Control
OSM
BMP2
TGFB
Treatment
6 hr
24 hr
E
Gremlin
Fold Increase (compared to Control)
2.5
2.0
1.5
1.0
0.5
0.0
Control
OSM
BMP2
TGFB
Treatment
6 hr
24 hr
F
Id1
Fold Increase (compared to Control)
8
6
4
2
0
Control
OSM
BMP2
TGFB
Treatment
6 hr
24 hr
G
ASMA
Fold Increase (compared to Control)
1.5
1.0
0.5
0.0
Control
OSM
BMP2
TGFB
Treatment
6 hr
24 hr

Figure 8

Figure 9: BALB/c MLF cultures were treated with recombinant OSM (5 ng/mL), BMP-2 (50 ng/mL), or TGF-β (5 ng/mL) for six and 24 hours. mRNA was extracted, reversed transcribed into cDNA, and assessed for steady state mRNA levels of IL-6 (A), fibronectin (B), collagen 1a1 (C), collagen 1a2 (D), gremlin-1 (E), Id1 (F), and α-SMA (G) via qRT-PCR

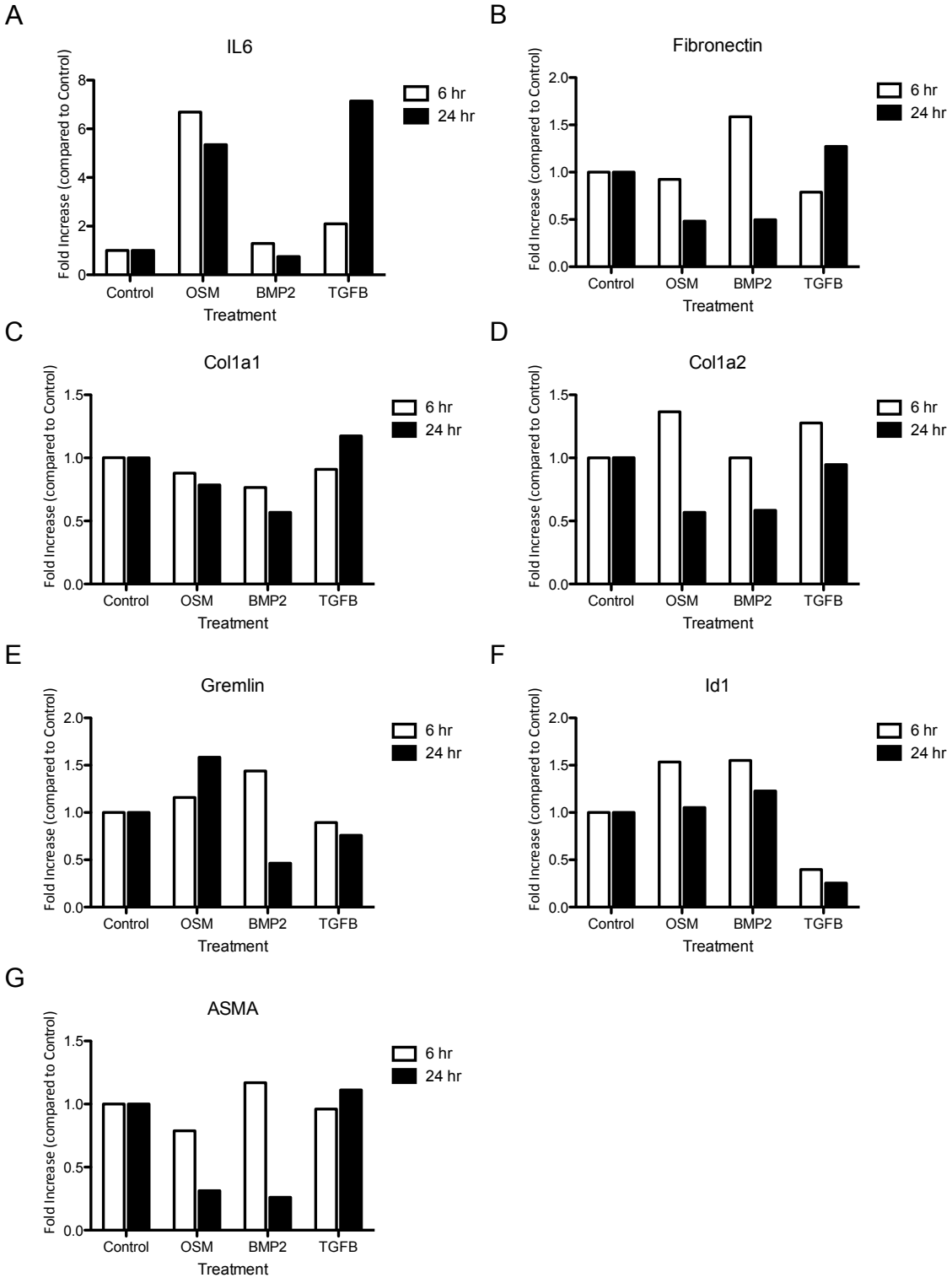
A
IL6
Fold Increase (compared to Control)
8
6
4
2
0
Control
OSM
BMP2
TGFB
Treatment
6 hr
24 hr
B
Fibronectin
Fold Increase (compared to Control)
2.0
1.5
1.0
0.5
0.0
Control
OSM
BMP2
TGFB
Treatment
6 hr
24 hr
C
Col1a1
Fold Increase (compared to Control)
1.5
1.0
0.5
0.0
Control
OSM
BMP2
TGFB
Treatment
6 hr
24 hr
D
Col1a2
Fold Increase (compared to Control)
1.5
1.0
0.5
0.0
Control
OSM
BMP2
TGFB
Treatment
6 hr
24 hr
E
Gremlin
Fold Increase (compared to Control)
2.0
1.5
1.0
0.5
0.0
Control
OSM
BMP2
TGFB
Treatment
6 hr
24 hr
F
Id1
Fold Increase (compared to Control)
2.0
1.5
1.0
0.5
0.0
Control
OSM
BMP2
TGFB
Treatment
6 hr
24 hr
G
ASMA
Fold Increase (compared to Control)
1.5
1.0
0.5
0.0
Control
OSM
BMP2
TGFB
Treatment
6 hr
24 hr

Figure 9

CHAPTER 4: Results of Aim 2

In this chapter is described the phenotype of OSM-induced lung ECM remodeling in both IL-6 -/- mice and SMAD3 -/- mice. This collection of work includes examining changes in pathology and BALF constituents.

4.1 Pathology of OSM-overexpression Model in IL-6 Knockout Mice

To examine the pathology of OSM-induced ECM remodeling in IL-6 -/- mice, IL-6 -/- and IL-6 +/+ mice were left untreated (naïve), or treated with $5x10^7$ pfu of AdOSM or the control vector AdDl70. After seven and 14 days, mice were culled, and lungs were extracted. The left lung was assessed using histology at 14 days (histology data at day seven not available). BALF collected from day seven was also analyzed by ELISA.

4.1.1 H&E staining of lung sections from AdOSM-treated IL-6 -/- mice

H&E-stained lung sections of AdOSM-treated mice from both IL-6-/- and IL-6 +/+ background consistently showed pathology in the airways and parenchyma compared to AdDl70-treated mice at 14 days (**Fig. 10**). These lungs were more affected than lungs from AdOSM-treated mice examined after seven days (**Fig. 1A**). This confirmed prior data collected in the laboratory that AdOSM-induced effects are more pronounced at day 14 than day seven. Regarding the histopathology, there was an accumulation of dense connective tissue in the parenchyma of both AdOSM-treated IL-6+/+ and IL-6-/- mice. Compared to AdDl70-treated mice, AdOSM-treated mice showed thicker alveolar walls. The airways of AdOSM-treated mice were also affected, with hyperplasia of the epithelial cells lining the large airways.

4.1.2 Collagen assessment in lungs of AdOSM-treated IL-6 -/- mice

Collagen content was assessed using histology via Masson's Trichrome and PSR. Masson's Trichrome staining accentuated the pathology previously described (**Fig. 10)** where lung sections were stained with H&E. Moreover, Masson's Trichrome staining showed in AdOSM-treated mice, but not AdDl70-treated mice, a thin network of blue staining throughout the lung parenchyma, indicative of parenchymal collagen (**Fig. 11A**). Similar conclusions were drawn when examining PSR-stained slides under polarized light (**Fig. 11B**). While OSM overexpression induced more cross-linked collagen fibers in the lung parenchyma, it appeared that the absence of IL-6 in IL-6 -/- mice did not markedly alter AdOSM-induced PSR staining 14 days after intubation.

Quantification of parenchymal collagen using the modified Ashcroft score confirmed the qualitative observation that IL-6 was not necessary for AdOSM-induced collagen deposition (**Fig. 12**). Assessors blinded to the animal identification assessed extent of PSR staining evident in the parenchyma, but not the airways or the pleural membranes. Thus, histology suggests that 14 days after intubation, AdOSM induced parenchymal collagen accumulation, though IL-6 is not required for this effect.

4.1.3 Inflammatory cells in BALF of AdOSM-treated IL-6 -/- mice

Total cell numbers in the BALF were counted. Compared to naïve IL-6 +/+ mice, AdOSM-treated IL-6 +/+ mice had significantly more total cells in the BALF (**Fig. 13A**). Furthermore, AdOSM-treated IL-6 -/- mice had significantly less total cells in the BALF compared to AdOSM-treated IL-6 +/+ mice (**Fig. 13A**). Cell differential from the BALF were also examined using cytocentrifuge smears, and similar trends were observed. AdOSM-treated IL-6 +/+ mice showed increased amounts of macrophages, eosinophils,

neutrophils, and lymphocytes relative to naïve-treated IL-6 +/+ mice (**Fig. 13B**). In addition, AdOSM-treated IL-6 -/- mice had fewer total macrophages, eosinophils, neutrophils, and lymphocytes compared to AdOSM-treated IL-6 +/+ mice (**Fig. 13B**). Admittedly, naïve IL-6 -/- mice may have different BALF cell constituency compared to naïve IL-6 +/+ mice, and having this control group would enable further interpretations regarding changes in BALF constituency in IL-6 -/- mice due to OSM overexpression.

4.1.4 Cytokine analyses of BALF from AdOSM-treated AdOSM-treated IL-6 -/- mice

BALF was assessed for OSM protein levels in AdOSM-treated mice using a specific in-house mouse OSM ELISA to confirm AdOSM-induced OSM protein production. AdOSM-treated IL-6 +/+ and IL-6 -/- mice had elevated levels of OSM compared to naïve IL-6 +/+ mice (**Fig. 14A**). However, OSM levels were significantly lower in AdOSM-treated IL-6 -/- mice than in AdOSM-treated IL-6 +/+ mice (average 800 pg/mL vs. 2500 pg/mL) (**Fig. 14A**).

IL-6 ELISA analysis on BALF confirmed that AdOSM expression induced IL-6 production in IL-6 +/+ mice, but that IL-6 -/- mice, by definition, are incapable of producing IL-6 even in the presence of AdOSM (**Fig. 14B**). BALF was also analyzed for MCP-1, as it has been shown to be upregulated in the BALF of IPF patients. MCP-1 levels were elevated at day seven in AdOSM-treated IL-6 +/+ mice, but were undetectable in AdOSM-treated IL-6 -/- mice (**Fig. 14C**). This suggests that IL-6 is required for OSM-induced MCP-1 production in this system.

Furthermore, BALF was analyzed for KC and VEGF levels, which were not detectable in both AdDl70 and AdOSM-treated mice (**Fig. 14D** and **Fig. 14E**).

4.2 Pathology of OSM-overexpression Model in SMAD3 Knockout Mice

To determine and compare the pathology of OSM-induced ECM remodeling in SMAD3 KO mice, SMAD3 -/- and SMAD3 +/+ mice were untreated (naïve), or treated with $5x10^7$ pfu of AdOSM. After seven days, mice were culled, and lungs were extracted. The left lung was assessed using histology whereas the right lung was used for hydroxyproline assay. BALF was also collected for cytokine analysis by ELISA.

4.2.1 H&E staining of lung sections from AdOSM-treated SMAD3 -/- mice

H&E-stained sections of AdOSM-treated SMAD3 -/- and SMAD3 +/+ mice consistently showed pathology in the airways and the parenchyma compared to AdDl70-treated mice at seven days (**Fig. 15**). There was comparable pathology in AdOSM-treated SMAD3 -/- and SMAD3 +/+ mice, with an accumulation of dense connective tissue in the lung parenchyma. Additionally, there was hyperplasia of the epithelial cells in the large airways in both AdOSM-treated SMAD3 -/- and SMAD3 +/+ mice.

4.2.2 Collagen assessment in lungs of AdOSM-treated SMAD3 -/- mice

Collagen content was assessed using histology as well as by hydroxyproline assay. Examination of the PSR-stained slides under polarized light showed increased PSR staining in the lung parenchyma at seven days, a phenomenon that occurred even in AdOSM-treated SMAD3 -/- mice (**Fig. 15**).

Quantification of parenchymal collagen using the modified Ashcroft score confirmed that relative to naïve SMAD3 +/+ mice, there was an accumulation of parenchymal collagen in both AdOSM-treated SMAD3 +/+ and SMAD3 -/- mice (**Fig. 16A**). However, since only two naïve-treated SMAD3 +/+ mice were examined,

statistical analyses could not be conducted. Total lung collagen was also quantified at day seven using a hydroxyproline assay. Relative to naïve SMAD3 +/+ mice, AdOSM-treated SMAD3 +/+ mice had elevated total collagen (**Fig. 16B**). However, naive SMAD3 +/+ mice had comparable hydroxyproline content compared to AdOSM-treated SMAD3 -/- mice, suggesting that there may be differences in morphology and basal collagen content in naïve SMAD3-/- mice compared to SMAD3+/+ mice. This suggestion is also made on the basis of phenotypic differences between SMAD3-/- and SMAD3+/+ mice, with the former group having an abnormally protruding chest cavity as well as enlarged airspaces. Further investigation is warranted to fully make interpretations of these results.

4.2.3 Inflammatory cells in BALF of AdOSM-treated SMAD3 -/- mice

Cell differentials of cells collected from the lung at day seven showed that AdOSM-treated mice had increased eosinophils, neutrophils, and lymphocytes compared to naïve-treated SMAD3+/+ mice (**Fig. 17**). Eosinophil and lymphocyte infiltration were comparable between AdOSM-treated SMAD3 -/- and AdOSM-treated SMAD3 +/+ mice, though it can be argued that there was less neutrophil infiltration in AdOSM-treated SMAD3 -/- mice compared to AdOSM-treated SMAD3 +/+ mice.

4.2.4 Cytokine analyses of BALF from AdOSM-treated SMAD3 -/- mice

BALF from AdOSM-treated SMAD3+/+ and SMAD3-/- mice was analyzed for mouse OSM and IL-6 by ELISA. Compared to naïve SMAD3 +/+ mice, elevated levels of OSM (**Fig. 18A**) and IL-6 (**Fig. 18B**) were found in AdOSM-treated SMAD3+/+ and SMAD3-/- mice. OSM and IL-6 levels were comparable between AdOSM-treated SMAD3+/+ and SMAD3-/- mice.

Figure 10: Age-matched IL-6 +/+ and IL-6-/- mice were endotracheally administered $5x10^7$ pfu of AdOSM or control vector AdDl70 (n=4 per group). Mice were culled after 14 days. The left lung of each mouse was fixed in 10% formalin and paraffin-embedded. Sections of the lung were stained with H&E. One representative mouse per group is shown using the 10x objective lenses.

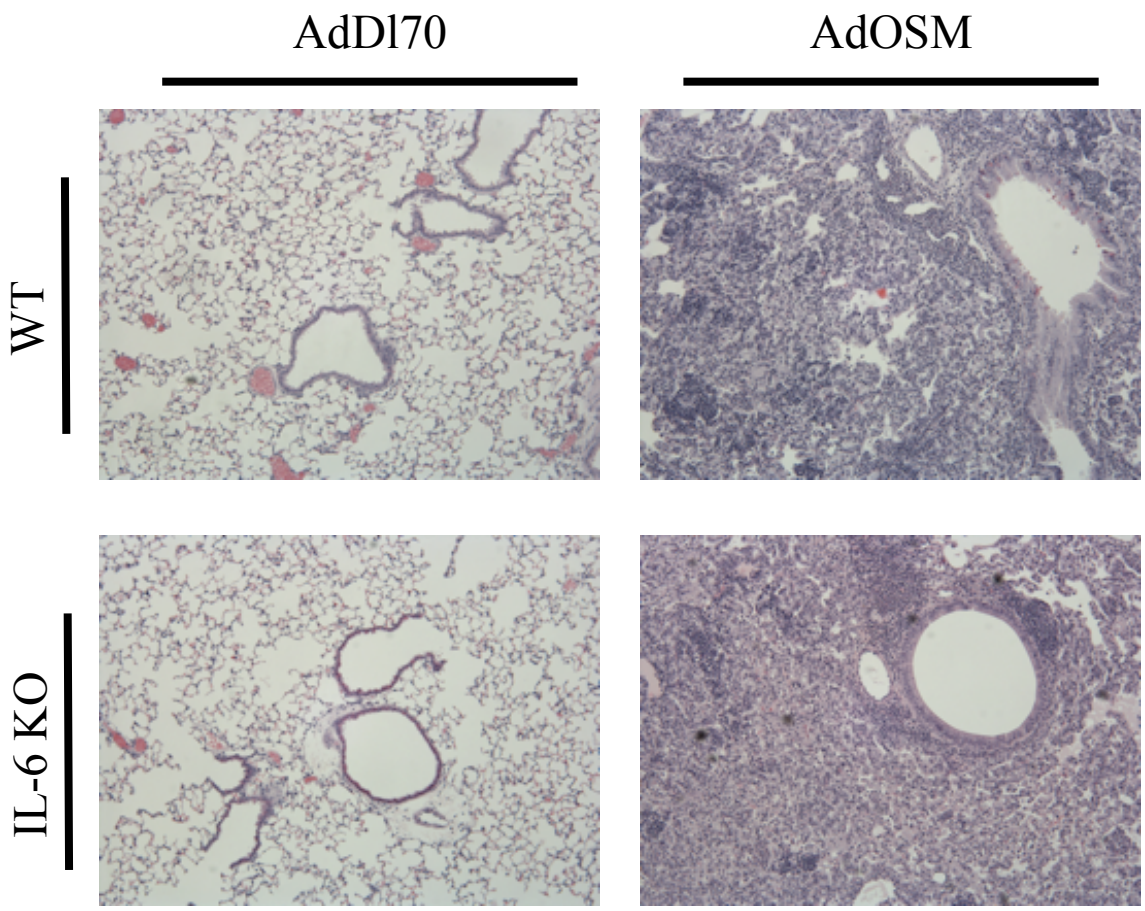

Figure 10

Figure 11: Age-matched IL-6 +/+ and IL-6-/- mice were endotracheally administered $5x10^7$ pfu of AdOSM or control vector AdDl70 (n=4 per group). Mice were culled after 14 days. The left lung of each mouse was fixed in 10% formalin and paraffin-embedded. Sections of the lung were stained with either Masson's Trichrome and viewed using the 10x objective lenses (A), or with PSR and examined using the 5x objective lenses (B). One representative mouse is shown per group.

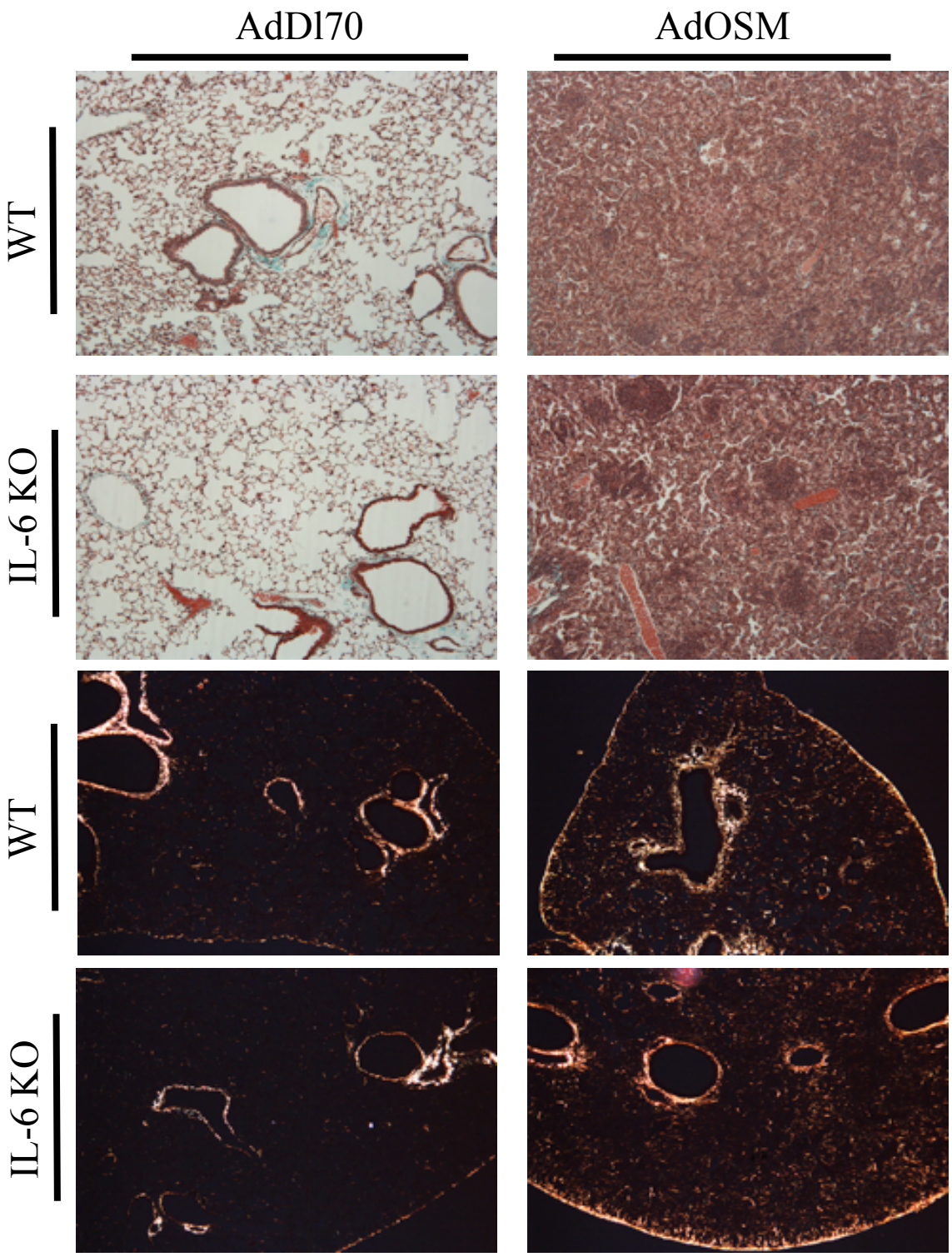

Figure 11

Figure 12: Age-matched IL-6 +/+ and -/- mice were endotracheally administered $5x10^7$ pfu of AdOSM or control vector AdDl70. Mice were culled after seven and 14 days. A quantification of parenchymal collagen in IL-6 +/+ and -/- mice mouse lung treated with AdOSM or AdDl70 14 days post-intubation was performed. Microphotographs were taken of PSR-stained slides examined under polarized light. Multiple microphotographs were taken to cover the entire lung. Subsequently, four blinded assessors rated each microphotograph on a score of 0-8 for amount of parenchymal collagen staining, with 8 being the highest score. Results are displayed relative to AdDl70-treated mice of each mouse strain. Statistical significance is shown where * = $p<0.05$, ** = $p<0.001$, *** = $p<0.0001$

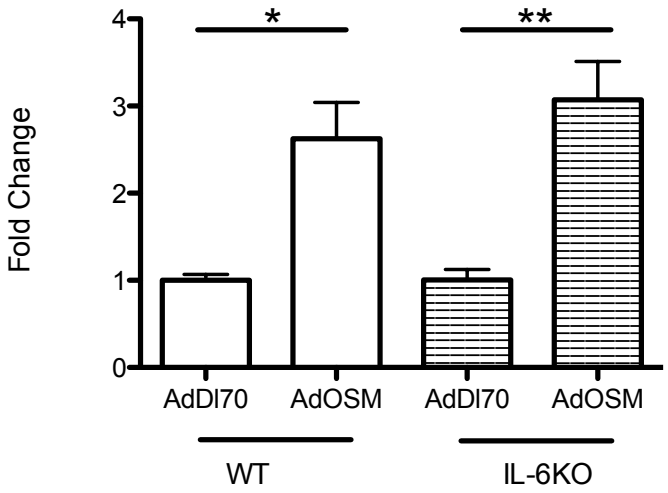

Figure 12

Figure 13: Age-matched IL-6 +/+ and -/- mice were endotracheally administered $5x10^7$ pfu of AdOSM (n=5 per group). A separate group of naïve, untreated IL-6 +/+ mice was utilized as a control group (n=3 mice). Mice were culled after seven days. Inflammatory cells were collected from the BALF and counted for total cell numbers (A). Cell differentials were then conducted using cytocentrifuge smears (B). Statistical significance is shown where * = $p<0.05$, ** = $p<0.001$, *** = $p<0.0001$

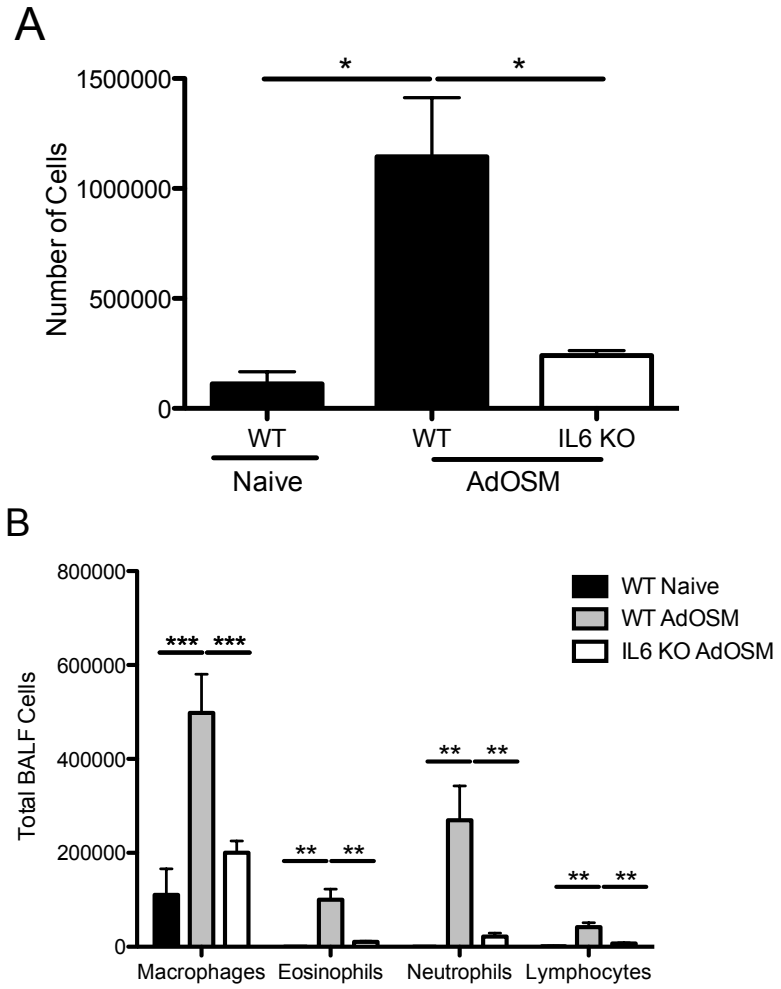
A
1500000
1000000
500000
0
Number of Cells
*
*
WT
WT
IL6 KO
Naive
AdOSM
B
800000
600000
400000
200000
0
Total BALF Cells
WT Naive
WT AdOSM
IL6 KO AdOSM
***
***
**
**
**
**
**
**
Macrophages
Eosinophils
Neutrophils
Lymphocytes

Figure 13

Figure 14: Age-matched IL-6 +/+ and -/- mice were endotracheally administered $5x10^7$ pfu of AdOSM (n=5 per group). A separate group of naïve, untreated IL-6 +/+ mice was utilized as a control group (n=3 mice). Mice were culled after seven days. BALF was collected and analyzed for OSM (A), IL-6 (B), MCP-1 (C), KC (D), and VEGF (E). Statistical significance is shown where * = $p<0.05$, ** = $p<0.001$, *** = $p<0.0001$

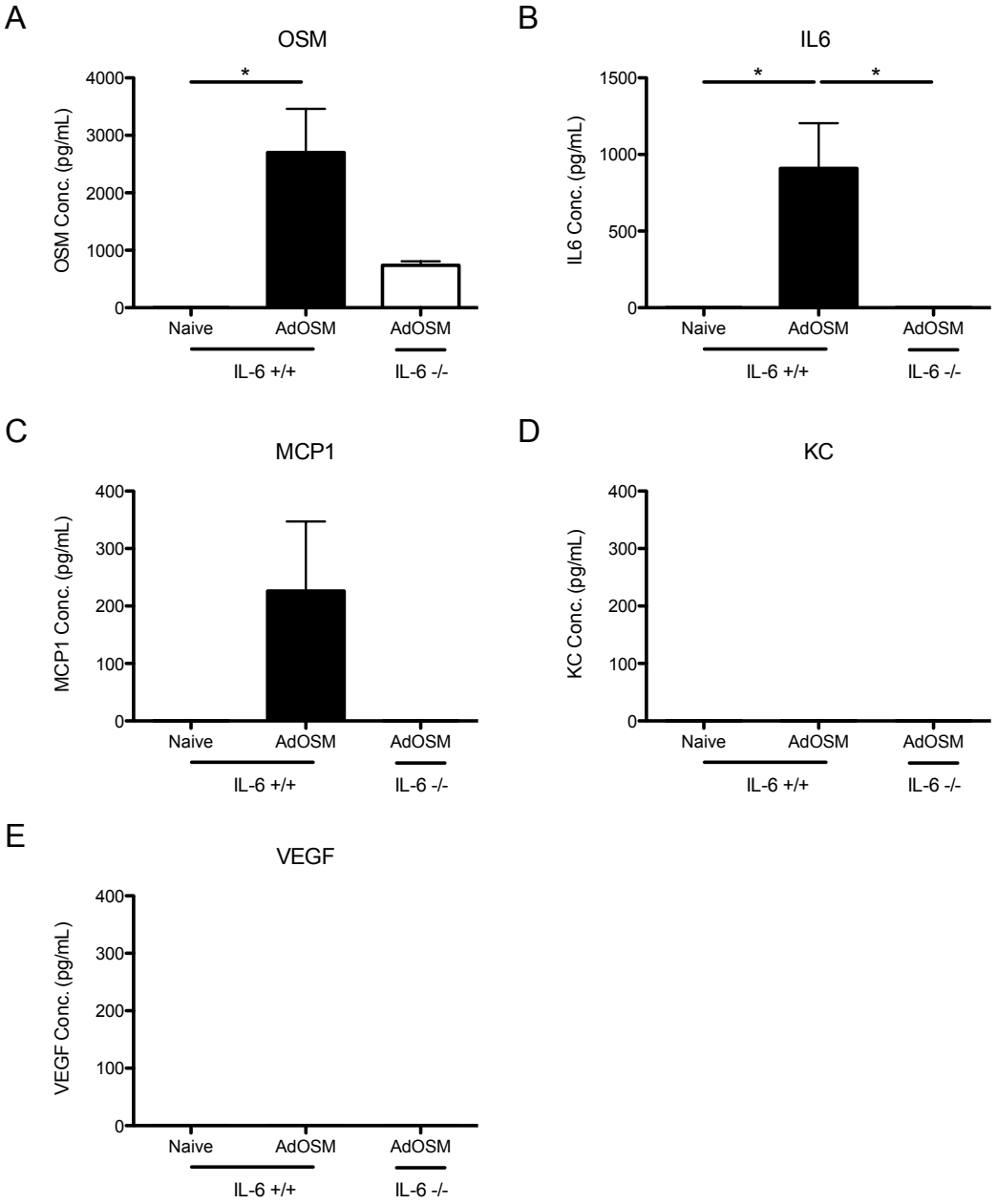
A
OSM
OSM Conc. (pg/mL)
4000
3000
2000
1000
0
*
Naive
AdOSM
AdOSM
IL-6 +/+
IL-6 -/-
B
IL6
IL6 Conc. (pg/mL)
1500
1000
500
0
*
*
Naive
AdOSM
AdOSM
IL-6 +/+
IL-6 -/-
C
MCP1
MCP1 Conc. (pg/mL)
400
300
200
100
0
Naive
AdOSM
AdOSM
IL-6 +/+
IL-6 -/-
D
KC
KC Conc. (pg/mL)
400
300
200
100
0
Naive
AdOSM
AdOSM
IL-6 +/+
IL-6 -/-
E
VEGF
VEGF Conc. (pg/mL)
400
300
200
100
0
Naive
AdOSM
AdOSM
IL-6 +/+
IL-6 -/-

Figure 14

Figure 15: Age-matched SMAD3 +/+ and -/- mice were endotracheally administered $5x10^7$ pfu of AdOSM (n=5 per group). A separate group of naïve, untreated SMAD3 +/+ mice was utilized as a control group (n=2 mice). Mice were culled after seven days. The left lung of each mouse was fixed in 10% formalin and paraffin-embedded. Sections of the lung were either stained with H&E and viewed using the 10x objective lenses (A), or with PSR and viewed using the 5x objective lenses (B). One representative m
Sections of the lung were either stained with Masson's Trichrome and examined using the 20x objective lenses (A), or PSR and examined using the 5x objective lenses (B). One representative mouse is shown per group.

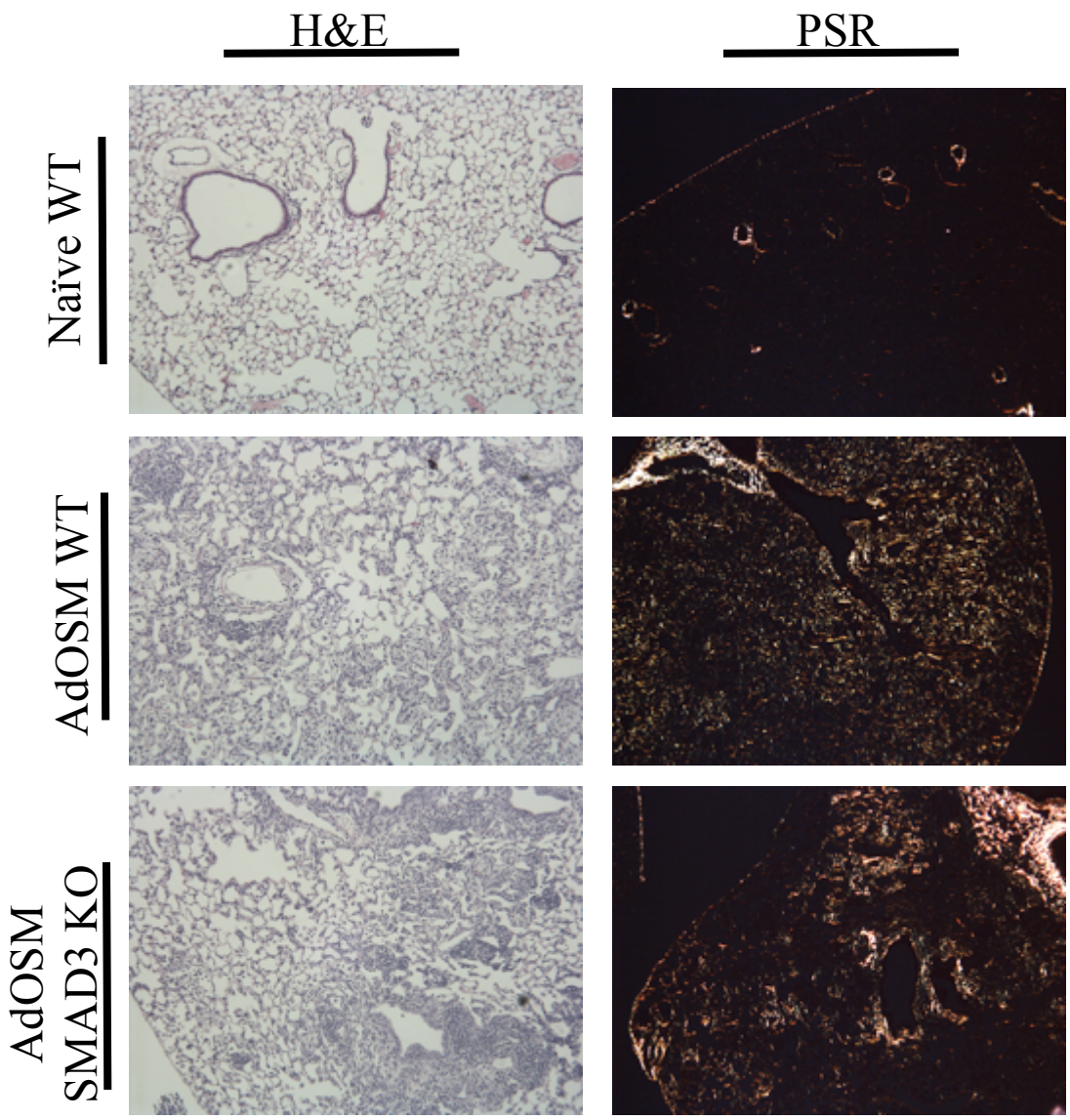

Figure 15

Figure 16: Age-matched SMAD3 +/+ and -/- mice were endotracheally administered $5x10^7$ pfu of AdOSM (n=5 per group). A separate group of naïve, untreated SMAD3 +/+ mice was utilized as a control group (n=2 mice). Mice were culled after seven days.
A - Quantification of parenchymal collagen in mouse lung using the modified Ashcroft score. 8-15 microphotographs were taken of PSR-stained lung sections viewed under polarized light using the 5x objective lenses to cover the entire lung area. Subsequently, four assessors blinded to the animal identification rated each microphotograph from a score of 0-8 for amount of parenchymal collagen staining, with 8 being the highest score. Results are displayed relative to AdDl70-treated mice of each mouse strain. Statistics could not be carried out because the naïve SMAD3 +/+ group contained two mice.
B – Right lung homogenates were put into a freeze dry lyophilizer to obtain dry weight tissue. Subsequently, a hydroxyproline assay was performed on dry tissue to assess total lung collagen. Statistics could not be carried out because the naïve SMAD3 +/+ group contained two mice.

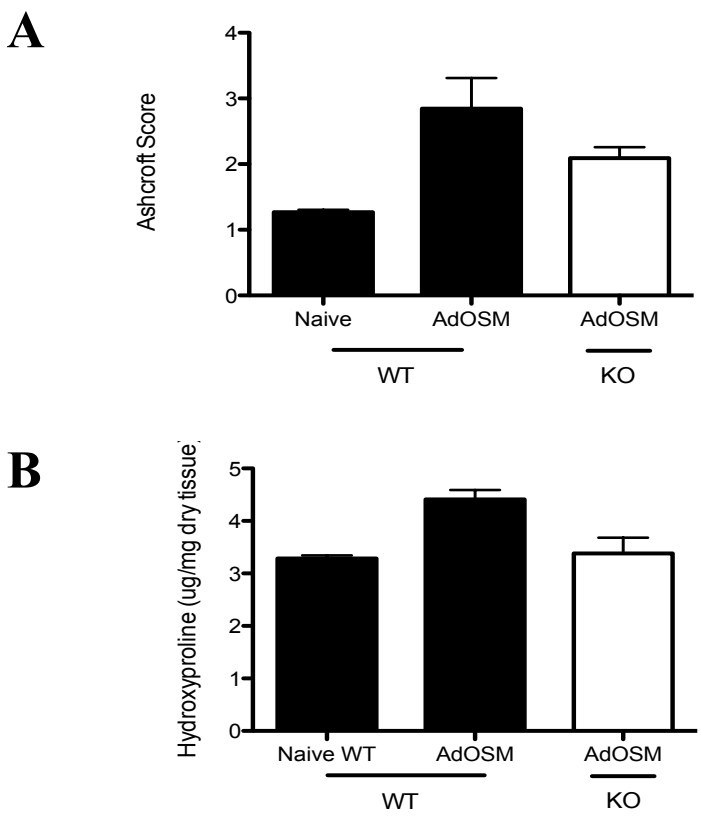
A
Ashcroft Score
0
1
2
3
4
Naive
AdOSM
AdOSM
WT
KO
B
Hydroxyproline (ug/mg dry tissue)
0
1
2
3
4
5
Naive WT
AdOSM
AdOSM
WT
KO

Figure 16

Figure 17: Age-matched SMAD3 +/+ and -/- mice were endotracheally administered $5x10^7$ pfu of AdOSM (n=5 per group). A separate group of naïve, untreated SMAD3 +/+ mice was utilized as a control group (n=2 mice). Mice were culled after seven days. Inflammatory cells were collected from the BALF, counted, and cell differentials were conducted using cytocentrifuge smears. Statistics could not be carried out because the naïve SMAD3 +/+ group contained two mice.

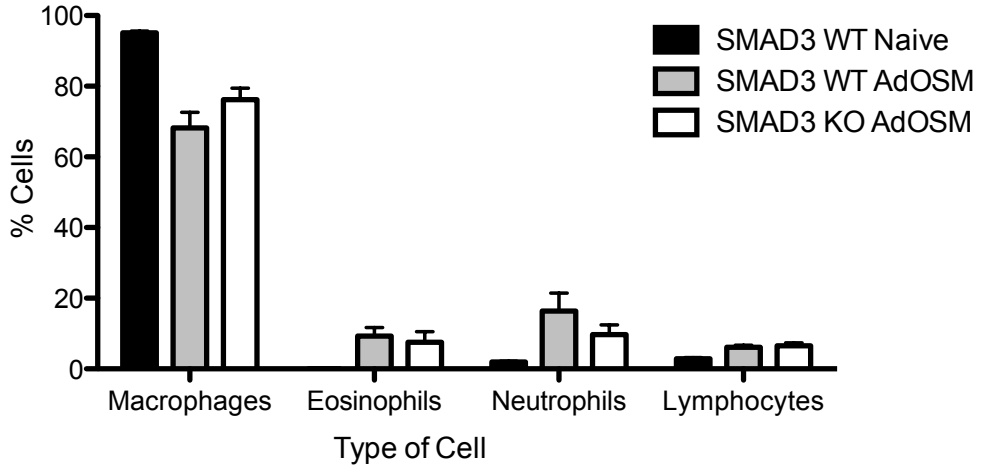
100
80
60
40
20
0
% Cells
SMAD3 WT Naive
SMAD3 WT AdOSM
SMAD3 KO AdOSM
Macrophages
Eosinophils
Neutrophils
Lymphocytes
Type of Cell

Figure 17

Figure 18: Age-matched SMAD3 +/+ and -/- mice were endotracheally administered $5x10^7$ pfu of AdOSM (n=5 per group). A separate group of naïve, untreated SMAD3 +/+ mice was utilized as a control group (n=2 mice). Mice were culled after seven days. BALF was collected and analyzed for OSM (A) and IL-6 (B)

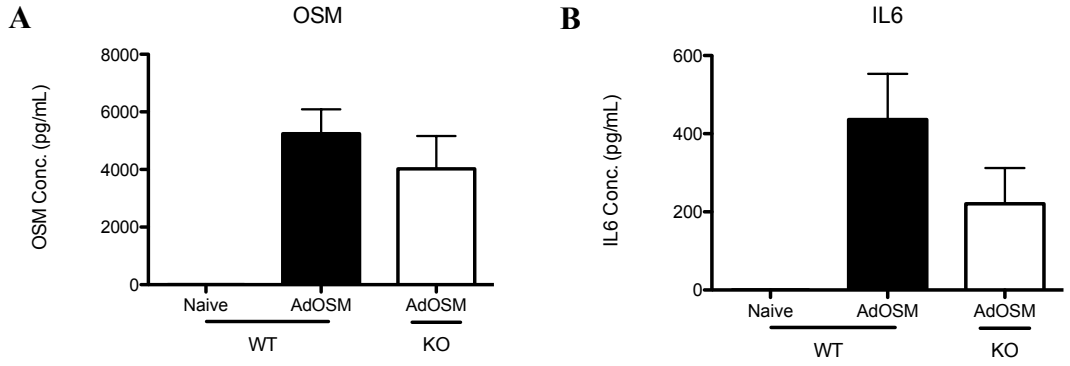
A
OSM
OSM Conc. (pg/mL)
8000
6000
4000
2000
0
Naive
AdOSM
AdOSM
WT
KO
B
IL6
IL6 Conc. (pg/mL)
600
400
200
0
Naive
AdOSM
AdOSM
WT
KO

Figure 18

CHAPTER 5: Results of Aim 3

In this chapter, STAT and SMAD signaling pathways are examined in the OSM-induced model of ECM remodeling. This body of work encompasses studies using both C57Bl/6 and BALB/c mice treated with AdOSM to examine SMAD signaling *in vivo*, and *in vitro* work using MLF cultures from both strains of mice, Beas 2B human airway epithelial cells, human A549 cells, and C10 mouse type two pneumocytes.

5.1 Cell Signaling *in vivo*

To examine regulation of the STAT and SMAD pathways *in vivo,* lung homogenates were generated from the right lung of C57Bl/6 and BALB/c mice seven days after intubation with $5x10^7$ pfu AdOSM or AdDl70. Lung homogenates were also generated from total lung homogenates of BALB/c mice two days after intubation with AdOSM or AdDl70. IHC for pSMAD1/5/8 and pSMAD2 was also completed on lung sections of AdOSM-treated mice to assess cell types that responded in this system.

5.1.1 STAT3 pathway regulation in both AdOSM-treated C57Bl/6 and BALB/c mice

Lung homogenates were probed for pSTAT3 by immunoblots as an indicator of STAT3 activation. All AdOSM-treated C57Bl/6 and BALB/c mouse lung homogenates showed increased levels of pSTAT3 signal relative to AdDl70-treated mice, suggesting that the STAT3 pathway is activated (**Fig. 19A**). This observation was also seen in AdOSM-treated BALB/c mouse lung homogenates at Day two in a dose-dependent manner (**Fig. 20**). To ensure that equivalent amounts of protein were loaded between samples, lung homogenates were probed for actin, of which signals indicated equivalent protein loading of all samples (**Fig. 19A** and **Fig. 20**).

5.1.2 SMAD1 pathway regulation in both AdOSM-treated C57Bl/6 and BALB/c mice

Mouse lung homogenates were then probed for pSMAD1/5 to investigate modulation of the SMAD1 pathway. AdOSM-treated mice from both mouse strains consistently showed decreased levels of pSMAD1/5 signal at Day 7 compared to AdDl70-treated mice (**Fig. 19C**). These results were verified using a second antibody to pSMAD1/5/8 (**Fig. 19D**). This decrease in pSMAD1/5 signal is in conjunction with unchanged levels of total SMAD1 protein in C57Bl/6 mice, and increased levels of total SMAD1 protein in AdOSM-treated BALB/c mice. Thus pSMAD1/5 decrease was not directly related to a decrease in total SMAD1 proteins.

The pSMAD1/5 and pSMAD1/5/8 antibodies gave conflicting results when used on Day two lung homogenates. There was a decrease in pSMAD1/5/8 signal in AdOSM-treated BALB/c mouse lung homogenates relative to naïve and AdDl70-treated mice (**Fig. 20**). In contrast, there was an increase in pSMAD1/5 signal in AdOSM-treated BALB/c mouse lung homogenates relative to naïve and AdDl70-treated mice (**Fig. 20**).

IHC was completed using the pSMAD1/5/8 antibody to confirm pSMAD1/5/8 regulation in AdOSM-treated mice and to determine cell types involved in this response. Qualitatively, levels of pSMAD1/5/8 were diminished in AdOSM-treated C57Bl/6 at Day 7 (**Fig. 21A**), as well as in AdOSM-treated BALB/c mice at both Day 2 and Day 7 (**Fig. 21B** and **Fig. 22**), compared to naïve and AdDl70-treated mice. A strong signal was detected around the large airways of naïve and AdDl70-treated mice that was not seen in either the AdOSM-treated mice nor the negative control/secondary antibody-alone stained control slide (**Fig. 21C**). Staining was also present, albeit more faint, around the lung

parenchyma of naïve and AdDl70-treated mice but not AdOSM-treated mice (**Fig. 21D**). This staining was localized to alveolar wall cells, which could include lung fibroblasts and type one and type two pneumocytes, but not cells within the alveolar spaces such as alveolar macrophages (**Fig. 21D**). These analyses were not completed using the pSMAD1/5 antibody since the manufacturer (Cell Signaling) does not recommend using this antibody for IHC. Collectively, this data suggests a suppression of the SMAD1/5/8 signaling pathway in lung tissue as a result of OSM overexpression.

To determine if OSM-induced suppression of SMAD1 signaling was associated with regulation of receptors of the BMP pathway, lung homogenates from the Day seven experiment were probed for BMPR2 and Alk3/BMPR1A by immunoblots. There was a consistent suppression of BMPR2 signal and a consistent upregulation of Alk3 signal in AdOSM-treated mice relative to AdDl70-treated mice (**Fig. 19F-G**).

5.1.3 SMAD2 pathway regulation in both AdOSM-treated C57Bl/6 and BALB/c mice

The literature suggests that BMPs and TGF-β have opposing roles in ECM remodeling. Thus, SMAD2 signaling was examined in the *in vivo* model as a comparator to SMAD1 signaling. Lung homogenates from Day 7 AdOSM-treated mice and Day 2 AdOSM-treated BALB/c mice were probed for pSMAD2 to investigate activation of the canonical TGF-β pathway. The results showed that there was no statistically significant difference between AdOSM-treated lung homogenates and AdDl70-treated lung homogenates from either C57Bl/6 or BALB/c background with respect to pSMAD2 signal (**Fig. 19C**). Similar observations were evident at day two (**Fig. 20**).

IHC was also completed for pSMAD2 on Day 7 AdOSM-treated C57Bl/6 and BALB/c mice, with AdDl70-treated mice serving as controls. Staining was positive in the airways and parenchyma of both AdOSM and AdDl70-treated mice (**Fig. 23A** and **Fig. 23B**). Although extent of staining was similar in the airways of AdDl70-treated and AdOSM-treated mice, it appeared that there was more parenchymal positive staining for pSMAD2 in AdOSM-treated mice than AdDl70-treated mice. Staining was not evident using the secondary antibody alone (**Fig. 23A** and **Fig. 23B**).

5.2 Cell Signaling in C57Bl/6 and BALB/c MLF cultures

Since fibroblasts are a major cell type implicated in pulmonary fibrosis pathogenesis, regulation of SMAD1 signaling in response to OSM was examined in both C57Bl/6 and BALB/c MLF cultures *in vitro*. The first set of experiments involved stimulating C57Bl/6 and BALB/c MLF cultures with 5 ng/mL of OSM over a time course of six hours. As a comparator, MLF cultures were also stimulated with 50 ng/mL BMP2 and 5 ng/mL of TGF-β for one hour. The actin blots in **Fig. 24A** and **Fig. 25A** showed that C57Bl/6 and BALB/c MLF cell lysates indicated equivalent levels of actin signal.

Cell signaling responses were also examined in C57Bl/6 and BALB/c MLF cultures over a longer stimulation period to determine the effects of longer exposure to OSM. This set of experiments involved stimulating C57Bl/6 and BALB/c MLF cultures with 5 ng/mL of OSM for 24 and 72 hours. As a comparator, MLF cultures were treated with 50 ng/mL BMP2 and 5 ng/mL of TGF-β, and combinations of these cytokines, for 24 and 72 hours. Immunoblots were initially probed for actin, and the actin signals in

lysates from both C57Bl/6 (**Fig. 26A**) and BALB/c MLF cultures (**Fig. 27A**) indicated that an equivalent amount of protein was loaded for each sample.

5.2.1 STAT3 signaling in C57Bl/6 and BALB/c MLF cultures

C57Bl/6 and BALB/c MLF cell lysates were probed for pSTAT3 to ensure that MLF cultures responded to OSM. OSM but not BMP2 or TGF-β elevated pSTAT3 signals in MLF extracts from both C57Bl/6 and BALB/c strains over a six hour time course (**Fig. 24B** and **Fig. 25B**). While pSTAT3 signal remained constant throughout the six hour time course in BALB/c MLF cultures, pSTAT3 signal decreased, but remained elevated compared to the zero hour time point, over the six hour time course.

Examining pSTAT3 signal at a later time point, OSM but not BMP2 or TGF-β elevated pSTAT3 signal in C57Bl/6 MLF cultures at 24 hours, although levels decreased to basal levels at 72 hours (**Fig. 26B**). In contrast, OSM but not BMP2 or TGF-β elevated pSTAT3 signal in BALB/c MLF cultures at both 24 and 72 hours (**Fig. 27B**), suggesting that the activation of the STAT3 pathway by OSM remained sustained in these primary cell cultures (passage seven).

5.2.2 SMAD1 signaling in C57Bl/6 and BALB/c MLF cultures

C57Bl/6 and BALB/c MLF cell lysates were then probed for SMAD1 signaling markers using both the pSMAD1/5 and the pSMAD1/5/8 antibodies. As a positive control, BMP2 induced pSMAD1/5 signal after one hour time stimulation in both C57Bl/6 and BALB/c MLF cell cultures (**Fig. 24D** and **Fig. 25D**). However, the pSMAD1/5/8 antibody did not complement the results obtained using the pSMAD1/5 antibody, as it showed that BMP2 did not regulate pSMAD1/5/8 signal in either C57Bl/6

and BALB/c MLF cell cultures after one hour stimulation (**Fig. 24E** and **Fig. 25E**). TGF-β also appeared to induce pSMAD1/5 signal in both cell lines after one hour stimulation, but not the pSMAD1/5/8 signal in BALB/c MLF cultures (**Fig. 24D-E** and **Fig. 25D-E**). OSM elevated pSMAD1/5 signal over the course of six hours in both C57Bl/6 and BALB/c MLF cultures (**Fig. 24D** and **Fig. 25D**). These results were observed when utilizing the pSMAD1/5/8 antibody (**Fig. 24E** and **Fig. 25E**).

At the later time points, BMP2 remained a positive control for SMAD1 signaling. After 72 hours stimulation, BMP2 but not OSM or TGF-β elevated pSMAD1/5 signal in C57Bl/6 MLF cell lysates (**Fig. 26C**). BMP2 but not TGF-β elevated levels of pSMAD1/5 at both 24 and 72 hours in BALB/c MLF cell lysates (**Fig. 27C**). These observations were also evident when probing with the pSMAD1/5/8 antibody (**Fig. 27D**). In contrast to BMP2 and TGF-β, OSM elevated the pSMAD1/5 signal in BALB/c MLF cultures at 24 hours (**Fig. 27C**), but suppressed pSMAD1/5 signal at 72 hours, observations that were also evident using the pSMAD1/5/8 antibody (**Fig. 27D**).

MLF cell lysates were also probed for BMPR2 to examine effects of OSM on BMP receptor expression in MLF cultures. BMPR2 signal was not regulated by OSM, BMP2, or TGF-β in C57Bl/6 MLF cultures after 24 or 72 hours stimulation (**Fig. 26E**). In BALB/c MLF cultures, OSM and BMP2 increased BMPR2 signal after 24 hours stimulation, whereas TGF-β decreased this signal (**Fig. 27E**). After 72 hours stimulation of these cells, TGF-β decreased BMPR2 signal, whereas the BMPR2 signal was unmodulated by OSM or BMP2 stimulation (**Fig. 27E**).

5.2.3 SMAD2 signaling in C57Bl/6 MLF and BALB/c MLF cultures

C57Bl/6 and BALB/c MLF lysates were probed for pSMAD2 as a comparator to SMAD1 signaling. TGF-β elevated levels of pSMAD2 signal after one hour stimulation in both C57Bl/6 and BALB/c MLF cell lysates (**Fig. 24C** and **Fig. 25C**). Interestingly, BMP2 also increased pSMAD2 signal in both C57Bl/6 and BALB/c MLF cultures after one hour stimulation (**Fig. 24C** and **Fig. 25C**). There is a trend towards an increase in OSM-induced pSMAD2 signal in C57Bl/6 MLF cell lysates relative that is not evident in the BALB/c MLF cell lysates (**Fig. 24C**).

TGF-β also elevated pSMAD2 signal in both C57Bl/6 and BALB/c MLF at 24 hours and 72 hours, with more of an increase in the latter cell line (**Fig. 26F** and **Fig. 27F**). In contrast, neither OSM nor BMP2 were able to regulate pSMAD2 signal at 24 or 72 hours relative to control (**Fig. 26F** and **Fig. 27F**). OSM did not modulate TGF-β-induced pSMAD2 signal at either 24 hour or 72 hours (**Fig. 26F** and **Fig. 27F**).

5.3 Cell Signaling in Beas 2B cells

Current literature also implicates epithelial cells in pulmonary fibrosis pathogenesis. *In vivo* data collected so far (**Fig. 20** and **Fig. 21**) suggested that OSM overexpression modulated cell signaling in the airway epithelial cells. To assess airway epithelial responses to human OSM, human Beas 2B cells were stimulated with 5 ng/mL OSM, 50 ng/mL BMP2, 5 ng/mL TGF-β, 5 ng/mL OSM with 50 ng/mL BMP2, 5 ng/mL OSM with 5 ng/mL TGF-β, and 50 ng/mL of BMP2 with 5 ng/mL TGF-β. Cells were examined both at one hour and at one day to look at early as well as late responses.

Beas 2B cells treated with OSM but not BMP2 or TGF-β showed increased pSTAT3 signal at both one hour and one day (**Fig. 29B** and **Fig. 30B**). Though BMP2

appeared to mildly decrease OSM-induced pSTAT3 signal at both the one hour and one day time point, it appeared that TGF-β augmented OSM-induced STAT3 activation (**Fig. 29B** and **Fig. 30B**).

Beas 2B cell lysates were then probed for regulation of the BMP-SMAD1 signaling axis. As a positive control, BMP2 but not TGF-β elevated pSMAD1/5 signal, an effect that was also observed using the pSMAD1/5/8 antibody (**Fig. 29C-D** and **Fig. 30C-D**). At both one hour and one day, OSM alone was able to suppress SMAD1/5 activation (**Fig. 29C** and **Fig. 30C**). These observations were also seen when using the pSMAD1/5/8 antibody (**Fig. 29D** and **Fig. 30D**).

BMPR2 was also probed to determine whether OSM regulation of the BMP-SMAD1 signaling axis correlated with modulation of this receptor chain. OSM, BMP2, and TGF-β all downregulated BMPR2, while combinations of these cytokines further downregulated BMPR2 after one hour stimulation (**Fig. 29F**). After one day stimulation, OSM and BMP2 alone or in combination slightly upregulated BMPR2, whereas TGF-β alone or in combination with either OSM or BMP2 downregulated BMPR2 (**Fig. 30F**).

Beas 2B cell lysates were also examined for regulation of the TGF-β-SMAD2 signaling axis. Unfortunately, TGF-β alone was unable to induce SMAD2 phosphorylation at either one hour or one day (**Fig. 29E** and **Fig. 30E**). This either suggests that these cells do not respond to TGF-β, or that TGF-β-induced SMAD2 phosphorylation occurs at a time point between one hour and one day. Neither OSM nor BMP2 was able to activate SMAD2 signaling in Beas 2B cells assessed at either one hour or one day time points (**Fig. 29E** and **Fig. 30E**).

5.4 Cell Signaling in A549 cells

To determine effects of OSM on a lung parenchymal epithelial cell line, human A549 cells were utilized. A549 cells were stimulated with 5 ng/mL OSM, 50 ng/mL BMP2, 5 ng/mL TGF-β, 5 ng/mL OSM with 50 ng/mL BMP2, 5 ng/mL OSM with 5 ng/mL TGF-β, and 50 ng/mL of BMP2 with 5 ng/mL TGF-β. Cells were examined both at one hour and at one day to look at early as well as late responses. Actin blots at both the 1 hour and 1 day time points for the A549 lysates showed that equivalent amounts of protein were loaded into each well (**Fig. 30A** and **Fig. 31A**).

The pSTAT3 blot showed that OSM increased pSTAT3 signal after one hour and one day stimulation (**Fig. 30A** and **Fig. 31A**). BMP2 and TGF-β do not affect OSM-induced pSTAT3 signal after one hour or one day stimulation (**Fig. 30A** and **Fig. 31A**).

Regulation of the BMP-SMAD1 signaling axis was next examined, and as a positive control, cells treated with BMP2 showed increased levels of pSMAD1/5 signal at both the one hour and one day time point (**Fig. 30C** and **Fig. 31C**). These results are also verified using a second pSMAD1/5/8 antibody (**Fig. 30D** and **Fig. 31D**). The data also suggests that while neither OSM nor TGF-β affected BMP2-induced pSMAD1/5 signal in A549 cells, OSM alone was capable of elevating the pSMAD1/5 signal at one hour and one day (**Fig. 30C** and **Fig. 31C**). This trend was also observed using the pSMAD1/5/8 antibody (**Fig. 30D** and **Fig. 31D**). In contrast, TGF-β did not appear to modulate the pSMAD1/5 signal one hour or one day stimulation (**Fig. 30C** and **Fig. 31C**).

In samples probed for pSMAD2, TGF-β, but not OSM or BMP2 alone, elevated levels of pSMAD2 signal compared to control at both one hour and one day (**Fig. 30E**

and **Fig. 31E**). However, it appeared that OSM as well as BMP2 decreased TGF-β-induced pSMAD2 protein levels upon co-stimulation. This observation is more evident at the one hour time point than at the one day time point (**Fig. 30E** and **Fig. 31E**).

5.5 Cell Signaling in C10 type two pneumocytes

To examine regulation of cell signaling pathways in a mouse epithelial cell line, C10 type two pneumocytes were used. C10 cells were stimulated with 5 ng/mL OSM, 50 ng/mL BMP2, 5 ng/mL TGF-β, 5 ng/mL OSM with 50 ng/mL BMP2, 5 ng/mL OSM with 5 ng/mL TGF-β, and 50 ng/mL of BMP2 with 5 ng/mL TGF-β. Cells were examined both at one hour, 24 hours, and 72 hours

Immunoblots for pSTAT3 on C10 cell lysates showed that OSM, but not BMP2 or TGF-β elevated pSTAT3 signal at one hour, one day, and three days (**Fig. 32B** and **Fig. 33B**). Neither BMP2 nor TGF-β did not modulate OSM-induced pSTAT3 signal.

Next, immunoblots were probed for pSMAD1/5/8 to examine regulation of the BMP-SMAD1 signaling axis. BMP2, but not TGF-β increased pSMAD1/5/8 signal after one and three days stimulation (**Fig. 33C-D**). However, this was not observed after one hour stimulation, suggesting that it requires longer than one hour for the SMAD1 pathway to be activated in response to BMP2 (**Fig. 32D-E**). Though not observed at one hour, OSM caused a decrease in pSMAD1/5/8 signal after one and three days stimulation.

Cell lysates were probed for modulation of pSMAD2 to assess the regulation of the TGF-β-SMAD2 signaling axis. As expected, TGF-β, but not OSM or BMP2 alone, elevated levels of pSMAD2 compared to control after one hour, one day, and three day stimulation (**Fig. 32E** and **Fig. 33E**).

Figure 19: Age-matched C57Bl/6 and BALB/c mice were endotracheally administered $5x10^7$ pfu of AdOSM or control vector AdDl70 (n=5 per group). Mice were culled after seven days. Lungs were collected, homogenized, and run on protein gels. Lung homogenates were probed for pSTAT3, pSMAD1/5, pSMAD1/5/8, SMAD1, pSMAD2, BMPR2, Alk3, and actin (A). Densitometry was carried out to quantify band intensity, corrected to actin, and expressed relative to AdDl70-treated mice (B-G)

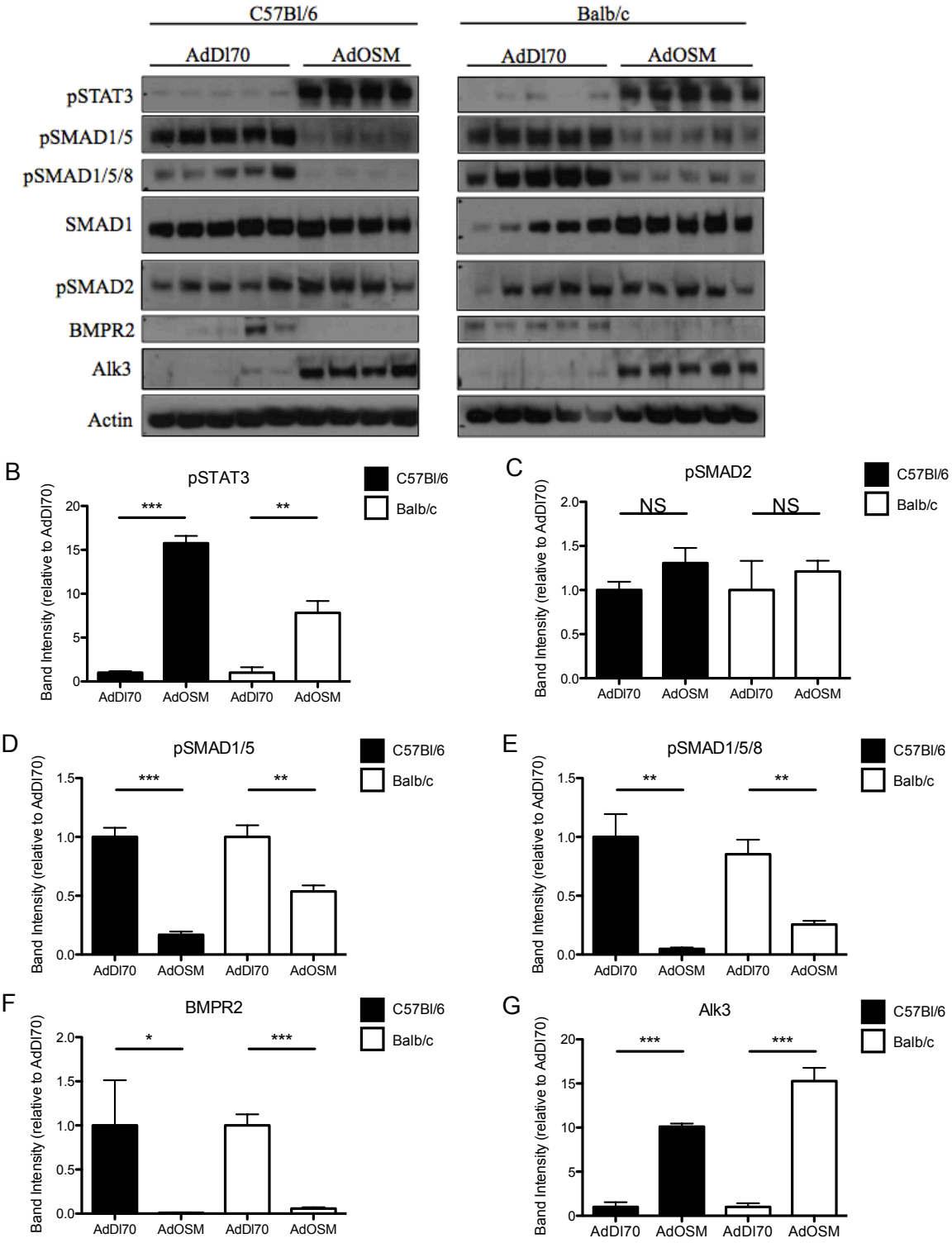
C57Bl/6
Balb/c
AdDl70
AdOSM
pSTAT3
pSMAD1/5
pSMAD1/5/8
SMAD1
pSMAD2
BMPR2
Alk3
Actin
B
pSTAT3
C57Bl/6
Balb/c
Band Intensity (relative to AdDl70)
***
**
C
pSMAD2
NS
D
pSMAD1/5
E
pSMAD1/5/8
F
BMPR2
*
G
Alk3

Figure 19

Figure 20: BALB/c mice were endotracheally administered varying dosages of AdOSM, $5x10^7$ pfu of AdDl70, or were left untreated (n=3 per treatment). Mice were culled after two days. Lungs were collected, homogenized, and run on protein gels. Lung homogenates were probed for pSTAT3, STAT3, pSMAD1/5, pSMAD1/5/8, pSMAD2, and actin.

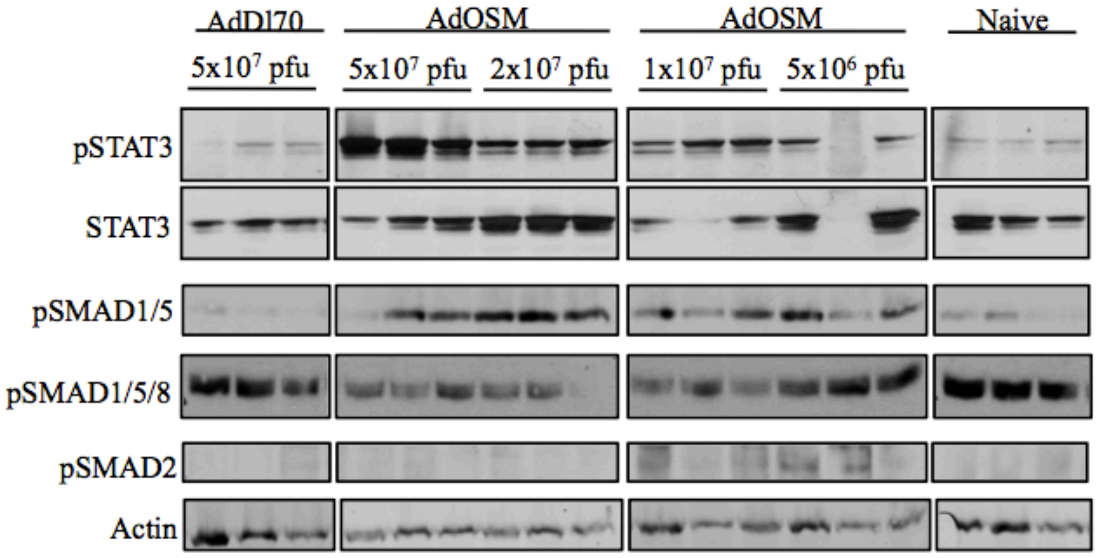
AdDl70
AdOSM
AdOSM
Naive
5x10^7 pfu
5x10^7 pfu
2x10^7 pfu
1x10^7 pfu
5x10^6 pfu
pSTAT3
STAT3
pSMAD1/5
pSMAD1/5/8
pSMAD2
Actin

Figure 20

Figure 21: Age-matched C57Bl/6 and BALB/c mice were endotracheally administered $5x10^7$ pfu of AdOSM or control vector AdDl70 (n=5 per group). Naïve mice from both strains were also kept as a control group. Mice were culled after seven days. The left lung of each mouse was fixed in 10% formalin and paraffin-embedded. IHC was conducted on lung sections for pSMAD1/5/8.

A: Overview of pSMAD1/5/8 staining in AdOSM, AdDl70, and naïve C57Bl/6 mice using a 5x objective lenses. One representative mouse is shown per group.

B: Overview of pSMAD1/5/8 staining in AdOSM, AdDl70, and naïve BALB/c mice using a 5x objective lenses. One representative mouse is shown per group.

C: Airways staining of pSMAD1/5/8 in AdOSM, AdDl70, and naïve C57Bl/6 and BALB/c mice using a 40x objective lenses. One representative mouse is shown per group, along with corresponding secondary antibody alone control.

D: Parenchymal staining of pSMAD1/5/8 in AdOSM, AdDl70, and naïve C57Bl/6 and BALB/c mice using a 40x objective lenses. One representative mouse is shown per group, along with corresponding secondary antibody alone control.

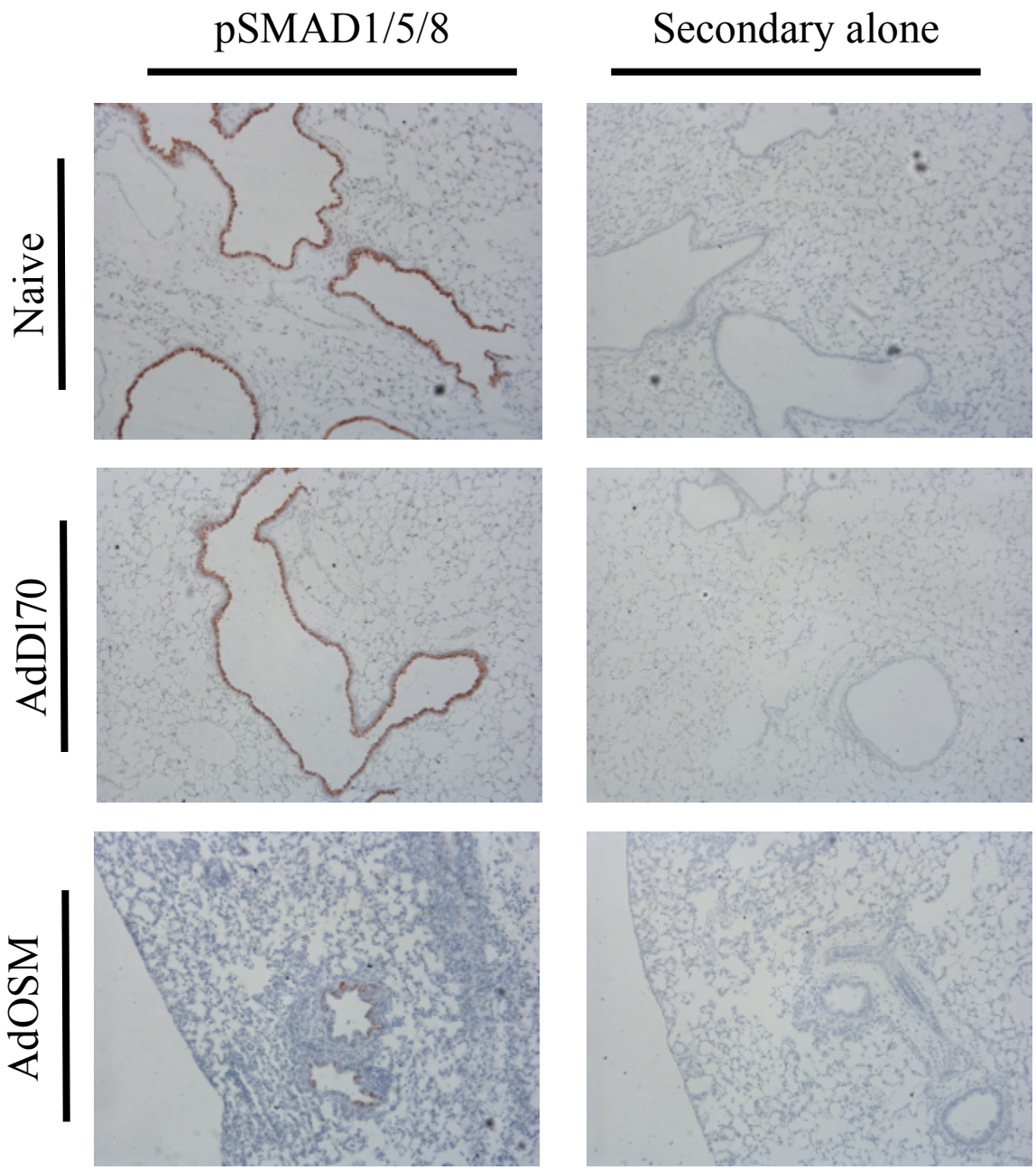

Figure 21A

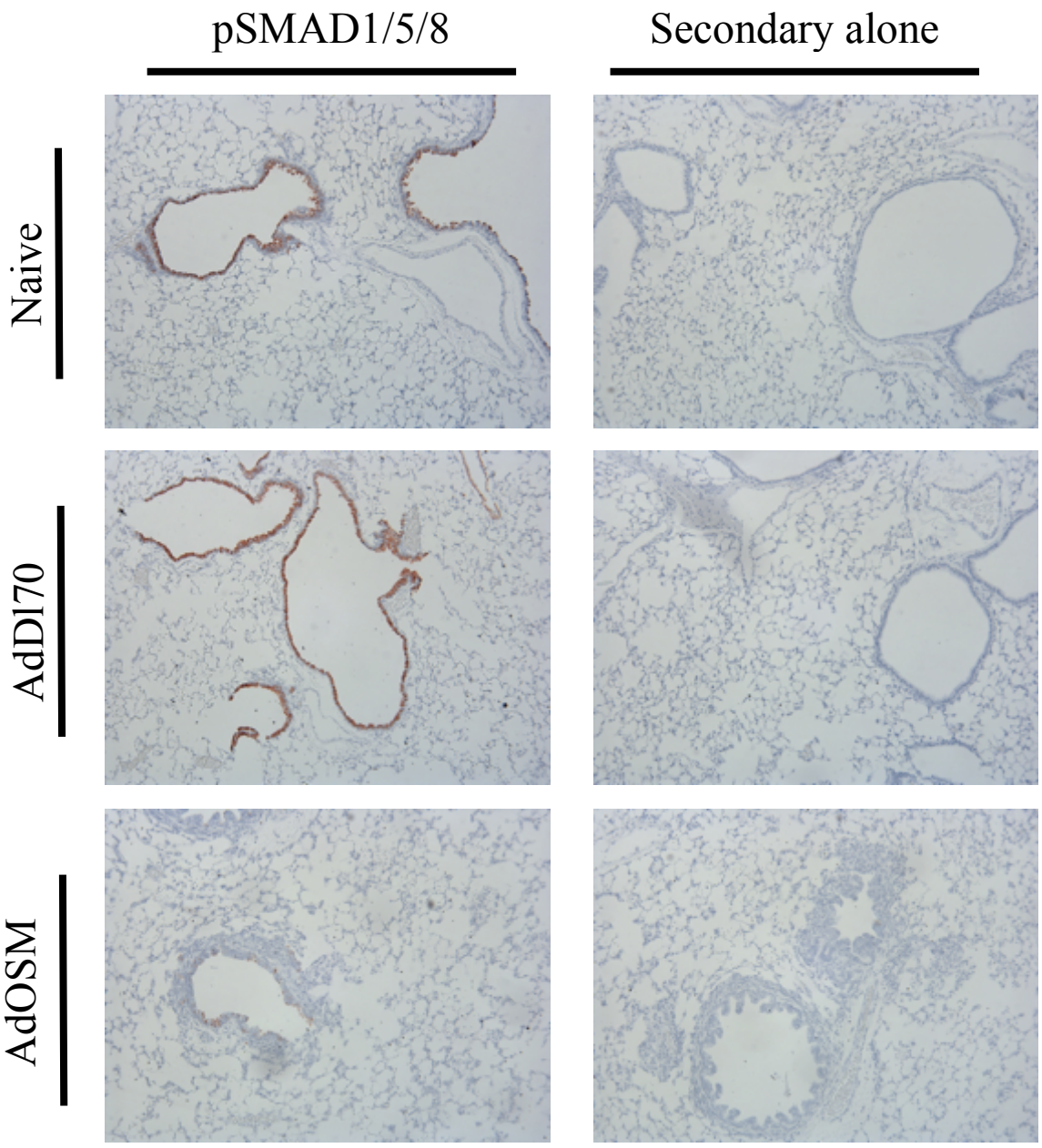

Figure 21B

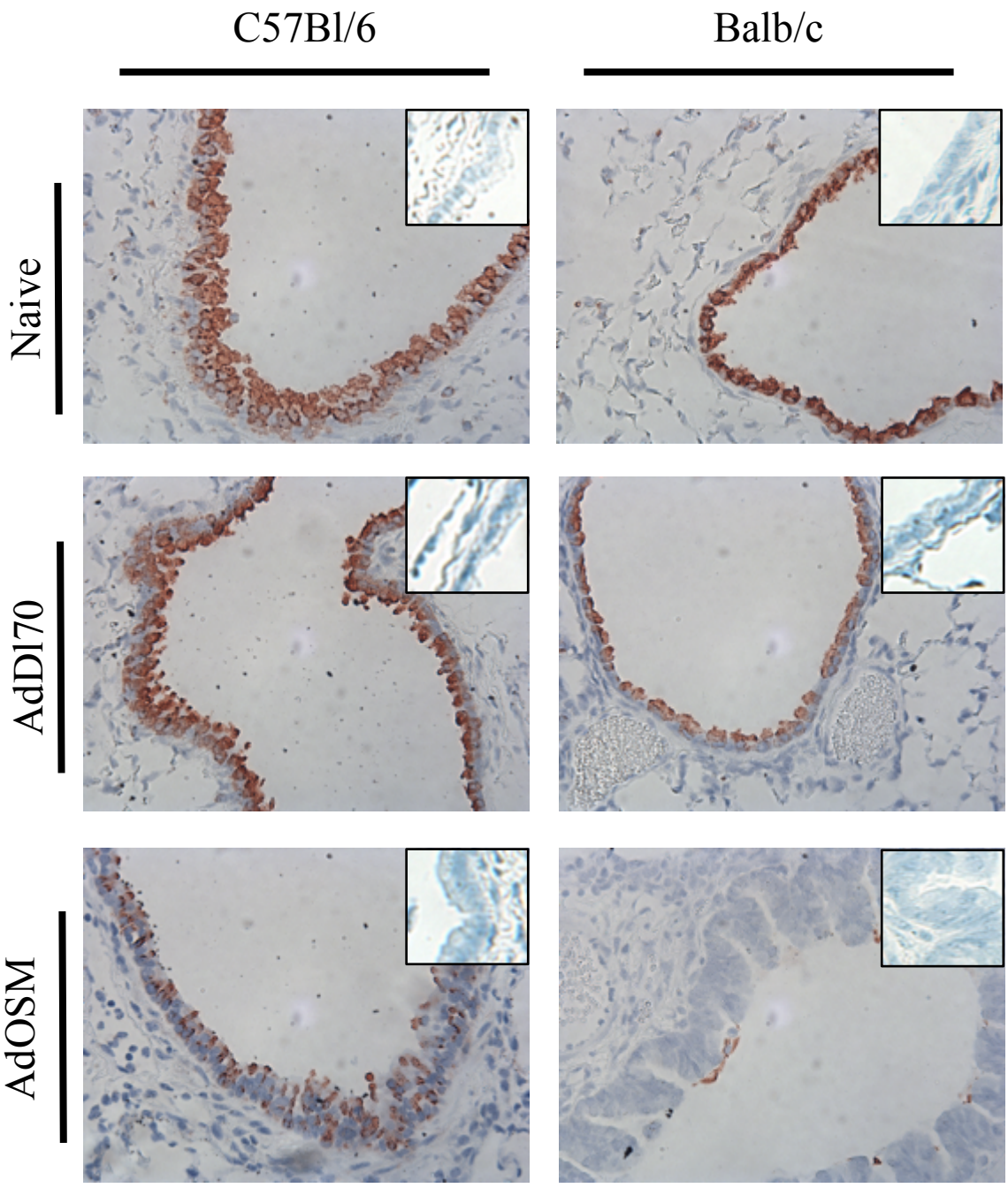

Figure 21C

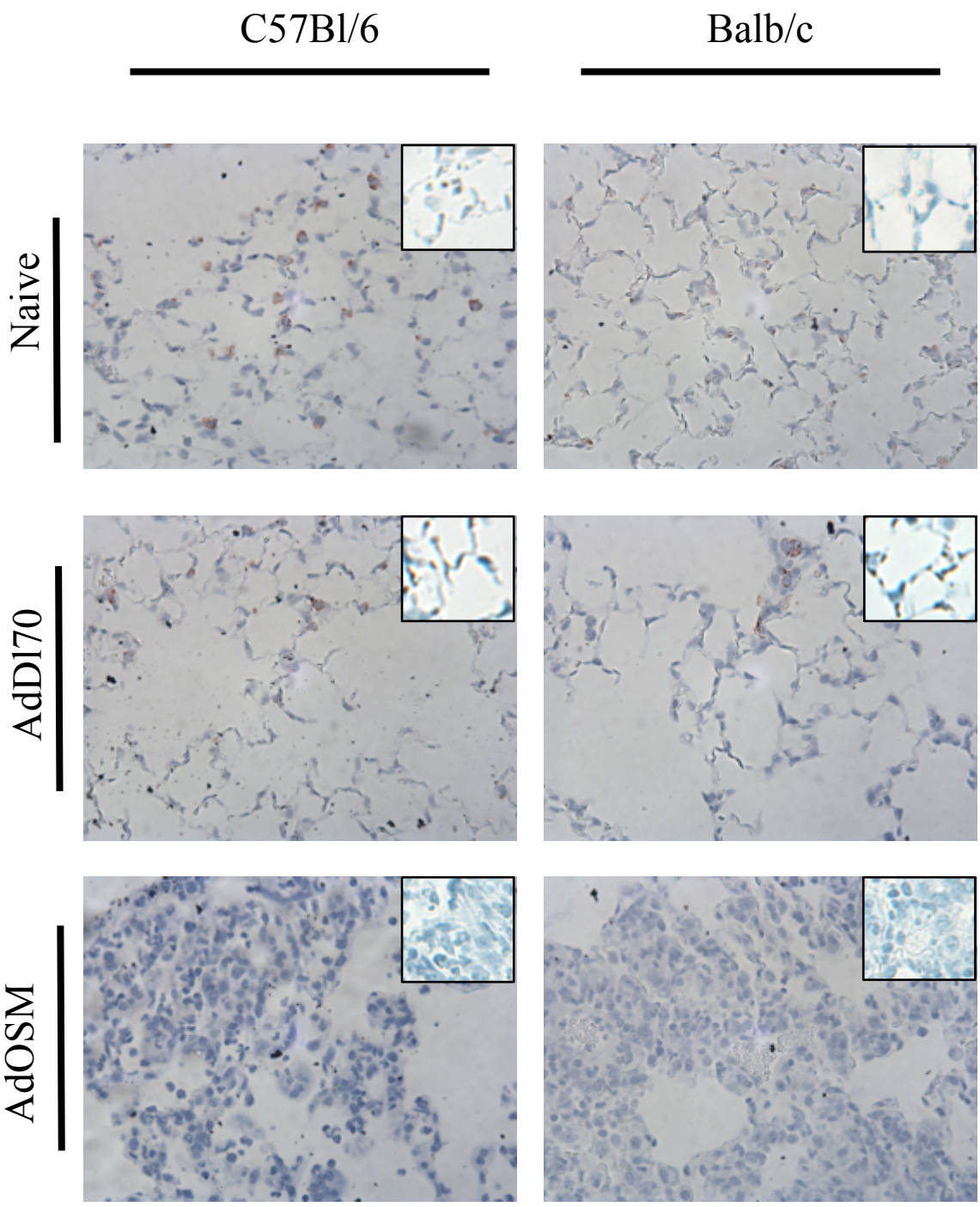

Figure 21D

Figure 22: BALB/c mice were endotracheally administered $5x10^7$ pfu of AdOSM, $5x10^7$ pfu of AdDl70, or were left untreated (n=3 per treatment). Mice were culled after two days. The left lung of each mouse was fixed in 10% formalin and paraffin-embedded. IHC was conducted on lung sections for pSMAD1/5/8. One representative mouse is shown per group using the 20x objective lenses

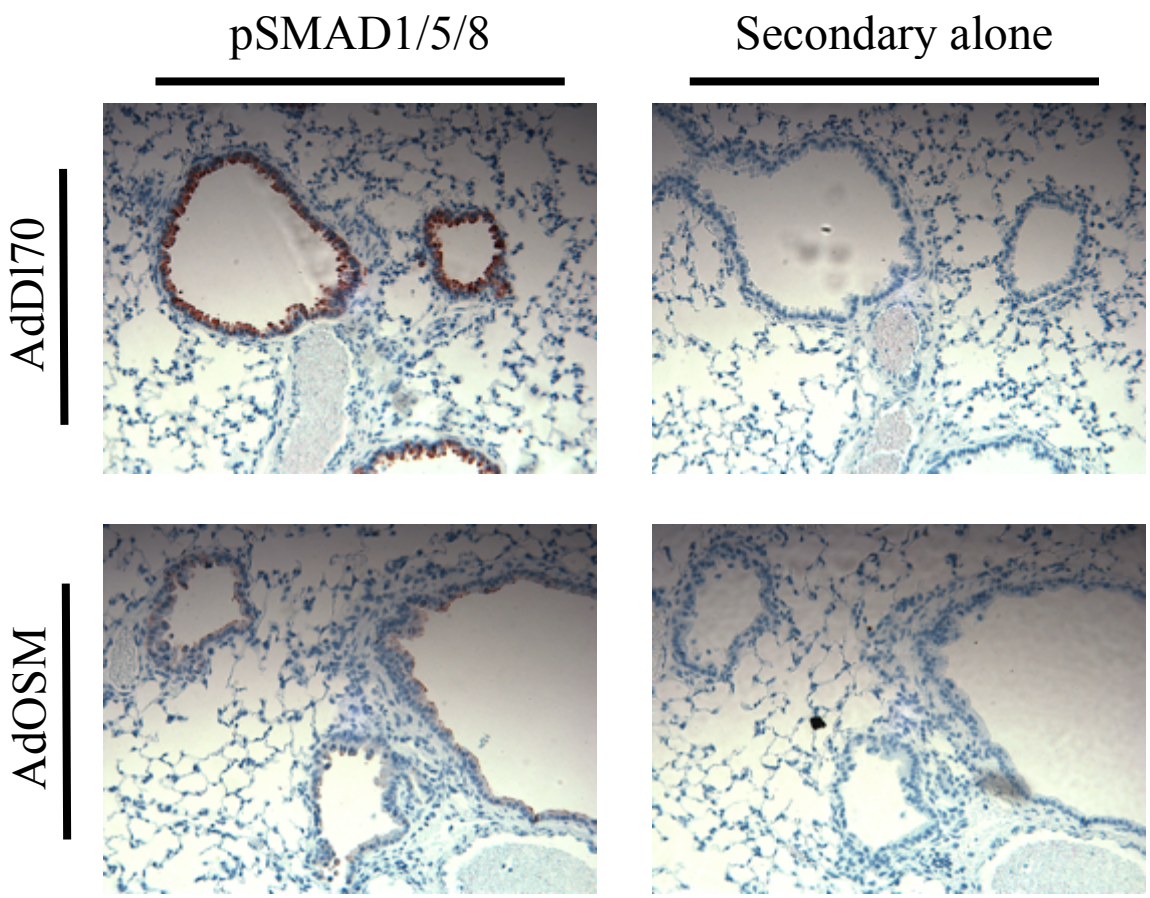

Figure 22

Figure 23: Age-matched C57Bl/6 and BALB/c mice were endotracheally administered $5x10^7$ pfu of AdOSM or control vector AdDl70. Naïve mice from both strains were also kept as a control group. Mice were culled after seven days. The left lung of each mouse was fixed in 10% formalin and paraffin-embedded. IHC was conducted on lung slice for pSMAD2.

A: Overview of pSMAD1/5/8 staining in AdOSM, AdDl70, and naïve C57Bl/6 mice using a 5x objective lenses. One representative mouse is shown per group.

B: Overview of pSMAD1/5/8 staining in AdOSM, AdDl70, and naïve BALB/c mice using a 5x objective lenses. One representative mouse is shown per group.

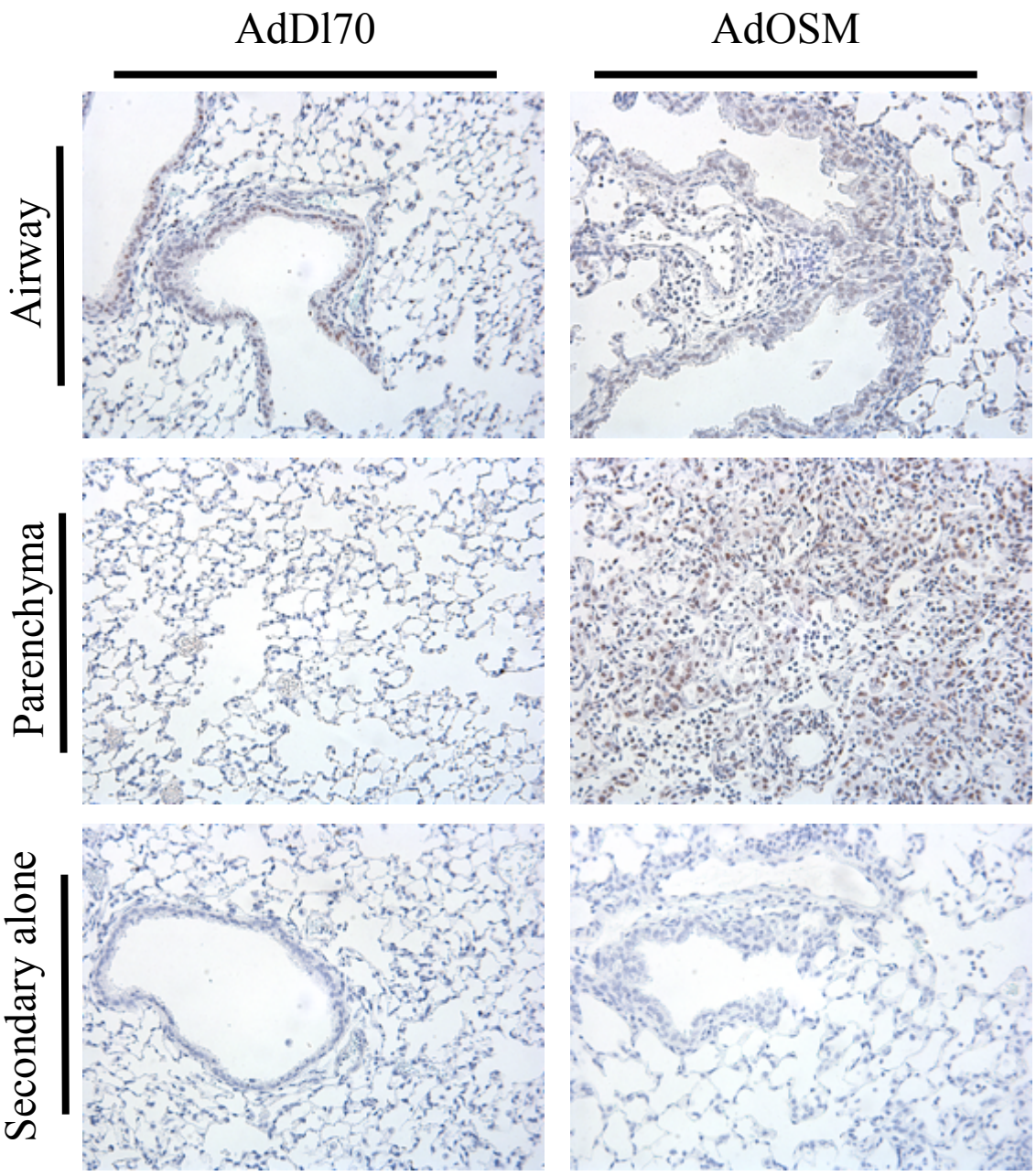

Figure 23A

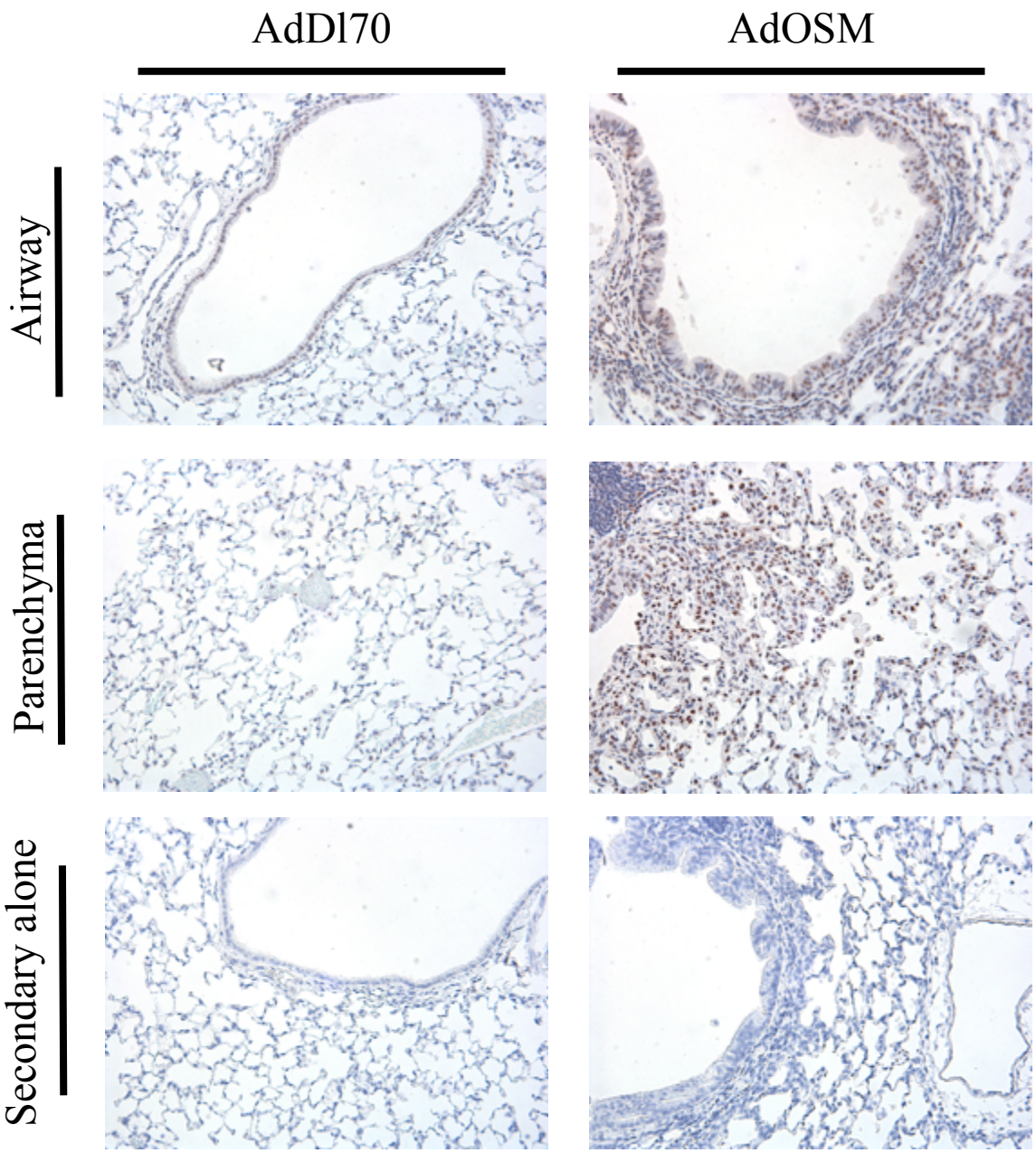

Figure 23B

Figure 24: Stimulation of subconfluent C57Bl/6 MLF cultures with 5 ng/mL mOSM in MEMF15 media containing 10% FBS over a time course of 0, 0.5, 1, 2, 4, and 6 hours. C57Bl/6 MLF cultures were also treated with 50 ng/mL BMP2, 5 ng/mL TGF-β, and combinations of OSM, BMP2, and TGF-β for 1 hour. Cell lysates were collected and probed for pSMAD1/5, SMAD1, pSMAD2, pSTAT3, and actin (A). Densitometry was carried out to quantify band intensity, corrected to actin, and expressed relative to untreated cells (B-E)

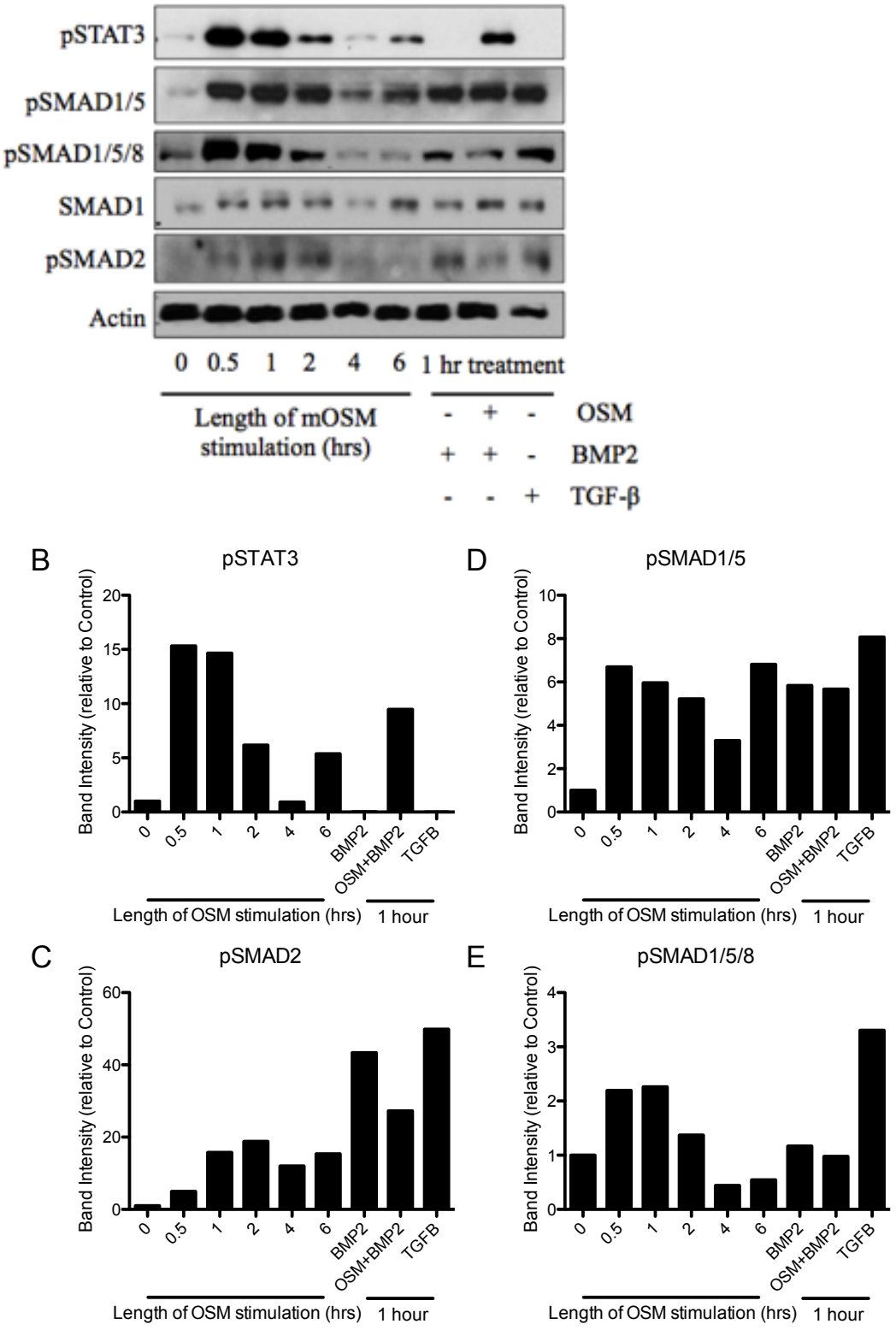
pSTAT3
pSMAD1/5
pSMAD1/5/8
SMAD1
pSMAD2
Actin
0 0.5 1 2 4 6 1 hr treatment
Length of mOSM stimulation (hrs)
- + - OSM
+ + - BMP2
- - + TGF-β
B
pSTAT3
Band Intensity (relative to Control)
0 0.5 1 2 4 6 BMP2 OSM+BMP2 TGFB
Length of OSM stimulation (hrs) 1 hour
D
pSMAD1/5
Band Intensity (relative to Control)
0 0.5 1 2 4 6 BMP2 OSM+BMP2 TGFB
Length of OSM stimulation (hrs) 1 hour
C
pSMAD2
Band Intensity (relative to Control)
0 0.5 1 2 4 6 BMP2 OSM+BMP2 TGFB
Length of OSM stimulation (hrs) 1 hour
E
pSMAD1/5/8
Band Intensity (relative to Control)
0 0.5 1 2 4 6 BMP2 OSM+BMP2 TGFB
Length of OSM stimulation (hrs) 1 hour

Figure 24

Figure 25: Stimulation of subconfluent BALB/c MLF cells with 5 ng/mL mOSM in MEMF15 media containing 10% FBS over a time course of 0, 0.5, 1, 2, 4, and 6 hours. BALB/c MLF were also treated with 50 ng/mL BMP2, 5 ng/mL TGF-β, and combinations of OSM, BMP2, and TGF-β for 1 hour. Cell lysates were collected and probed for pSMAD1/5, pSMAD1/5/8, SMAD1, pSTAT2, pSMAD2, and actin (A). Densitometry was carried out to quantify band intensity, corrected to actin, and expressed relative to untreated cells (B-E)

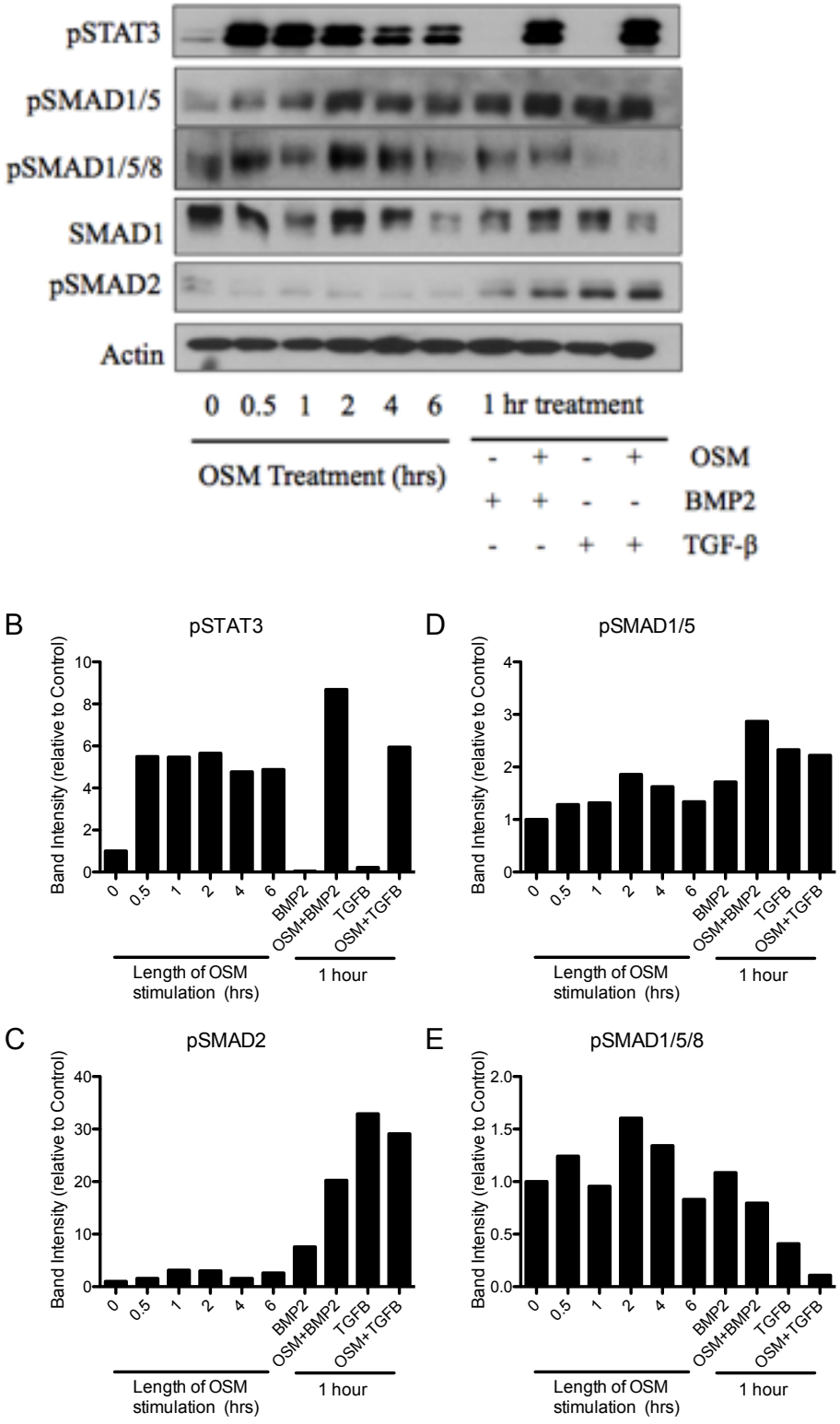
pSTAT3
pSMAD1/5
pSMAD1/5/8
SMAD1
pSMAD2
Actin
0 0.5 1 2 4 6
OSM Treatment (hrs)
1 hr treatment
- + - + OSM
+ + - - BMP2
- - + + TGF-β
B
pSTAT3
Band Intensity (relative to Control)
0 0.5 1 2 4 6 BMP2 OSM+BMP2 TGFB OSM+TGFB
Length of OSM stimulation (hrs)
1 hour
D
pSMAD1/5
Band Intensity (relative to Control)
0 0.5 1 2 4 6 BMP2 OSM+BMP2 TGFB OSM+TGFB
Length of OSM stimulation (hrs)
1 hour
C
pSMAD2
Band Intensity (relative to Control)
0 0.5 1 2 4 6 BMP2 OSM+BMP2 TGFB OSM+TGFB
Length of OSM stimulation (hrs)
1 hour
E
pSMAD1/5/8
Band Intensity (relative to Control)
0 0.5 1 2 4 6 BMP2 OSM+BMP2 TGFB OSM+TGFB
Length of OSM stimulation (hrs)
1 hour

Figure 25

Figure 26: Stimulation of subconfluent C57Bl/6 MLF cells with 5 ng/mL mOSM, 50 ng/mL of BMP2, 5 ng/mL TGF-β, and combinations of these three cytokines in MEMF15 media containing 10% FBS for 1 day and 3 days. Cell lysates were collected and probed for pSTAT3, pSMAD1/5, pSMAD1/5/8, SMAD1, BMPR2, pSMAD2 and actin (A). Densitometry was carried out to quantify band intensity, corrected to actin, and expressed relative to untreated cells (B-F)

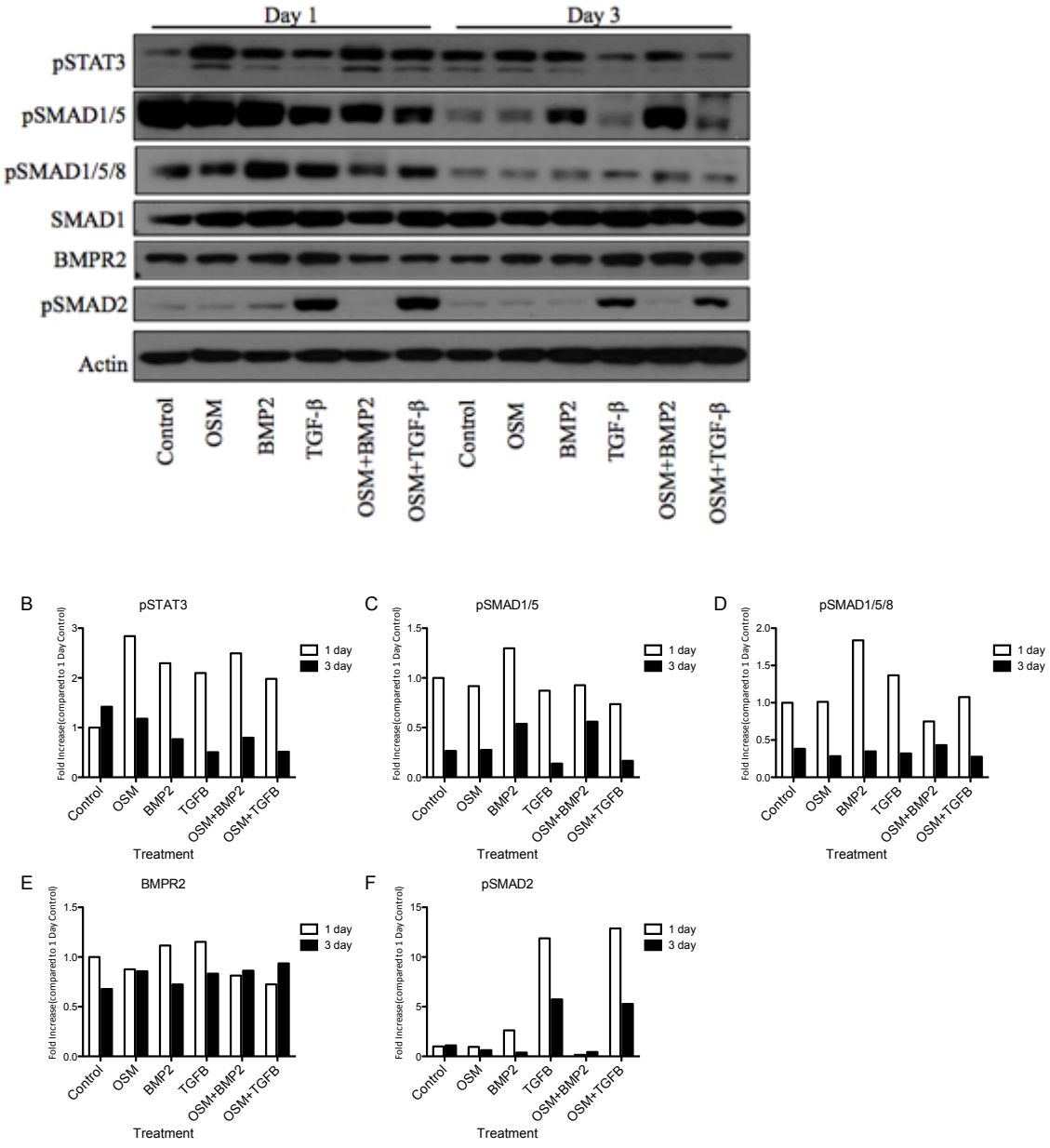
Day 1
Day 3
pSTAT3
pSMAD1/5
pSMAD1/5/8
SMAD1
BMPR2
pSMAD2
Actin
Control
OSM
BMP2
TGF-β
OSM+BMP2
OSM+TGF-β
B
pSTAT3
C
pSMAD1/5
D
pSMAD1/5/8
E
BMPR2
F
pSMAD2
Fold Increase(compared to 1 Day Control)
1 day
3 day
Control
OSM
BMP2
TGFB
OSM+BMP2
OSM+TGFB
Treatment

Figure 26

Figure 27: Stimulation of subconfluent BALB/c MLF cells with 5 ng/mL mOSM, 50 ng/mL of BMP2, 5 ng/mL TGF-β, and combinations of these three cytokines in MEMF15 media containing 10% FBS for 1 day and 3 days. Cell lysates were collected and probed for pSTAT3, pSMAD1/5, pSMAD1/5/8, SMAD1, BMPR2, pSMAD2 and actin (A). Densitometry was carried out to quantify band intensity, corrected to actin, and expressed relative to untreated cells (B-F)

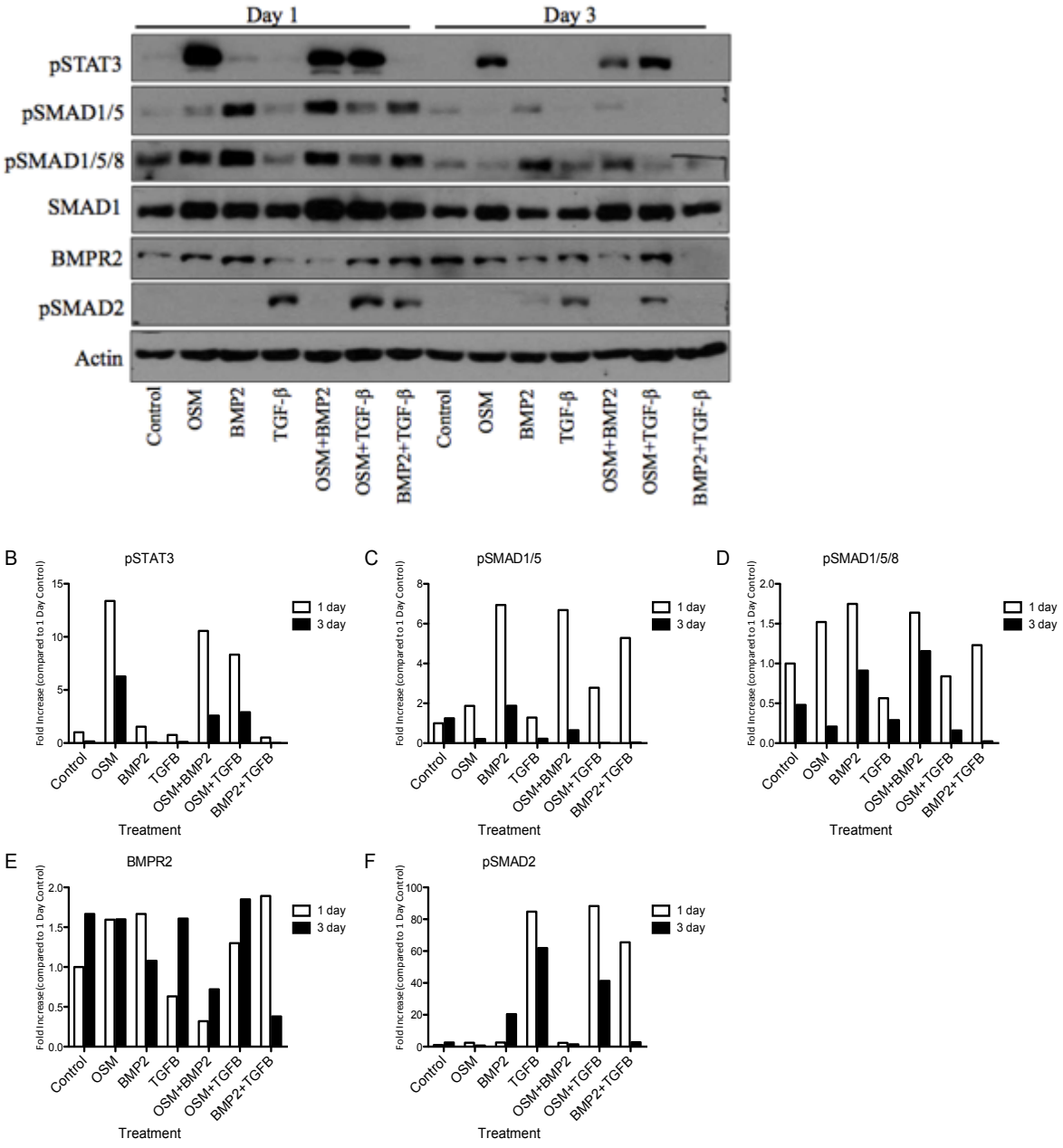
Day 1
Day 3
pSTAT3
pSMAD1/5
pSMAD1/5/8
SMAD1
BMPR2
pSMAD2
Actin
Control
OSM
BMP2
TGF-β
OSM+BMP2
OSM+TGF-β
BMP2+TGF-β
B
pSTAT3
C
pSMAD1/5
D
pSMAD1/5/8
E
BMPR2
F
pSMAD2
Fold Increase (compared to 1 Day Control)
1 day
3 day
Control
OSM
BMP2
TGFB
OSM+BMP2
OSM+TGFB
BMP2+TGFB
Treatment

Figure 27

Figure 28: Stimulation of Beas 2B cells with 5 ng/mL OSM, 50 ng/mL of BMP2, 5 ng/mL TGF-β, and combinations of these three cytokines in LHC-9 media containing 10% FBS for 1 hour. Cell lysates were collected and probed for pSTAT3, SMAD1/5, pSMAD1/5/8, SMAD1, pSMAD2, BMPR2 and actin (A). Densitometry was carried out to quantify band intensity, corrected to actin, and expressed relative to untreated cells (B-F)

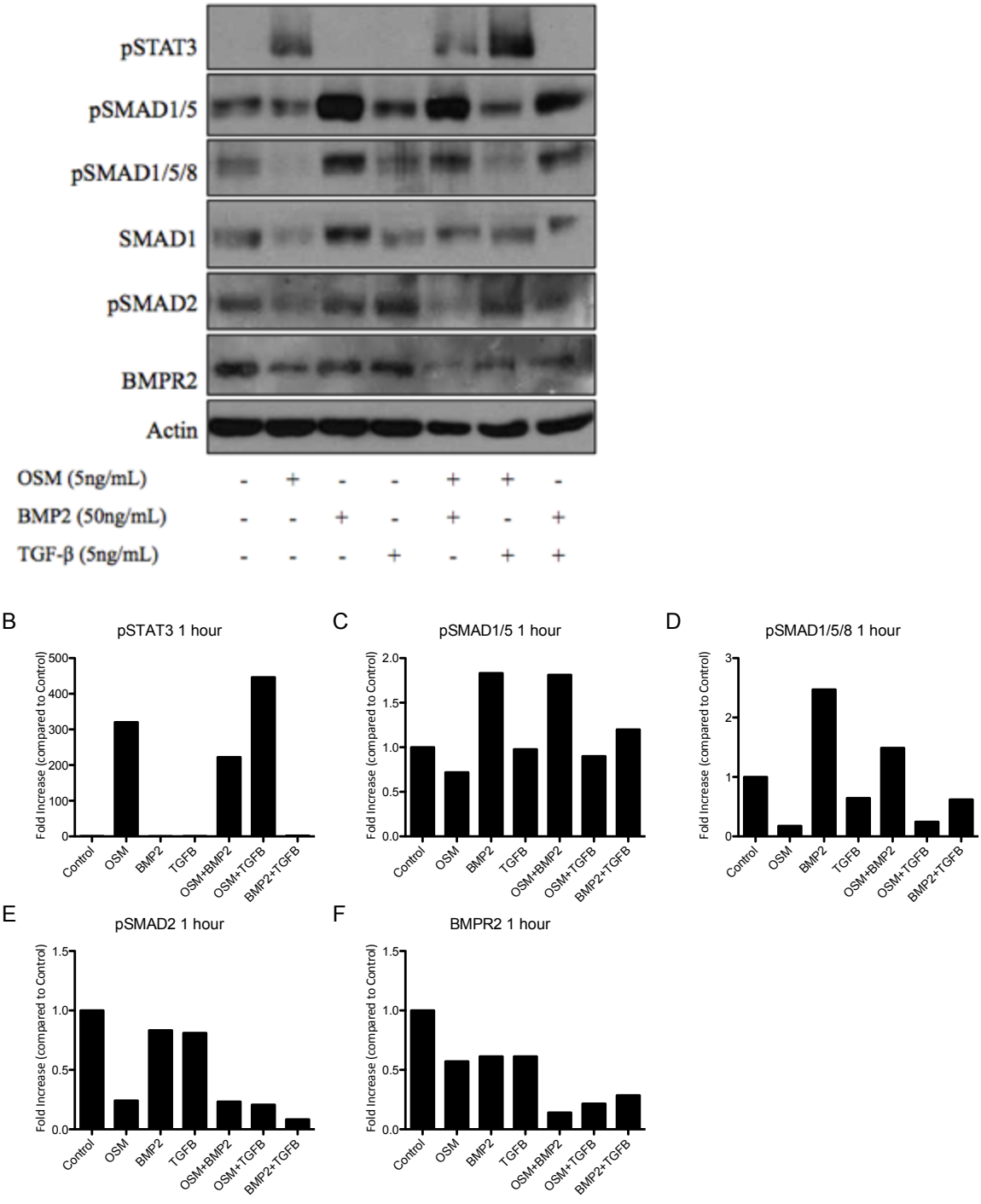
pSTAT3
pSMAD1/5
pSMAD1/5/8
SMAD1
pSMAD2
BMPR2
Actin
OSM (5ng/mL) - + - - + + -
BMP2 (50ng/mL) - - + - + - +
TGF-β (5ng/mL) - - - + - + +
B
pSTAT3 1 hour
C
pSMAD1/5 1 hour
D
pSMAD1/5/8 1 hour
E
pSMAD2 1 hour
F
BMPR2 1 hour
Fold Increase (compared to Control)
Control
OSM
BMP2
TGFB
OSM+BMP2
OSM+TGFB
BMP2+TGFB

Figure 28

Figure 29: Stimulation of Beas 2B cells with 5 ng/mL OSM, 50 ng/mL of BMP2, 5 ng/mL TGF-β, and combinations of these three cytokines in LHC-9 media containing 10% FBS for 1 day. Cell lysates were collected and probed for pSTAT3, SMAD1/5, pSMAD1/5/8, SMAD1, pSMAD2, BMPR2 and actin (A). Densitometry was carried out to quantify band intensity, corrected to actin, and expressed relative to untreated cells (B-F)

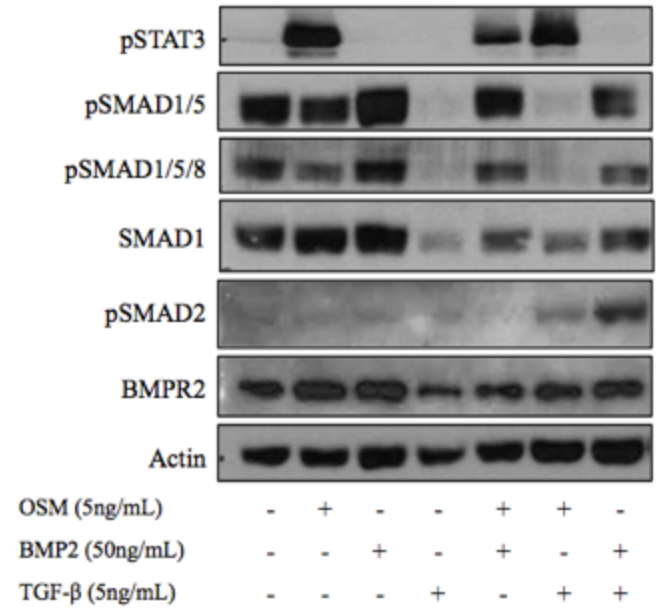
pSTAT3
pSMAD1/5
pSMAD1/5/8
SMAD1
pSMAD2
BMPR2
Actin
OSM (5ng/mL) - + - - + + -
BMP2 (50ng/mL) - - + - + - +
TGF-β (5ng/mL) - - - + - + +

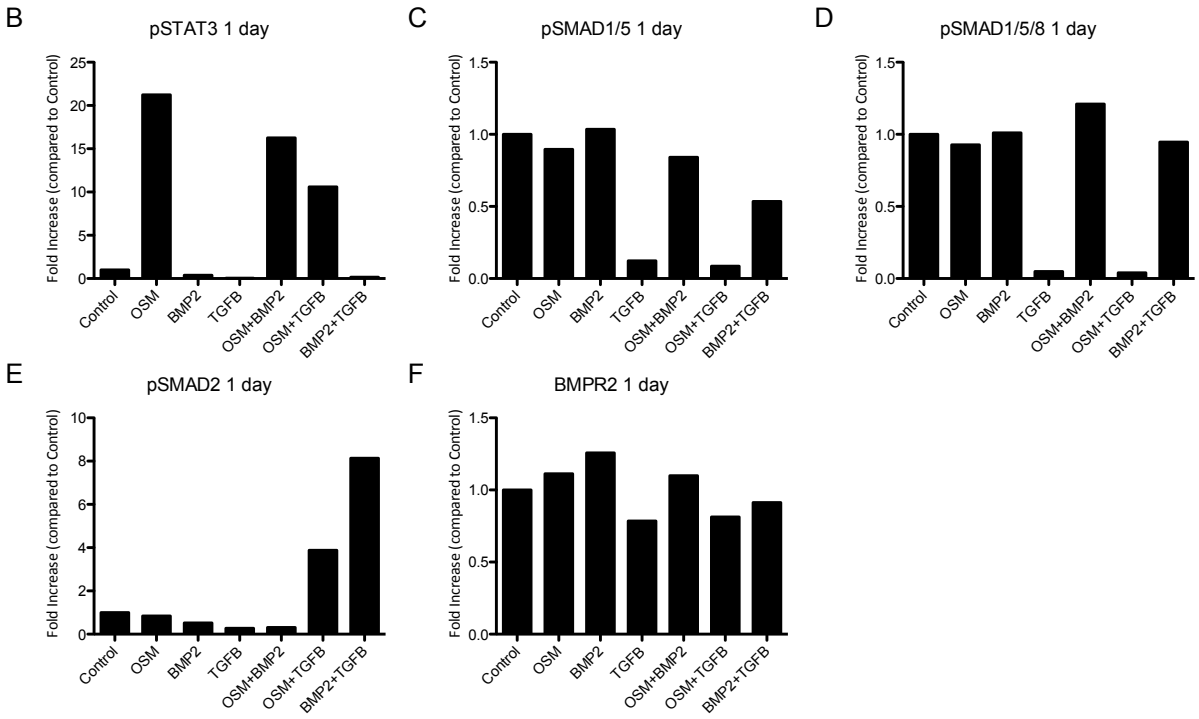
B
pSTAT3 1 day
C
pSMAD1/5 1 day
D
pSMAD1/5/8 1 day
E
pSMAD2 1 day
F
BMPR2 1 day
Fold Increase (compared to Control)
Control
OSM
BMP2
TGFB
OSM+BMP2
OSM+TGFB
BMP2+TGFB

Figure 29

Figure 30: Stimulation of A549 cells with 5 ng/mL OSM, 50 ng/mL of BMP2, 5 ng/mL TGF-β, and combinations of these three cytokines in α-MEM media containing 10% FBS for 1 hour. Cell lysates were collected and probed for pSTAT3, SMAD1/5, pSMAD1/5/8, SMAD1, pSMAD2, and actin (A). Densitometry was carried out to quantify band intensity, corrected to actin, and expressed relative to untreated cells (B-E)

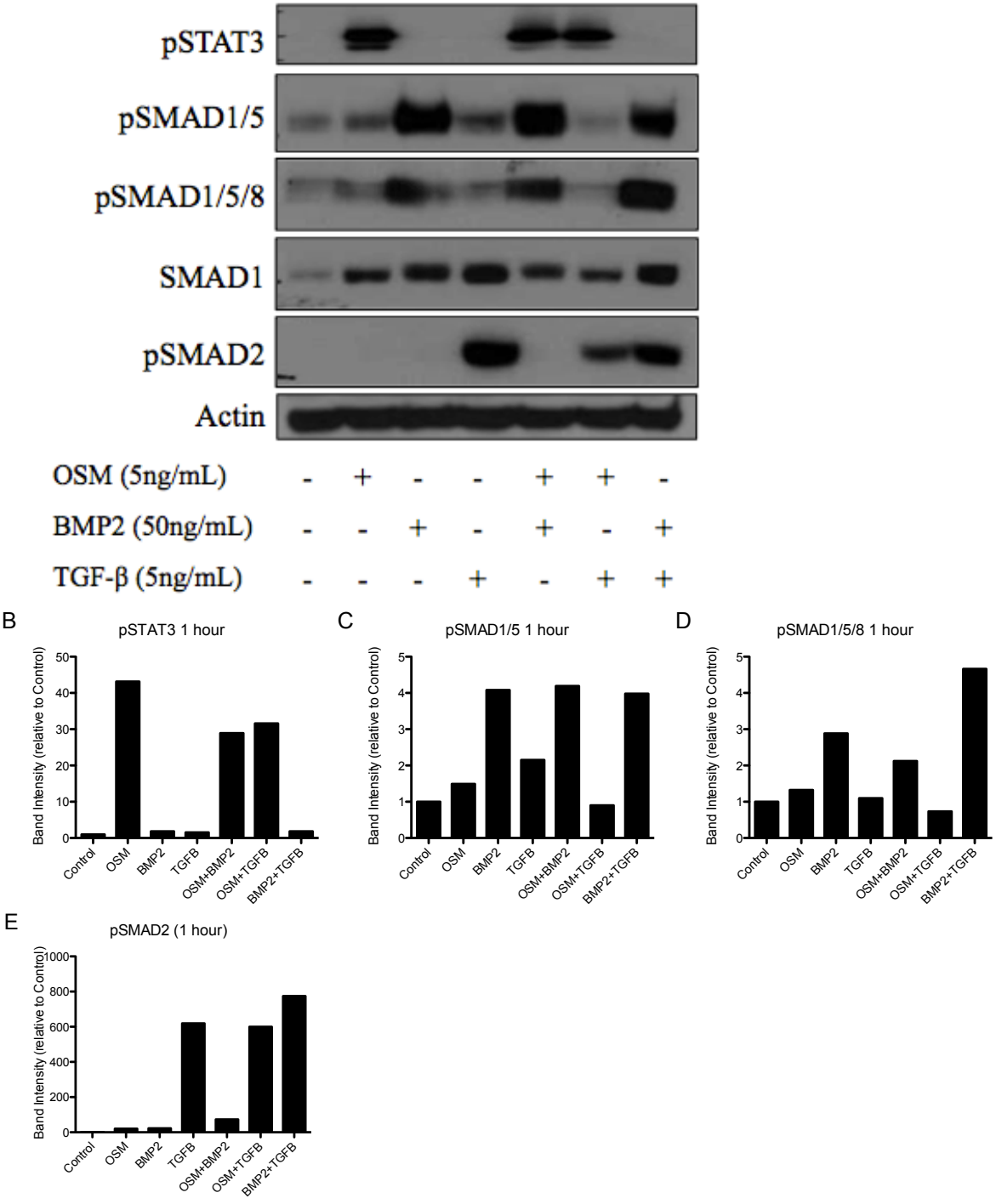
pSTAT3
pSMAD1/5
pSMAD1/5/8
SMAD1
pSMAD2
Actin
OSM (5ng/mL) - + - - + + -
BMP2 (50ng/mL) - - + - + - +
TGF-β (5ng/mL) - - - + - + +
B
pSTAT3 1 hour
C
pSMAD1/5 1 hour
D
pSMAD1/5/8 1 hour
E
pSMAD2 (1 hour)
Band Intensity (relative to Control)
Control
OSM
BMP2
TGFB
OSM+BMP2
OSM+TGFB
BMP2+TGFB

Figure 30

Figure 31: Stimulation of A549 cells with 5 ng/mL OSM, 50 ng/mL of BMP2, 5 ng/mL TGF-β, and combinations of these three cytokines in α-MEM media containing 10% FBS for 1 day. Cell lysates were collected and probed for pSTAT3, SMAD1/5, pSMAD1/5/8, SMAD1, pSMAD2, and actin (A). Densitometry was carried out to quantify band intensity, corrected to actin, and expressed relative to untreated cells (B-E)

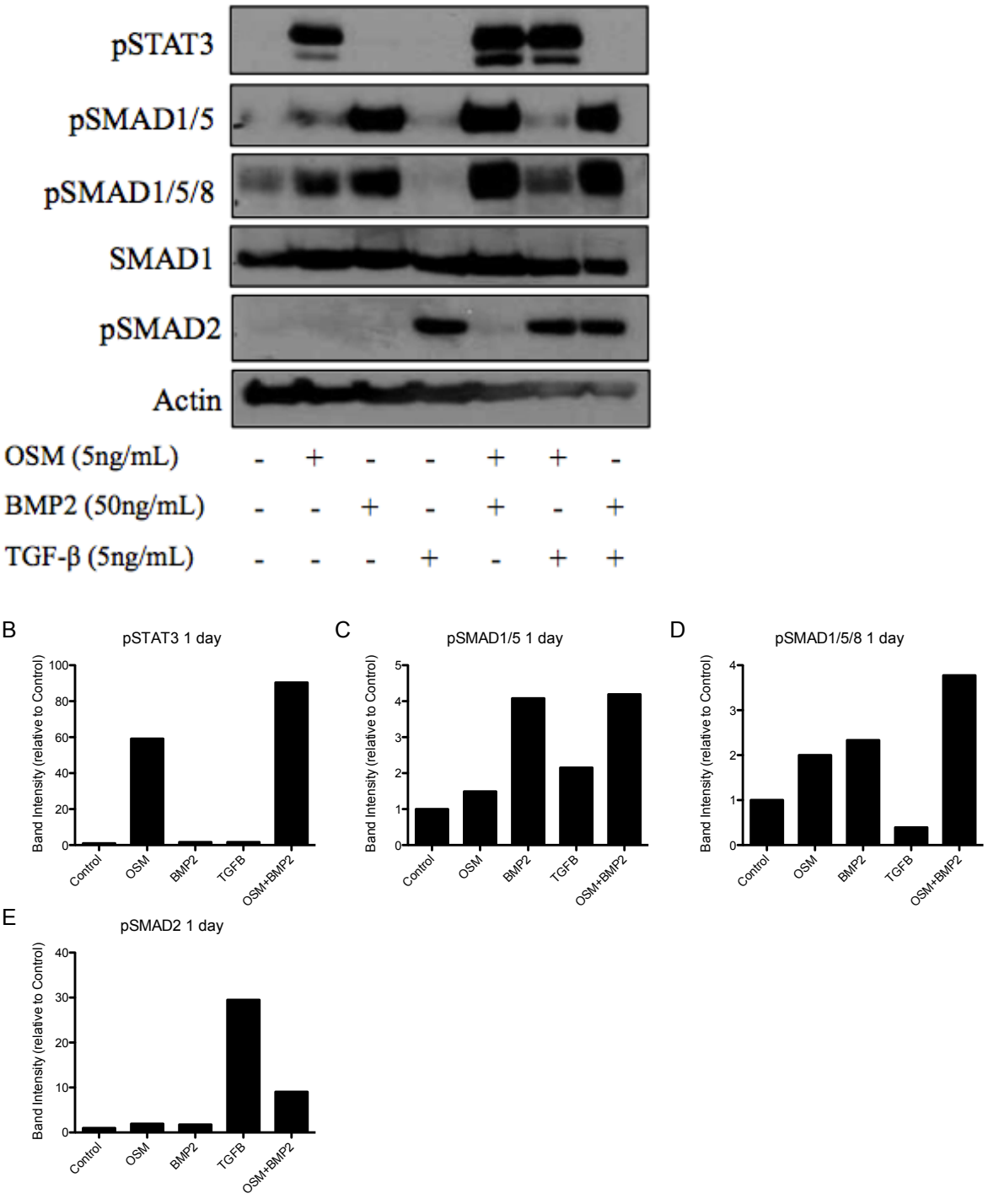
pSTAT3
pSMAD1/5
pSMAD1/5/8
SMAD1
pSMAD2
Actin
OSM (5ng/mL) - + - - + + -
BMP2 (50ng/mL) - - + - + - +
TGF-β (5ng/mL) - - - + - + +
B
pSTAT3 1 day
C
pSMAD1/5 1 day
D
pSMAD1/5/8 1 day
E
pSMAD2 1 day
Band Intensity (relative to Control)
Control
OSM
BMP2
TGFB
OSM+BMP2

Figure 31

Figure 32: Stimulation of C10 type two pneumocytes with 5 ng/mL OSM, 50 ng/mL of BMP2, 5 ng/mL TGF-β, and combinations of these three cytokines in RPMI media containing 10% FBS for one hour. Cell lysates were collected and probed for pSTAT3, SMAD1/5, pSMAD1/5/8, SMAD1, pSMAD2, and actin (A). Densitometry was carried out to quantify band intensity, corrected to actin, and expressed relative to untreated cells (B-E)

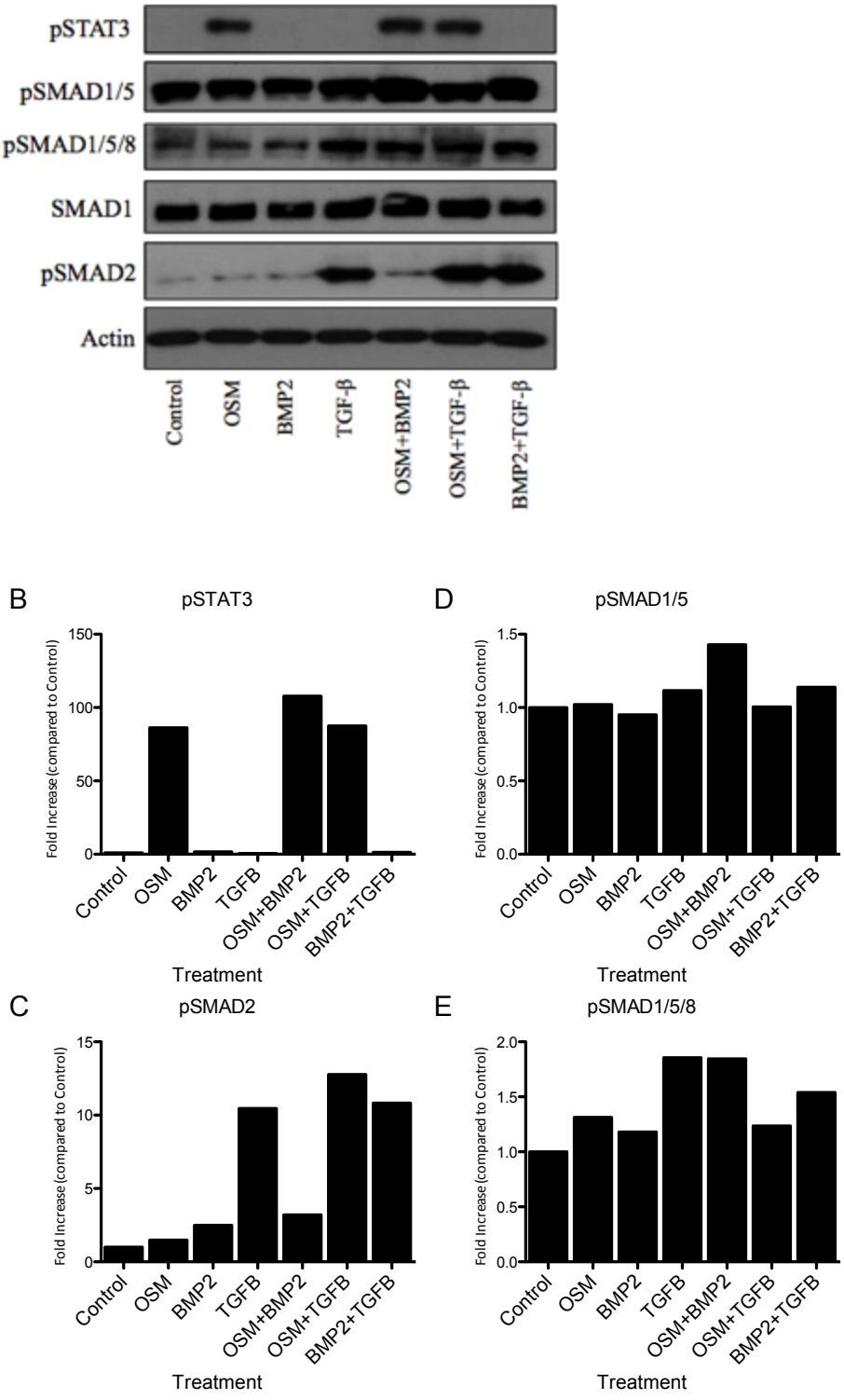
pSTAT3
pSMAD1/5
pSMAD1/5/8
SMAD1
pSMAD2
Actin
Control
OSM
BMP2
TGF-β
OSM+BMP2
OSM+TGF-β
BMP2+TGF-β
B
pSTAT3
Fold Increase (compared to Control)
150
100
50
0
Control
OSM
BMP2
TGFB
OSM+BMP2
OSM+TGFB
BMP2+TGFB
Treatment
D
pSMAD1/5
Fold Increase (compared to Control)
1.5
1.0
0.5
0.0
Control
OSM
BMP2
TGFB
OSM+BMP2
OSM+TGFB
BMP2+TGFB
Treatment
C
pSMAD2
Fold Increase (compared to Control)
15
10
5
0
Control
OSM
BMP2
TGFB
OSM+BMP2
OSM+TGFB
BMP2+TGFB
Treatment
E
pSMAD1/5/8
Fold Increase (compared to Control)
2.0
1.5
1.0
0.5
0.0
Control
OSM
BMP2
TGFB
OSM+BMP2
OSM+TGFB
BMP2+TGFB
Treatment

Figure 32

Figure 33: Stimulation of C10 type two pneumocytes with 5 ng/mL OSM, 50 ng/mL of BMP2, 5 ng/mL TGF-β, and combinations of these three cytokines in RPMI media containing 10% FBS for 24 or 72 hours. Cell lysates were collected and probed for pSTAT3, SMAD1/5, pSMAD1/5/8, SMAD1, BMPR2, pSMAD2, and actin (A). Densitometry was carried out to quantify band intensity, corrected to actin, and expressed relative to untreated cells (B-E)

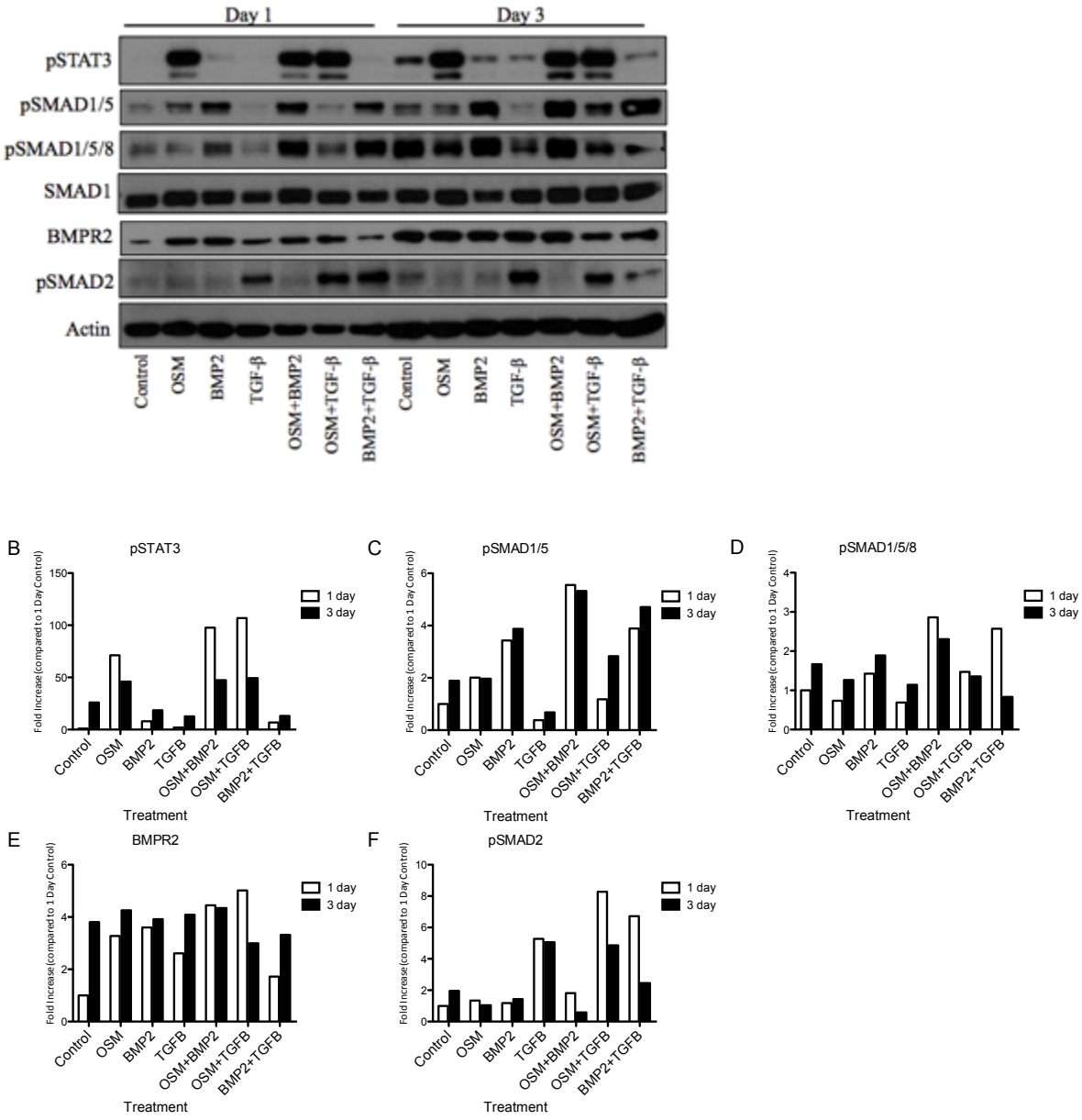
Day 1
Day 3
pSTAT3
pSMAD1/5
pSMAD1/5/8
SMAD1
BMPR2
pSMAD2
Actin
Control
OSM
BMP2
TGF-β
OSM+BMP2
OSM+TGF-β
BMP2+TGF-β
B
pSTAT3
C
pSMAD1/5
D
pSMAD1/5/8
E
BMPR2
F
pSMAD2
Fold Increase (compared to 1 Day Control)
1 day
3 day
Control
OSM
BMP2
TGFB
OSM+BMP2
OSM+TGFB
BMP2+TGFB
Treatment

Figure 33

CHAPTER 6: Discussion

6.1 Summary of Findings

The data collected *in vivo* demonstrate that endotracheal administration of the AdOSM vector induced rapid lung ECM remodeling by seven days in BALB/c mice as effectively as in C57Bl/6 mice, despite BALB/c mice being relatively fibrosis-resistant in the bleomycin and AdTGF-β model of lung ECM accumulation. The lung pathology of AdOSM-treated mice was characterized by thicker alveolar septa and airway epithelial cell hyperplasia (**Fig. 1**), as well as an accumulation of parenchymal collagen (**Fig. 3A**). Furthermore, morphological changes to the airway, but not the lung parenchyma, remained apparent in AdOSM-treated BALB/c mice after 28 days (**Fig. 6**). AdOSM-treated mice after seven days had elevated levels of IL-6 and KC protein (**Fig. 4B-C**) in the BALF, elevated levels of steady state mRNA for TIMP1 and gremlin, but decreased levels of α-SMA steady state mRNA (**Fig. 5A-C**). Although OSM increased steady state mRNA levels of gremlin in MLF cultures, there was no consistent regulation by OSM of collagen 1a1, collagen 1a2, fibronectin, nor α-SMA steady state mRNA (**Fig. 8-9**). This suggests that OSM does not directly induce myofibroblast differentiation nor modulates ECM remodeling in resident lung fibroblasts, and that other cell types such as fibrocytes, epithelial cells, and endothelial cells may be involved in OSM-induced ECM remodeling.

OSM overexpression induced lung ECM remodeling in the absence of IL-6 (**Fig. 10**), which suggests that IL-6 associated inflammation is not required. OSM-induced ECM remodeling also did not require SMAD3 (**Fig. 15**) as PSR staining was similar between AdOSM-treated knockout and wildtype mice, suggesting that other mechanisms

than TGF-β are involved in OSM-induced ECM remodeling. Although the TGF-β-SMAD2 signaling axis was not altered in total in lung homogenates of AdOSM-treated mice (**Fig. 19C**), there was an elevation of the STAT3 (**Fig. 19B**) and suppression of the SMAD1 (**Fig. 19D-E**) pathway, and SMAD1 reduction could be localized to airway epithelial cells by IHC (**Fig. 21C**).

In cell culture systems, OSM induced STAT3 phosphorylation while TGF-β induced SMAD2 phosphorylation in MLF cultures from C57Bl/6 (**Fig. 24B-C**) and BALB/c mice (**Fig. 25B-C**), Beas 2B airway epithelial cells (**Fig. 28B**), A549 cells (**Fig. 30B** and **Fig. 30E**), and C10 type two pneumocytes (**Fig. 32B-C**). While BMP2 induced SMAD1 phosphorylation in MLF cultures (**Fig. 26C** and **Fig. 27C**), Beas 2B airway epithelial cells (**Fig. 28C**), A549 cells (**Fig. 30C**), and C10 type two pneumocytes (**Fig. 33C**), OSM stimulation suppressed the SMAD1 pathway in C10 pneumocytes (**Fig. 33D**) and Beas 2B airway epithelial cells (**Fig. 28C**), particularly when corrected to SMAD1. Furthermore, OSM induced the steady state mRNA expression of the BMP antagonist gremlin in both C57Bl/6 and BALB/c MLF cultures (**Fig. 8E** and **Fig. 9E**).

6.2 OSM-induced ECM remodeling in C57Bl/6 mice

Transient OSM overexpression induced lung ECM remodeling in C57BL/6 mice by seven days, as seen through histologic analyses (**Fig. 1**), assessment of PSR-stained lung (**Fig. 3A**), and hydroxyproline assay (**Fig. 3B**). This is consistent with previous results of Fritz *et al*., 2011[126]. Fritz *et al.*, 2011 also showed parenchymal staining for α-SMA by IHC in AdOSM-treated C57Bl/6 mice after seven days, suggesting the presence of myofibroblasts that contribute to the accumulation of the ECM in the parenchyma[126].

The observation that steady state mRNA levels of α-SMA were decreased in AdOSM-treated C57Bl/6 mouse lung homogenates at day seven was unexpected (**Fig. 5A**). One explanation for this inverse correlation between mRNA and protein levels of α-SMA is that steady state mRNA levels for α-SMA may have peaked at an earlier time point in this model. Moreover, an analysis of BALF indicated that levels of IL-6 (**Fig. 4B**) and KC (**Fig. 4C**) were elevated in AdOSM-treated C57Bl/6 mice. IL-6, along with having inflammatory properties, has also been shown to contribute to ECM remodeling through regulating fibroblast proliferation, whereas KC, a mouse homolog of human IL-8, has been shown to act as a neutrophil chemoattractant[147,148]. Efforts were made to further characterize the AdOSM model in C57Bl/6 mice to determine how OSM overexpression induces ECM remodeling. Unpublished data from the Richards laboratory showed that AdOSM-treated C57Bl/6 mice have increased CD45+col1+ cells in the lung after seven days, suggesting the recruitment of fibrocytes that contribute to lung ECM accumulation. To explore chemotactic factors that may be responsible for driving fibrocyte recruitment into the lungs, MCP-5 was analyzed in the BALF and found to be elevated in AdOSM-treated C57Bl/6 mice after seven days (**Fig. 4E**). This provides one possible mechanism as to how OSM overexpression induces ECM remodeling in C57Bl/6 mice.

Experiments were also completed *in vitro* using C57Bl/6 MLF cultures to supplement *in vivo* data. Despite previous work (Fritz *et al.*, 2011) and unpublished data collected in the Richards laboratory showing that total lung homogenates from AdOSM-treated C57Bl/6 mice have increased levels of collagen 1a1, collagen 1a2, and fibronectin steady state mRNA at both day five and seven, as well as increased α-SMA protein

staining in the lung parenchyma by day seven, C57Bl/6 MLF cell culture mRNA were not modulated in a similar fashion (**Fig. 8**)[126]. Surprisingly, TGF-β was also unable to induce steady state mRNA expression of fibronectin in C57Bl/6 MLF cultures after 24 hours stimulation, which has been previously reported in the literature (**Fig. 8B**)[149–151]. One possible explanation involves the culture conditions. Research from the Hinz lab and others show that tissue culture plastic has an extremely high stiffness that represents a damaged tissue environment[152,153]. Recent work from the Hinz group showed that stiff culture substrates can drive the differentiation of a fibroblast into a myofibroblast in the absence of TGF-β, raising the possibility that the MLF cultures used for experimentation may have an altered phenotype[152]. One suggestion for future work would be to grow fibroblasts on a less stiff culture substrate, such as silicone. An examination of responses of these fibroblasts to OSM may give a more accurate reflection of fibroblast cellular behavior *in vivo.* Another explanation for this data is that resident MLF do not modulate ECM as profoundly as other sources of myofibroblasts, including fibrocytes, epithelial cells, and endothelial cells. Alternatively, this data may indicate that OSM mediates collagen levels, at both the mRNA and protein level, through an indirect mechanism that likely involves other cytokines. Lastly, there is a possibility that the explant methodology used in the laboratory to isolate MLF cultures from mice results in a selection of a subpopulation of lung fibroblasts that are collagen 1+ and α-SMA+, where expanding cultures from lung tissue pieces is dependent on the outgrowth and adherence of proliferating MLF cells to tissue culture plastic. This coincides with research showing that human lung fibroblasts isolated from the parenchyma have increased TGF-β and α-

SMA expression compared to fibroblasts isolated from the proximal bronchi[53]. Thus, further experiments need to be carried out to further elucidate or verify the role of OSM on MLF cultures.

6.3 OSM-induced ECM remodeling in BALB/c mice

Responses to OSM overexpression were also examined in BALB/c mice and compared to C57Bl/6 mice, since BALB/c mice are more resistant to ECM remodeling than C57Bl/6 mice in both the bleomycin model as well as the AdTGF-β model of ECM remodeling[154,155]. BALB/c mice may be more resistant to bleomycin due to elevated levels of bleomycin hydrolase compared to C57Bl/6 mice[81]. This enzyme is responsible for inactivating the drug before it can carry out its' biological function. Other groups have also shown that active TGF-β becomes internalized for lysosome degradation in BALB/c 3T3 fibroblasts upon binding to the TGF-β receptor complex, thus attenuating TGF-β-elicited effects[156]. Since fibroblasts are an important cell population in the modulation of the ECM, this may explain why AdTGF-β-treated BALB/c mice are more resistant to ECM modeling compared to C57Bl/6 mice. In contrast to the bleomycin and AdTGF-β model of ECM remodeling, endotracheal administration of the same dosage of AdOSM ($5x10^7$ pfu) in C57Bl/6 mice induced similar histopathological effects as well as lung parenchymal collagen accumulation in BALB/c mice after seven days (**Fig. 1**). Taken together with immunoblot analysis on lung homogenates from AdOSM-treated BALB/c mice, which showed no regulation of the TGF-β-SMAD2/3 signaling axis (**Fig. 19C**), this data supports the notion that ECM remodeling and fibrosis can occur in certain conditions in the absence of TGF-β/SMAD3 signaling. One could speculate that targeting OSM may

present a potential therapeutic option for IPF patients who do not respond positively to TGF-β treatment although much analysis of human cells and tissue is required. Though this work was completed using mice, which do not spontaneously develop IPF, elevated levels of OSM have been reported in IPF patients and patients with pulmonary fibrosis arising from systemic sclerosis[122]. This study along with data from this thesis suggests a profibrotic role for OSM in lung ECM remodeling, even in the absence of TGF-β activity.

Data from the Richards laboratory show that like C57Bl/6 mice, AdOSM-treated BALB/c mice have increased CD45+col1+ cells in the lung by day seven, suggesting that the presence of fibrocytes in the lung that contribute to ECM remodeling. BALF from AdOSM-treated mice showed undetectable levels of MCP-5, unlike C57Bl/6 mice (**Fig. 4E**). One possible explanation for the differences in MCP-5 observed is that the kinetics of MCP-5 protein expression may vary between the two mice strains and the analysis missed a MCP-5 peak in AdOSM-treated BALB/c mice. Alternatively, other chemotactic factors may be responsible for the process of fibrocyte recruitment to the lung in this system, though data from the Richards laboratory has ruled out SDF-1.

Experiments were also completed using BALB/c MLF cultures to supplement *in vivo* data. While responses to TGF-β by C57Bl/6 MLF cultures have previously been characterized in the literature, to our knowledge, there are no reports on the role of TGF-β on BALB/c MLF cultures. Data collected during this project showed that TGF-β did not elevate steady state mRNA expression of collagen 1a1, collagen 1a2, fibronectin, or α-SMA after six or 24 hours stimulation (**Fig. 9**). One interpretation of this data is that it supports the notion that BALB/c mice are more resistant to AdTGF-β-induced ECM

remodeling. However, the data could also reflect that the BALB/c MLF cultures were phenotypically activated, as suggested previously (Chapter 6.2). In contrast to TGF-β, it appeared that OSM decreased steady state mRNA expression of collagen 1a1, collagen 1a2, fibronectin and α-SMA after 24 hours stimulation in BALB/c MLF cultures, although the culture conditions may affect responses (**Fig. 9**). Thus, further investigation is needed to determine the role of OSM on BALB/c MLF cultures on other substrates.

While OSM overexpression induced rapid ECM remodeling, it was also important to address whether these effects were transient and representative of fibrogenesis, or sustained and representative of fibrosis. Although not completed in C57Bl/6 mice for this thesis, BALB/c mice were examined 28 days after endotracheal administration of AdOSM. Preliminary results showed that while parenchymal ECM remodeling was largely resolved, there were morphological differences in the airway epithelium of AdOSM-treated BALB/c mice relative to AdDL70-treated BALB/c mice (**Fig. 6**). While levels of OSM and IL-6 were undetectable in the BALF of AdOSM-treated BALB/c mice, total cell numbers, macrophages, and lymphocytes in the BALF were elevated in AdOSM-treated BALB/c mice, indicating that some of the effects of OSM overexpression are long-lasting (**Fig. 7**). Resolution of parenchymal ECM accumulation 28 days post endotracheal administration of AdOSM is likely due to the reduction of vector expressing OSM, suggesting high OSM levels are required to maintain lung parenchymal ECM accumulation. It is well documented that expression of the transgene in these vectors (typically 2-12 days) is reduced due to immune response towards the adenovirus[157]. This is consistent with the lack of OSM detected in the BALF of AdOSM-

treated BALB/c mice after 28 days (**Fig. 7C**). In contrast, OSM is detectable in the BALF of IPF patients, although modulation of levels over time in individual patients is unknown[122]. Sustained OSM in mouse models using different vectors may induce chronic ECM remodeling, however this remains to be investigated. In conclusion, the data suggests in BALB/c mice that the AdOSM-induced parenchymal ECM accumulation remodeling is a transient model of fibrogenesis unlike the AdTGF-β model in the rat.

6.4 Role of IL-6 in OSM-induced ECM remodeling

Controversy remains over the role of inflammation in fibrosis, with evidence to support both sides of the argument. AdOSM effects in IL-6 -/- mice have recently been shown to be markedly reduced in cytokine and inflammatory cell infiltration[158]. To disengage inflammation from ECM remodeling, IL-6 -/- mice were intubated with AdOSM, and lungs were examined seven days later. Despite a reduction in inflammatory cells accumulation in the airspace of AdOSM-treated IL-6 -/- mice compared to AdOSM-treated IL-6 +/+ mice (**Fig. 13A**), the histopathology was similar between AdOSM-treated IL-6 -/- and IL-6 +/+ mice (**Fig. 10-12**), implying that IL-6 is not required for OSM-induced ECM remodeling. This also suggests that prominent inflammatory cell accumulation in the BALF was not required for ECM remodeling in this model, or that after inflammatory cells reach a threshold number in the BALF, there is no change to the extent of ECM remodeling. This contrasts the role of IL-6 in other models of ECM remodeling, such as the bleomycin model of ECM remodeling. Bleomycin-treated IL-6 -/- mice had attenuated ECM remodeling relative to bleomycin-treated IL-6 +/+ mice at day 21[112]. However, the same group observed a decrease in inflammatory cell

accumulation in bleomycin-treated IL-6 -/- mice at day two but not day seven[112]. One possible explanation to address the discrepancy between data collected from the AdOSM model and the bleomycin model of ECM remodeling is that the using an overexpression system induces higher than physiological levels of OSM protein in the BALF. Thus, OSM may be driving ECM accumulation and masking the effects of a decrease in inflammatory cell numbers in the BALF of AdOSM-treated IL-6 -/- mice. Perhaps using a suboptimal dose of AdOSM, lower than what was used during this thesis, may provide a different outcome. Alternatively, it can be argued that the bleomycin and AdOSM model of lung ECM remodeling are not comparable, as one relies on epithelial damage induced by a drug to instigate ECM remodeling, whereas the other relies on adverse effects initiated by the presence of a specific cytokine.

An interesting observation from this phase of the thesis was that OSM levels were lower in the BALF of AdOSM-treated IL-6 -/- mice relative to AdOSM-treated IL-6 +/+ mice after seven days, despite the same dosage of AdOSM being endotracheally administered to each group (**Fig. 14A**). This suggests that IL-6, which can be produced by fibroblasts, lung epithelial cells, and airway smooth muscle cells in response to OSM stimulation, directly or indirectly stimulates endogenous OSM production through a positive feedback loop. Cells that have been reported to produce OSM are T cells, granulocytes, and macrophages, and decreased infiltration of these cells in IL-6 -/- mice could result in decreased production of endogenous OSM. Alternatively, IL-6 may directly regulate OSM expression in macrophages or other cells but this would be the subject of future work.

6.4 Role of TGF-β/SMAD3 pathway during lung injury

TGF-β has been shown to have a profibrotic role in many models of ECM remodeling, and the TGF-β-induced SMAD2/3 signaling pathway has been shown to be central in this process. It has been shown that ECM remodeling is attenuated in bleomycin-treated SMAD3 -/- mice compared to SMAD3 +/+ mice[159]. Animal models using AdTGF-β and AdIL-1β also show a similar trend in SMAD3 -/- mice[160,161]. Interestingly, this thesis shows that the AdOSM model of ECM remodeling is SMAD3 independent, as AdOSM-treated SMAD3 -/- mice had similar severity of ECM remodeling as AdOSM-treated SMAD3 +/+ mice after seven days (**Fig. 15-16**). In addition, OSM overexpression was able to induce ECM remodeling in BALB/c mice, a mouse strain that is resistant to bleomycin and AdTGF-β-induced ECM remodeling (**Fig. 1-3**). Furthermore, lung homogenates from AdOSM-treated C57Bl/6 and BALB/c mice showed little change in the pSMAD2 signal relative to AdDl70-treated mice, as assessed by immunoblots, in contrast to STAT3 activation and SMAD1 suppression (**Fig. 19B-D**). This implies that the SMAD2/3 pathway was not activated or regulated in this model at the time point assessed. It cannot be ruled out that TGF-β may be modulating ECM remodeling through SMAD3-independent pathways, although evidence from other experimental models including the AdIL-1β model suggests otherwise[161]. To determine if TGF-β protein is present and or regulated by OSM overexpression, lung homogenates or BALF from AdOSM-treated mice could be probed for active TGF-β by immunoblots or ELISA, respectively. If TGF-β protein levels were unchanged using either methodology, this would give stronger support that TGF-β does not modulate ECM remodeling in this

in vivo model. At this time, the results collectively support a TGF-β-SMAD3 independent mechanis by which OSM overexpression mediates ECM accumulation. Whether lower levels of OSM expression can also drive similar effects in SMAD3 -/- mice is not clear at this time. To test this, a lower suboptimal dosage of AdOSM could be used to compare responses between AdOSM-treated SMAD3 +/+ and AdOSM-treated SMAD3 -/- mice.

Although levels of pSMAD2 signal were not significantly modulated in AdOSM-treated mice by immunoblot analysis (**Fig. 19C**), qualitative observations suggested a pronounced increase in pSMAD2 staining by IHC analysis, particularly in the lung parenchyma (**Fig. 23**). These results were obtained using the same pSMAD2 antibody (Cell Signaling), raising the question of how the two methodologies produced different results. While the left lung was used for histological analysis, the right lung was used for protein and RNA analysis, and thus it is possible that the right lung was not as affected as the left lung by the OSM vector. Therefore, immunoblot analysis would not have detected changes in pSMAD2 signal. It is also possible that while parenchymal staining for pSMAD2 is significantly increased in AdOSM-treated mice, staining is more pronounced in the airways, masking any pSMAD2 regulation in the parenchyma as detected by immunoblot. Alternatively, the pSMAD2 antibody may have higher specificity towards a folded epitope found on a lung section than a two-dimensional denatured protein.

One limitation of the SMAD3 -/- model is that it is assumed that knockout of this gene abolishes canonical TGF-β signaling. However, it cannot be ruled out that SMAD2 might drive canonical TGF-β signaling in the absence of SMAD3. This claim is supported by recent reports showing that SMAD2 and SMAD3 are redundantly necessary

for TGF-β mediated regulation of T cell plasticity and Th1 development[162]. Probing lung homogenates of AdOSM-treated SMAD3 -/- mice for pSMAD2 by immunoblot could be used to test this hypothesis.

6.5 Role of STAT3 pathway during lung injury

There is an emerging body of literature suggesting a profibrotic role for STAT3 in lung ECM remodeling. For instance, O'Donoghue *et al., 2012* showed that that $Gp130^{757F}$ mice with hyperactive STAT3 showed exacerbated ECM remodeling in response to bleomycin, whereas $gp130^{\Delta STAT}$ mice with hypoactive STAT3 showed attenuated effects upon bleomycin treatment[163]. Furthermore, Nagayama *et al.*, 2013 showed that OSM regulated lung fibroblast function, such as the differentiation of fibroblasts into myofibroblasts, and this process was dependent on the STAT3 pathway[164]. The data collected in this thesis also implicate STAT3 activation in OSM-induced ECM remodeling. OSM overexpression in BALB/c mice increased pSTAT3 signal two days after intubation in a dose-dependent fashion (**Fig. 20**), and was sustained at day seven (**Fig. 19B**). Whether STAT3 remains activated in AdOSM-treated BALB/c mice 28 days post-intubation is subject to future analysis.

OSM was also able to activate the STAT3 pathway within one hour *in vitro* in MLFs derived from C57Bl/6 and BALB/c mice (**Fig. 24B** and **Fig. 25B**), as well as alveolar and airway epithelial cell lines (**Fig. 32B** and **Fig. 28B**). These results collectively show that that OSM is able to act on numerous cell types in the lung, though the consequences of STAT3 activation in each cell type in the OSM overexpression remain unclear. While it may appear as though STAT3 activation leads to profibrotic

outcomes, it is important to note that STAT3 activation may play differential roles dependent on the cell type, and even subpopulations of a cell type. Kotaru *et al*., 2006 emphasized that the lung is made of subpopulations of lung fibroblasts, each of which has its own gene expression profile and phenotype[165]. In a more recent publication from the Knight group, it was shown that a subpopulation of lung fibroblasts with constitutive phosphorylated STAT3 had increased expression of α-SMA, more collagen secretion, and was more responsiveness to TGF-β upon suppression of STAT3 activation[53]. On the other hand, it has also been suggested that STAT3 signaling is correlated with antifibrotic mechanisms such as premature senescence of lung fibroblasts[166]. Thus, since STAT3 activation has a range of effects in different cell types, the precise mechanisms of its function in lung ECM remodeling is complex.

STAT3 activation has also been shown to have an important role in modulating airway inflammation in a murine model of airway hyperresponsiveness involving house dust mite (HDM)[167]. STAT3 activation induced by HDM was localized to airway smooth muscle cells, airway epithelial cells, and inflammatory cells[167]. HDM-treated mice with STAT3 conditionally knocked out from the airway epithelium had less eosinophilia, less of a Th2 response, and decreased levels of KC compared to wildtype mice[167]. These results were also observed when delivering STAT kinase inhibitors through the intranasal route to mice already treated with HDM for three weeks[167]. The histology from AdOSM-treated BALB/c mice after 28 days treatment showed morphological changes in the airway architecture compared to AdDl70-treated mice (**Fig. 6**). Perhaps STAT3 activation is persistent in the airways, but not in the parenchyma, after 28 days, and this may give a

reason why ECM remodeling has resolved in the lung parenchyma. To address this hypothesis, IHC for pSTAT3 could be completed on lung sections from AdOSM-treated BALB/c mice after 28 days treatment.

With evidence supporting both a profibrotic and an antifibrotic role for STAT3 pathway in the lung environment, it is important to delineate the role of STAT3 activation in the AdOSM model of ECM remodeling. The fact that OSM receptor is expressed on numerous cell types found in the lung mileau suggests that the STAT3 pathway may have many roles, dependent on the cell type[118]. At this given time, whether STAT3 activation mediates EMT or EndoMT directly is unclear, and could be examined in the future. The use of a STAT3 inhibitor *in vivo* could help to determine whether STAT3 is required for OSM-induced ECM remodeling, while the use of a STAT3 inhibitor *in vitro* may help to delineate its function in the various cell types.

6.6 Role of SMAD1 pathway during lung injury

The findings from this thesis are consistent with the prevailing notion that pulmonary fibrosis is associated with a suppression of BMP-SMAD1/5/8 signaling axis. Firstly, based on qRT-PCR experiments conducted on MLF cultures, BMP2 appeared to be an antifbrotic agent, as it decreased the steady state mRNA levels of α-SMA, fibronectin, collagen 1a1, and collagen 1a2 in C57Bl/6 and BALB/c MLF cultures after six hours of stimulation and one day of stimulation, respectively (**Fig. 8** and **Fig. 9**). However, the AdOSM model of lung ECM remodeling in both C57Bl/6 and BALB/c mice showed a decrease in pSMAD1/5, pSMAD1/5/8, and BMPR2 signal, all suggesting a suppression of the SMAD1 pathway (**Fig. 19D-F**). Using IHC, it was identified that the

airway epithelial cells were the major cell type exhibiting the suppression of SMAD1/5 signaling (**Fig. 21C**). mRNA levels of gremlin, a BMP antagonist, were upregulated in both AdOSM-treated BALB/c and C57Bl/6 mice seven days after intubation (**Fig. 5C**). Furthermore, OSM suppressed pSMAD1/5/8 signal in airway (**Fig. 27C**) as well as alveolar epithelial cells (**Fig. 33D**) *in vitro*. Lastly, data from the laboratory showed that steady state mRNA levels of the BMP ligands BMP2, BMP, and BMP4 are downregulated in AdOSM-treated mouse lung homogenates (Rodrigues, unpublished).

One conflicting observation to this collection of work is the observation that OSM elevated pSMAD1/5/8 signal in C57Bl/6 and BALB/c MLF cultures, albeit at early time points (**Fig. 24D** and **Fig. 25D**). However, based on the minimal pSMAD1/5/8 staining in the lung parenchyma by IHC analysis relative to the large airways (**Fig. 21D**), as well as trends in pSMAD1/5 signal seen using immunoblots on lung homogenates (**Fig. 19D**), it is possible that SMAD1/5 regulation in fibroblasts is not as dominant compared to SMAD1/5 regulation in airway epithelial cells. Another possibility is that the observation seen in fibroblasts cultured in isolation may not be an accurate representation of the events that unfold *in vivo*, as discussed previously.

BMPs are thought to contribute to tissue homeostasis by counterbalancing the effects of TGF-β[168–170]. For instance, BMP4 has been shown to inhibit TGF-β-induced ECM protein production in human lung fibroblasts[168]. It is thought that upon tissue injury, the BMP-SMAD1 signaling axis is activated in order to initiate wound healing, a process that draws parallels to lung development. In fact, SMAD1 activation has been reported to occur within days of exposure of mice to bleomycin, although the kinetics of SMAD1

activation at later points in the bleomycin model, especially during the onset of pathology, is unknown[143]. On the other hand, SMAD1 signaling has been shown to be suppressed in the silica model of ECM remodeling at Day 20, consistent with the AdOSM-induced effects in this thesis[171]. This suggests that OSM may be involved in the silica model of ECM remodeling but not bleomycin.

Based on our results, one possible explanation as to how OSM regulates the BMP-SMAD1 signaling axis is through gremlin. Findings both *in vivo* and *in vitro* indicate OSM induces gremlin mRNA expression (**Fig. 5C**, **Fig. 8E**, and **Fig. 9E**), and this may have important implications in the modulation of the BMP pathway. Recent work has shown that overexpression of gremlin using an adenovirus is able to induce transient ECM remodeling[146]. Other studies show that an upregulation of gremlin skews the BMP-TGF-β equilibrium towards a fibrotic environment. For example, gremlin inactivation of BMP inhibits epithelial regeneration, as well as BMP-mediated apoptosis of fibroblasts and myofibroblasts[102]. Overall, these findings suggest that OSM induction of ECM remodeling *in vivo* involves suppression of the BMP-SMAD1 signaling axis. With recent literature showing that a BMP agonist is able to ameliorate ECM remodeling, a similar approach could be taken to assess functional consequences of the BMP-SMAD1 signaling axis in the AdOSM models.

6.7 Future directions

In addition to suggestions for future work proposed throughout Chapter 6, there are other suggestions that may help in characterizing the OSM-induced model of ECM remodeling accumulation. Myofibroblasts are thought to originate from at least four

different sources: resident fibroblasts, circulating fibrocytes, epithelial cells through EMT, and endothelial cells through EndoMT[55,58,60,61]. Data collected for this thesis, along with unpublished data have tried to address the role of OSM on resident fibroblasts as well as circulating fibrocytes. However, the role of OSM on epithelial cells and endothelial cells remains unclear with regards to ECM accumulation. It would therefore be of interest to determine whether OSM can stimulate C10 epithelial cell or endothelial cell differentiation into a myofibroblast through EMT and EndoMT, respectively.

BMP2 is only one of around 20 BMP proteins that have been characterized[172]. To date, BMP2, BMP4, and BMP7 are predominantly the focus of fibrosis studies. BMP2 was chosen as a candidate for this thesis to investigate *in vitro* effects as it has been previously shown to synergize OSM-induced alkaline phosphatase activity in C2C12 cells[121]. However, one of the limitations of only examining BMP2 responses in *in vitro* cell lines is that it may not represent responses of other BMP family members. Therefore, it would be of interest to look at the roles of BMP4 as well as BMP7, two other well studied members of the BMP family.

Many of the cell signaling pathways activated during lung development are also activated upon lung injury, and it is thought that aberrant signaling of these pathways contributes to ECM accumulation. This provided one rationale for examining the BMP pathway in OSM models of ECM remodeling. However, other pathways, including the wnt/β-catenin and the sonic hedgehog (SHH) pathways, are activated during lung development, raising the possibility that these pathways are modulated in the OSM overexpression system[173]. The wnt/β-catenin pathway activation been detected in

epithelial and mesenchymal cells in IPF patients, and is implicated in various processes such as epithelial cell proliferation, EMT, and inflammation[174]. In fact, it has been suggested that modulating this pathway may be a plausible approach for IPF therapy. However, preliminary work from the Richards laboratory was unable to detect modulation of the Wnt/β-catenin pathway in OSM models of ECM remodeling. The SHH pathway, the most broadly expressed of three hedgehog homologs identified in humans, is responsible for lung branching morphogenesis. Recently, it has been shown that IPF patients, but not control patients, have elevated levels of SHH markers in the alveolar epithelium[175]. The same group also showed that human lung fibroblasts treated with recombinant SHH showed increased cell proliferation, collagen and fibronectin expression, and migration relative to untreated cells[175]. Therefore, it would be of interest to investigate the role of other lung developmental pathways in models of OSM-induced lung ECM remodeling.

Lastly, the observation that transient pulmonary overexpression of OSM decreased BMPR2 signal in total lung homogenates of both BALB/C and C57Bl/6 mice at Day 7 gives rise to the possibility that OSM overexpression is linked to familial pulmonary arterial hypertension (FPAH), a condition associated with IPF. Genetic studies have implicated defects in BMPR2 to exaggerated TGF-β signaling, endothelial cell apoptosis, and ultimately FPAH. First, it would be important to determine if the OSM overexpression system is associated with hypertension. OSMR -/- mice could also be used in experimental models of FPAH such as chronic hypoxia or monocrotaline exposure to determine whether OSM signaling modulates hypertension[176]. Finally, recent

studies have shown that gene delivery of BMPR2 attenuates pulmonary hypertension, and it would be of interest to examine whether gene therapy could induce similar effects in OSM models of ECM remodeling[177].

CHAPTER 7: Conclusions

In this thesis, the effects of pulmonary overexpression of OSM were assessed in BALB/c mice and compared to C57Bl/6 mice using adenovirus vectors. Although the literature indicates that BALB/c mice are relatively resistant to bleomycin and AdTGF-β-induced lung ECM accumulation, in this thesis AdOSM-treated BALB/c mice showed comparable lung ECM accumulation to C57Bl/6 mice seven days after exposure to AdOSM, whereas the control vector (AdDl70) had no detectable effect. This suggests different mechanisms are involved in the AdOSM model compared to other models of lung ECM remodeling. Furthermore, histological analyses of AdOSM-treated BALB/c mice showed sustained airway epithelial alterations after 28 days, whereas effects in the lung parenchyma appear resolved. Ongoing studies will determine longer time point effects in both C57Bl/6 and BALB/c strains of mice. Analysis of MLF cultures from both mouse strains indicated that OSM did not directly modulate fibroblast production of ECM-related genes such as collagen 1a1 and fibronectin *in vitro*, suggesting that other cells, including fibrocytes, epithelial cells, and endothelial cells, may be involved in this process. However, this would be subject to further investigation.

IL-6 -/- and SMAD3 -/- mice were also utilized to examine the roles of inflammation and the canonical TGF-β pathway, respectively, in OSM-induced ECM remodeling. Although there was a decrease in cell infiltration, AdOSM-treated IL-6 -/- mice had similar severity of ECM accumulation after seven and 14 days. Similar histopathological findings were observed using SMAD3 -/- mice.

STAT3 and SMAD signaling were also assessed in the OSM overexpression system. While pSMAD2 signal was unregulated by OSM, based on immunoblot analysis, the STAT3 pathway was activated while the SMAD1 pathway was suppressed. SMAD1 signaling is thought to have a protective role during lung homeostasis, and the suppression of this pathway, also observed in other models of lung ECM remodeling, may promote ECM accumulation. Furthermore, there is a growing body of literature showing that the STAT3 pathway, which is activated in numerous cell types and appears to have many functions, may contribute to pulmonary fibrosis. While OSM overexpression was associated with STAT3 activation and SMAD1 suppression, additional experiments would be required to determine if the regulation of these pathways had functional consequences in the AdOSM models of ECM remodeling. Collectively, this data suggests that OSM induces novel pathways in lung ECM remodeling, although further investigation in other animal models of ECM accumulation as well as clinical studies are needed. This may have implications in understanding mechanisms in pulmonary fibrosis conditions that are not responsive to targeting of TGF-β/SMAD3 signaling or inflammation.

CHAPTER 8: References

1. Davidson, R. W. Canadian Pulmonary Fibrosis Foundation. **2012,** (2012).

2. Gross, T. J. & Hunninghake, G. W. Idiopathic pulmonary fibrosis. *N Engl J Med* **345,** 517–525 (2001).

3. Meuten, T. *et al.* WNT7B in fibroblastic foci of idiopathic pulmonary fibrosis. *Respir Res* **13,** 62 (2012).

4. American Thoracic Society. Idiopathic pulmonary fibrosis: diagnosis and treatment. International consensus statement. American Thoracic Society (ATS), and the European Respiratory Society (ERS). *American journal of respiratory and critical care medicine* **161,** 646–64 (2000).

5. Katzenstein, A. L. & Myers, J. L. Idiopathic pulmonary fibrosis: clinical relevance of pathologic classification. *Am J Respir Crit Care Med* **157,** 1301–1315 (1998).

6. Wynn, T. A. Integrating mechanisms of pulmonary fibrosis. *The Journal of experimental medicine* **208,** 1339–50 (2011).

7. Gaensler, E. A., Jederlinic, P. J. & Churg, A. Idiopathic pulmonary fibrosis in asbestos-exposed workers. *The American review of respiratory disease* **144,** 689–96 (1991).

8. Oh, C. K., Murray, L. A. & Molfino, N. A. Smoking and idiopathic pulmonary fibrosis. *Pulmonary medicine* **2012,** 808260 (2012).

9. Yagoda, A. *et al.* Bleomycin, an antitumor antibiotic. Clinical experience in 274 patients. *Annals of internal medicine* **77,** 861–70 (1972).

10. Young, A. *et al.* Mortality in rheumatoid arthritis. Increased in the early course of disease, in ischaemic heart disease and in pulmonary fibrosis. *Rheumatology (Oxford, England)* **46,** 350–7 (2007).

11. Steen, V. D., Conte, C., Owens, G. R. & Medsger, T. A. Severe restrictive lung disease in systemic sclerosis. *Arthritis and rheumatism* **37,** 1283–9 (1994).

12. Khalil, N. & O'Connor, R. Idiopathic pulmonary fibrosis: current understanding of the pathogenesis and the status of treatment. *CMAJ* **171,** 153–160 (2004).

13. Khalil, N. *et al.* Increased production and immunohistochemical localization of transforming growth factor-beta in idiopathic pulmonary fibrosis. *Am J Respir Cell Mol Biol* **5,** 155–162 (1991).

14. Selman, M., King, T. E. & Pardo, A. Idiopathic pulmonary fibrosis: prevailing and evolving hypotheses about its pathogenesis and implications for therapy. *Ann Intern Med* **134,** 136–151 (2001).

15. Society, C. C. Prostate cancer statistics at a glance. *Canadian Cancer Society* **2012,** (2011).

16. Meltzer, E. B. & Noble, P. W. Idiopathic pulmonary fibrosis. *Orphanet J Rare Dis* **3,** 8 (2008).

17. Thabut, G. *et al.* Survival after bilateral versus single-lung transplantation for idiopathic pulmonary fibrosis. *Annals of internal medicine* **151,** 767–74 (2009).

18. Moeller, A., Ask, K., Warburton, D., Gauldie, J. & Kolb, M. The bleomycin animal model: a useful tool to investigate treatment options for idiopathic pulmonary fibrosis? *The international journal of biochemistry & cell biology* **40,** 362–82 (2008).

19. Dik, W. A. *et al.* Dexamethasone treatment does not inhibit fibroproliferation in chronic lung disease of prematurity. *The European respiratory journal : official journal of the European Society for Clinical Respiratory Physiology* **21,** 842–7 (2003).

20. Kisseleva, T. & Brenner, D. A. Mechanisms of fibrogenesis. *Exp Biol Med (Maywood)* **233,** 109–122 (2008).

21. Peterson, M. W. & Kirschbaum, J. Asbestos-induced lung epithelial permeability: potential role of nonoxidant pathways. *Am J Physiol* **275,** L262–8 (1998).

22. Magro, C. M. *et al.* Idiopathic pulmonary fibrosis related to endothelial injury and antiendothelial cell antibodies. *Hum Immunol* **67,** 284–297 (2006).

23. Thannickal, V. J., Toews, G. B., White, E. S., Lynch 3rd, J. P. & Martinez, F. J. Mechanisms of pulmonary fibrosis. *Annu Rev Med* **55,** 395–417 (2004).

24. Gereke, M. *et al.* Phenotypic alterations in type II alveolar epithelial cells in CD4+ T cell mediated lung inflammation. *Respiratory research* **8,** 47 (2007).

25. Santiago, B., Galindo, M., Palao, G. & Pablos, J. L. Intracellular regulation of Fas-induced apoptosis in human fibroblasts by extracellular factors and cycloheximide. *J Immunol* **172,** 560–566 (2004).

26. Hasegawa, M., Sato, S. & Takehara, K. Augmented production of chemokines (monocyte chemotactic protein-1 (MCP-1), macrophage inflammatory protein-1alpha (MIP-1alpha) and MIP-1beta) in patients with systemic sclerosis: MCP-1 and MIP-1alpha may be involved in the development of pulmonary fibros. *Clin Exp Immunol* **117,** 159–165 (1999).

27. Laurent, G. J., Chambers, R. C., Hill, M. R. & McAnulty, R. J. Regulation of matrix turnover: fibroblasts, forces, factors and fibrosis. *Biochemical Society transactions* **35,** 647–51 (2007).

28. Henry, M. T. *et al.* Matrix metalloproteinases and tissue inhibitor of metalloproteinase-1 in sarcoidosis and IPF. *The European respiratory journal : official journal of the European Society for Clinical Respiratory Physiology* **20,** 1220–7 (2002).

29. Checa, M. *et al.* MMP-1 polymorphisms and the risk of idiopathic pulmonary fibrosis. *Human genetics* **124,** 465–72 (2008).

30. Bienkowski, R. S. & Gotkin, M. G. Control of collagen deposition in mammalian lung. *Proc Soc Exp Biol Med* **209,** 118–140 (1995).

31. Chen, C. Z. & Raghunath, M. Focus on collagen: in vitro systems to study fibrogenesis and antifibrosis state of the art. *Fibrogenesis Tissue Repair* **2,** 7 (2009).

32. Akasaka, Y. *et al.* The mechanisms underlying fibroblast apoptosis regulated by growth factors during wound healing. *J Pathol* **221,** 285–299 (2010).

33. Herzog, E. L., Brody, A. R., Colby, T. V, Mason, R. & Williams, M. C. Knowns and unknowns of the alveolus. *Proceedings of the American Thoracic Society* **5,** 778–82 (2008).

34. McAnulty, R. J. Fibroblasts and myofibroblasts: their source, function and role in disease. *The international journal of biochemistry & cell biology* **39,** 666–71 (2007).

35. Todd, N. W., Luzina, I. G. & Atamas, S. P. Molecular and cellular mechanisms of pulmonary fibrosis. *Fibrogenesis & tissue repair* **5,** 11 (2012).

36. Quan, T. E., Cowper, S. E. & Bucala, R. The role of circulating fibrocytes in fibrosis. *Curr Rheumatol Rep* **8,** 145–150 (2006).

37. Garcia-Alvarez, J. *et al.* Membrane type-matrix metalloproteinases in idiopathic pulmonary fibrosis. *Sarcoidosis Vasc Diffuse Lung Dis* **23,** 13–21 (2006).

38. Manoury, B., Caulet-Maugendre, S., Guénon, I., Lagente, V. & Boichot, E. TIMP-1 is a key factor of fibrogenic response to bleomycin in mouse lung. *International journal of immunopathology and pharmacology* **19,** 471–87 (2009).

39. Selman, M., Montaño, M., Ramos, C. & Chapela, R. Concentration, biosynthesis and degradation of collagen in idiopathic pulmonary fibrosis. *Thorax* **41,** 355–9 (1986).

40. Hernnäs, J. *et al.* Alveolar accumulation of fibronectin and hyaluronan precedes bleomycin-induced pulmonary fibrosis in the rat. *The European respiratory journal : official journal of the European Society for Clinical Respiratory Physiology* **5,** 404–10 (1992).

41. Ashcroft, T., Simpson, J. M. & Timbrell, V. Simple method of estimating severity of pulmonary fibrosis on a numerical scale. *Journal of clinical pathology* **41,** 467–70 (1988).

42. Faress, J. A. *et al.* Bleomycin-induced pulmonary fibrosis is attenuated by a monoclonal antibody targeting HER2. *Journal of applied physiology (Bethesda, Md. : 1985)* **103,** 2077–83 (2007).

43. Kroll, M. H. & Afshar-Kharghan, V. Platelets in pulmonary vascular physiology and pathology. *Pulmonary circulation* **2,** 291–308 (2012).

44. Jones, H. A., Schofield, J. B., Krausz, T., Boobis, A. R. & Haslett, C. Pulmonary fibrosis correlates with duration of tissue neutrophil activation. *American journal of respiratory and critical care medicine* **158,** 620–8 (1998).

45. Sullivan, D. E., Ferris, M., Nguyen, H., Abboud, E. & Brody, A. R. TNF-alpha induces TGF-beta1 expression in lung fibroblasts at the transcriptional level via AP-1 activation. *Journal of cellular and molecular medicine* **13,** 1866–76 (2009).

46. Elias, J. A., Reynolds, M. M., Kotloff, R. M. & Kern, J. A. Fibroblast interleukin 1 beta: synergistic stimulation by recombinant interleukin 1 and tumor necrosis factor and posttranscriptional regulation. *Proceedings of the National Academy of Sciences of the United States of America* **86,** 6171–5 (1989).

47. Murphy, K. *Janeway's Immunobiology*. 888 (Garland Science, 2012).

48. Frantz, C., Stewart, K. M. & Weaver, V. M. The extracellular matrix at a glance. *Journal of cell science* **123,** 4195–200 (2010).

49. Aszódi, A., Legate, K. R., Nakchbandi, I. & Fässler, R. What mouse mutants teach us about extracellular matrix function. *Annual review of cell and developmental biology* **22,** 591–621 (2006).

50. Dunsmore, S. E. & Rannels, D. E. Extracellular matrix biology in the lung. *The American journal of physiology* **270,** L3–27 (1996).

51. Ramos, C. *et al.* Fibroblasts from idiopathic pulmonary fibrosis and normal lungs differ in growth rate, apoptosis, and tissue inhibitor of metalloproteinases expression. *Am J Respir Cell Mol Biol* **24,** 591–598 (2001).

52. Fujitsu, Y., Fukuda, K., Kumagai, N. & Nishida, T. IL-4-induced cell proliferation and production of extracellular matrix proteins in human conjunctival fibroblasts. *Experimental eye research* **76,** 107–14 (2003).

53. Pechkovsky, D. V *et al.* Human lung parenchyma but not proximal bronchi produces fibroblasts with enhanced TGF-beta signaling and alpha-SMA expression. *American journal of respiratory cell and molecular biology* **43,** 641–51 (2010).

54. Jordana, M. *et al.* Heterogeneous proliferative characteristics of human adult lung fibroblast lines and clonally derived fibroblasts from control and fibrotic tissue. *Am Rev Respir Dis* **137,** 579–584 (1988).

55. Willis, B. C. *et al.* Induction of epithelial-mesenchymal transition in alveolar epithelial cells by transforming growth factor-beta1: potential role in idiopathic pulmonary fibrosis. *Am J Pathol* **166,** 1321–1332 (2005).

56. Kim, K. K. *et al.* Alveolar epithelial cell mesenchymal transition develops in vivo during pulmonary fibrosis and is regulated by the extracellular matrix. *Proceedings of the National Academy of Sciences of the United States of America* **103,** 13180–5 (2006).

57. Hinz, B. *et al.* The myofibroblast: one function, multiple origins. *Am J Pathol* **170,** 1807–1816 (2007).

58. Barnes, J. L. & Gorin, Y. Myofibroblast differentiation during fibrosis: role of NAD(P)H oxidases. *Kidney Int* **79,** 944–956 (2011).

59. Chen, H., Zhou, X., Shi, Y. & Yang, J. Roles of p38 MAPK and JNK in TGF-β1-induced human alveolar epithelial to mesenchymal transition. *Archives of medical research* **44,** 93–8 (2013).

60. Li, J. & Bertram, J. F. Review: Endothelial-myofibroblast transition, a new player in diabetic renal fibrosis. *Nephrology (Carlton)* **15,** 507–512 (2010).

61. Mori, L., Bellini, A., Stacey, M. A., Schmidt, M. & Mattoli, S. Fibrocytes contribute to the myofibroblast population in wounded skin and originate from the bone marrow. *Exp Cell Res* **304,** 81–90 (2005).

62. Varcoe, R. L. *et al.* The role of the fibrocyte in intimal hyperplasia. *Journal of thrombosis and haemostasis : JTH* **4,** 1125–33 (2006).

63. Moore, B. B. & Hogaboam, C. M. Murine models of pulmonary fibrosis. *Am J Physiol Lung Cell Mol Physiol* **294,** L152–60 (2008).

64. Garibaldi, B. T. *et al.* Regulatory T cells reduce acute lung injury fibroproliferation by decreasing fibrocyte recruitment. *American journal of respiratory cell and molecular biology* **48,** 35–43 (2013).

65. Gabbiani, G. The myofibroblast in wound healing and fibrocontractive diseases. *J Pathol* **200,** 500–503 (2003).

66. Micallef, L. *et al.* The myofibroblast, multiple origins for major roles in normal and pathological tissue repair. *Fibrogenesis & tissue repair* **5 Suppl 1,** S5 (2012).

67. Hinz, B., Pittet, P., Smith-Clerc, J., Chaponnier, C. & Meister, J.-J. Myofibroblast development is characterized by specific cell-cell adherens junctions. *Molecular biology of the cell* **15,** 4310–20 (2004).

68. Hinz, B. Formation and function of the myofibroblast during tissue repair. *J Invest Dermatol* **127,** 526–537 (2007).

69. Li, Y. *et al.* Severe lung fibrosis requires an invasive fibroblast phenotype regulated by hyaluronan and CD44. *The Journal of experimental medicine* **208,** 1459–71 (2011).

70. Lawson, W. E. *et al.* Increased and prolonged pulmonary fibrosis in surfactant protein C-deficient mice following intratracheal bleomycin. *The American journal of pathology* **167,** 1267–77 (2005).

71. Ono, S. *et al.* Surfactant protein C G100S mutation causes familial pulmonary fibrosis in Japanese kindred. *The European respiratory journal : official journal of the European Society for Clinical Respiratory Physiology* **38,** 861–9 (2011).

72. Selman, M. & Pardo, A. Role of epithelial cells in idiopathic pulmonary fibrosis: from innocent targets to serial killers. *Proceedings of the American Thoracic Society* **3,** 364–72 (2006).

73. Sisson, T. H. *et al.* Targeted injury of type II alveolar epithelial cells induces pulmonary fibrosis. *American journal of respiratory and critical care medicine* **181,** 254–63 (2010).

74. Williams, K. *et al.* Identification of spontaneous feline idiopathic pulmonary fibrosis: morphology and ultrastructural evidence for a type II pneumocyte defect. *Chest* **125,** 2278–88 (2004).

75. Johnston, C. J., Williams, J. P., Okunieff, P. & Finkelstein, J. N. Radiation-induced pulmonary fibrosis: examination of chemokine and chemokine receptor families. *Radiation research* **157,** 256–65 (2002).

76. Shimbori, C., Shiota, N. & Okunishi, H. Involvement of leukotrienes in the pathogenesis of silica-induced pulmonary fibrosis in mice. *Experimental lung research* **36,** 292–301 (2010).

77. Quinlan, T. R. *et al.* Dose-responsive increases in pulmonary fibrosis after inhalation of asbestos. *American journal of respiratory and critical care medicine* **150,** 200–6 (1994).

78. Sime, P. J., Xing, Z., Graham, F. L., Csaky, K. G. & Gauldie, J. Adenovector-mediated gene transfer of active transforming growth factor-beta1 induces prolonged severe fibrosis in rat lung. *J Clin Invest* **100,** 768–776 (1997).

79. Mouratis, M. A. & Aidinis, V. Modeling pulmonary fibrosis with bleomycin. *Current opinion in pulmonary medicine* **17,** 355–61 (2011).

80. Kim, J. H. *et al.* Natural killer T (NKT) cells attenuate bleomycin-induced pulmonary fibrosis by producing interferon-gamma. *The American journal of pathology* **167,** 1231–41 (2005).

81. Chung, M. P. *et al.* Role of repeated lung injury and genetic background in bleomycin-induced fibrosis. *American journal of respiratory cell and molecular biology* **29,** 375–80 (2003).

82. Izbicki, G., Segel, M. J., Christensen, T. G., Conner, M. W. & Breuer, R. Time course of bleomycin-induced lung fibrosis. *International journal of experimental pathology* **83,** 111–9 (2002).

83. Degryse, A. L. *et al.* Repetitive intratracheal bleomycin models several features of idiopathic pulmonary fibrosis. *American journal of physiology. Lung cellular and molecular physiology* **299,** L442–52 (2010).

84. Bringardner, B. D., Baran, C. P., Eubank, T. D. & Marsh, C. B. The role of inflammation in the pathogenesis of idiopathic pulmonary fibrosis. *Antioxidants & redox signaling* **10,** 287–301 (2008).

85. Luzina, I. G., Todd, N. W., Iacono, A. T. & Atamas, S. P. Roles of T lymphocytes in pulmonary fibrosis. *Journal of leukocyte biology* **83,** 237–44 (2008).

86. Marchal-Sommé, J. *et al.* Cutting edge: nonproliferating mature immune cells form a novel type of organized lymphoid structure in idiopathic pulmonary fibrosis. *Journal of immunology (Baltimore, Md. : 1950)* **176,** 5735–9 (2006).

87. Helene, M. *et al.* T cell independence of bleomycin-induced pulmonary fibrosis. *Journal of leukocyte biology* **65,** 187–95 (1999).

88. Janick-Buckner, D., Ranges, G. E. & Hacker, M. P. Effect of cytotoxic monoclonal antibody depletion of T-lymphocyte subpopulations on bleomycin-induced lung damage in C57BL/6J mice. *Toxicology and applied pharmacology* **100,** 474–84 (1989).

89. Massague, J. & Wotton, D. Transcriptional control by the TGF-beta/Smad signaling system. *EMBO J* **19,** 1745–1754 (2000).

90. Cao, B., Guo, Z., Zhu, Y. & Xu, W. The potential role of PDGF, IGF-1, TGF-beta expression in idiopathic pulmonary fibrosis. *Chinese medical journal* **113,** 776–82 (2000).

91. Giri, S. N., Hyde, D. M. & Hollinger, M. A. Effect of antibody to transforming growth factor beta on bleomycin induced accumulation of lung collagen in mice. *Thorax* **48,** 959–66 (1993).

92. Horan, G. S. *et al.* Partial inhibition of integrin alpha(v)beta6 prevents pulmonary fibrosis without exacerbating inflammation. *American journal of respiratory and critical care medicine* **177,** 56–65 (2008).

93. Li, J., He, B. & Weng, B. [The therapeutic effect of TGF-beta monoclonal antibody to bleomycin-induced pulmonary fibrosis in rats]. *Zhonghua jie he he hu*

xi za zhi = Zhonghua jiehe he huxi zazhi = Chinese journal of tuberculosis and respiratory diseases **20,** 347–9 (1997).

94. Ali, N. A. *et al.* Latency associated peptide has in vitro and in vivo immune effects independent of TGF-beta1. *PloS one* **3,** e1914 (2008).

95. Lutz, M. & Knaus, P. Integration of the TGF-beta pathway into the cellular signalling network. *Cell Signal* **14,** 977–988 (2002).

96. Miyazono, K., Kamiya, Y. & Morikawa, M. Bone morphogenetic protein receptors and signal transduction. *J Biochem* **147,** 35–51 (2010).

97. Tarantal, A. F. *et al.* Overexpression of transforming growth factor-beta1 in fetal monkey lung results in prenatal pulmonary fibrosis. *Eur Respir J* **36,** 907–914 (2010).

98. Munger, J. S. *et al.* The integrin alpha v beta 6 binds and activates latent TGF beta 1: a mechanism for regulating pulmonary inflammation and fibrosis. *Cell* **96,** 319–28 (1999).

99. Nakao, A. *et al.* Transient gene transfer and expression of Smad7 prevents bleomycin-induced lung fibrosis in mice. *The Journal of clinical investigation* **104,** 5–11 (1999).

100. Wipff, P.-J., Rifkin, D. B., Meister, J.-J. & Hinz, B. Myofibroblast contraction activates latent TGF-beta1 from the extracellular matrix. *The Journal of cell biology* **179,** 1311–23 (2007).

101. Kalter, V. G. & Brody, A. R. Receptors for transforming growth factor-beta (TGF-beta) on rat lung fibroblasts have higher affinity for TGF-beta 1 than for TGF-beta 2. *American journal of respiratory cell and molecular biology* **4,** 397–407 (1991).

102. Koli, K. *et al.* Bone morphogenetic protein-4 inhibitor gremlin is overexpressed in idiopathic pulmonary fibrosis. *Am J Pathol* **169,** 61–71 (2006).

103. Murray, L. A. *et al.* TGF-beta driven lung fibrosis is macrophage dependent and blocked by Serum amyloid P. *Int J Biochem Cell Biol* **43,** 154–162 (2011).

104. Taylor, L. M. & Khachigian, L. M. Induction of platelet-derived growth factor B-chain expression by transforming growth factor-beta involves transactivation by Smads. *The Journal of biological chemistry* **275,** 16709–16 (2000).

105. LeBleu, V. S. & Kalluri, R. Blockade of PDGF receptor signaling reduces myofibroblast number and attenuates renal fibrosis. *Kidney international* **80,** 1119–21 (2011).

106. White, U. A. & Stephens, J. M. The gp130 receptor cytokine family: regulators of adipocyte development and function. *Curr Pharm Des* **17,** 340–346 (2011).

107. Silver, J. S. & Hunter, C. A. gp130 at the nexus of inflammation, autoimmunity, and cancer. *J Leukoc Biol* **88,** 1145–1156 (2010).

108. Bravo, J. & Heath, J. K. Receptor recognition by gp130 cytokines. *EMBO J* **19,** 2399–2411 (2000).

109. Heinrich, P. C. *et al.* Principles of interleukin (IL)-6-type cytokine signalling and its regulation. *Biochem J* **374,** 1–20 (2003).

110. Knight, D. A., Ernst, M., Anderson, G. P., Moodley, Y. P. & Mutsaers, S. E. The role of gp130/IL-6 cytokines in the development of pulmonary fibrosis: critical determinants of disease susceptibility and progression? *Pharmacol Ther* **99,** 327–338 (2003).

111. Park, C. S. *et al.* Increased levels of interleukin-6 are associated with lymphocytosis in bronchoalveolar lavage fluids of idiopathic nonspecific interstitial pneumonia. *American journal of respiratory and critical care medicine* **162,** 1162–8 (2000).

112. Saito, F. *et al.* Role of interleukin-6 in bleomycin-induced lung inflammatory changes in mice. *American journal of respiratory cell and molecular biology* **38,** 566–71 (2008).

113. Dumas, A., Lagarde, S., Laflamme, C. & Pouliot, M. Oncostatin M decreases interleukin-1beta secretion by human synovial fibroblasts and attenuates an acute inflammatory reaction in vivo. *J Cell Mol Med* (2011). doi:10.1111/j.1582-4934.2011.01412.x

114. Kozlowska, K., Cichorek, M. & Zarzeczna, M. Estimation of oncostatin M (OSM) secretion by peritoneal macrophages with regard to the progression of transplantable melanomas. *Neoplasma* **45,** 369–372 (1998).

115. Chauhan, D. *et al.* Oncostatin M induces association of Grb2 with Janus kinase JAK2 in multiple myeloma cells. *The Journal of experimental medicine* **182,** 1801–6 (1995).

116. Stross, C. *et al.* Oncostatin M receptor-mediated signal transduction is negatively regulated by SOCS3 through a receptor tyrosine-independent mechanism. *The Journal of biological chemistry* **281,** 8458–68 (2006).

117. Brown, T. J., Rowe, J. M., Liu, J. W. & Shoyab, M. Regulation of IL-6 expression by oncostatin M. *Journal of immunology (Baltimore, Md. : 1950)* **147,** 2175–80 (1991).

118. Pelletier, J. P. & Martel-Pelletier, J. Oncostatin M: foe or friend? *Arthritis Rheum* **48,** 3301–3303 (2003).

119. Albasanz-Puig, A. *et al.* Oncostatin M is expressed in atherosclerotic lesions: a role for Oncostatin M in the pathogenesis of atherosclerosis. *Atherosclerosis* **216,** 292–298 (2011).

120. Hui, W., Bell, M. & Carroll, G. Detection of oncostatin M in synovial fluid from patients with rheumatoid arthritis. *Ann Rheum Dis* **56,** 184–187 (1997).

121. De Hooge, A. S. *et al.* Adenoviral transfer of murine oncostatin M elicits periosteal bone apposition in knee joints of mice, despite synovial inflammation and up-regulated expression of interleukin-6 and receptor activator of nuclear factor-kappa B ligand. *Am J Pathol* **160,** 1733–1743 (2002).

122. Mozaffarian, A. *et al.* Mechanisms of oncostatin M-induced pulmonary inflammation and fibrosis. *J Immunol* **181,** 7243–7253 (2008).

123. Simpson, J. L., Baines, K. J., Boyle, M. J., Scott, R. J. & Gibson, P. G. Oncostatin M (OSM) is increased in asthma with incompletely reversible airflow obstruction. *Exp Lung Res* **35,** 781–794 (2009).

124. Li, W. Q. & Zafarullah, M. Oncostatin M up-regulates tissue inhibitor of metalloproteinases-3 gene expression in articular chondrocytes via de novo transcription, protein synthesis, and tyrosine kinase- and mitogen-activated protein kinase-dependent mechanisms. *J Immunol* **161,** 5000–5007 (1998).

125. Nagata, T. *et al.* Oncostatin M, an interleukin-6 family cytokine, upregulates matrix metalloproteinase-9 through the mitogen-activated protein kinase kinase-extracellular signal-regulated kinase pathway in cultured smooth muscle cells. *Arterioscler Thromb Vasc Biol* **23,** 588–593 (2003).

126. Fritz, D. K. *et al.* A mouse model of airway disease: oncostatin M-induced pulmonary eosinophilia, goblet cell hyperplasia, and airway hyperresponsiveness are STAT6 dependent, and interstitial pulmonary fibrosis is STAT6 independent. *J Immunol* **186,** 1107–1118 (2011).

127. Venkayya, R. *et al.* The Th2 lymphocyte products IL-4 and IL-13 rapidly induce airway hyperresponsiveness through direct effects on resident airway cells. *American journal of respiratory cell and molecular biology* **26,** 202–8 (2002).

128. Saito, A., Okazaki, H., Sugawara, I., Yamamoto, K. & Takizawa, H. Potential action of IL-4 and IL-13 as fibrogenic factors on lung fibroblasts in vitro. *International archives of allergy and immunology* **132,** 168–76 (2003).

129. Scaffidi, A. K. *et al.* Oncostatin M stimulates proliferation, induces collagen production and inhibits apoptosis of human lung fibroblasts. *British journal of pharmacology* **136,** 793–801 (2002).

130. Cao, X. & Chen, D. The BMP signaling and in vivo bone formation. *Gene* **357,** 1–8 (2005).

131. Chen, D. *et al.* Differential roles for bone morphogenetic protein (BMP) receptor type IB and IA in differentiation and specification of mesenchymal precursor cells to osteoblast and adipocyte lineages. *J Cell Biol* **142,** 295–305 (1998).

132. Wagner, D. O. *et al.* BMPs: from bone to body morphogenetic proteins. *Science signaling* **3,** mr1 (2010).

133. Dudley, A. T., Lyons, K. M. & Robertson, E. J. A requirement for bone morphogenetic protein-7 during development of the mammalian kidney and eye. *Genes Dev* **9,** 2795–2807 (1995).

134. Zhang, H. & Bradley, A. Mice deficient for BMP2 are nonviable and have defects in amnion/chorion and cardiac development. *Development* **122,** 2977–2986 (1996).

135. McKay, B. & Sandhu, H. S. Use of recombinant human bone morphogenetic protein-2 in spinal fusion applications. *Spine (Phila Pa 1976)* **27,** S66–85 (2002).

136. Myllarniemi, M. *et al.* Gremlin-mediated decrease in bone morphogenetic protein signaling promotes pulmonary fibrosis. *Am J Respir Crit Care Med* **177,** 321–329 (2008).

137. Susperregui, A. R. G. *et al.* Noncanonical BMP signaling regulates cyclooxygenase-2 transcription. *Molecular endocrinology (Baltimore, Md.)* **25,** 1006–17 (2011).

138. Zhang, Y. E. Non-Smad pathways in TGF-beta signaling. *Cell research* **19,** 128–39 (2009).

139. Gamell, C., Susperregui, A. G., Bernard, O., Rosa, J. L. & Ventura, F. The p38/MK2/Hsp25 pathway is required for BMP-2-induced cell migration. *PloS one* **6,** e16477 (2011).

140. Xu, B. *et al.* Smad1 and its target gene Wif1 coordinate BMP and Wnt signaling activities to regulate fetal lung development. *Development (Cambridge, England)* **138,** 925–35 (2011).

141. Morrell, N. W. Pulmonary hypertension due to BMPR2 mutation: a new paradigm for tissue remodeling? *Proceedings of the American Thoracic Society* **3,** 680–6 (2006).

142. Yu, P. B. *et al.* BMP type I receptor inhibition reduces heterotopic [corrected] ossification. *Nature medicine* **14,** 1363–9 (2008).

143. Sountoulidis, A. *et al.* Activation of the canonical Bone Morphogenetic Protein (BMP) pathway during lung morphogenesis and adult lung tissue repair. *PloS one* **7,** e41460 (2012).

144. Chang, H. *et al.* Smad5 knockout mice die at mid-gestation due to multiple embryonic and extraembryonic defects. *Development* **126,** 1631–1642 (1999).

145. Tremblay, K. D., Dunn, N. R. & Robertson, E. J. Mouse embryos lacking Smad1 signals display defects in extra-embryonic tissues and germ cell formation. *Development* **128,** 3609–3621 (2001).

146. Farkas, L. *et al.* Transient overexpression of Gremlin results in epithelial activation and reversible fibrosis in rat lungs. *Am J Respir Cell Mol Biol* **44,** 870–878 (2011).

147. Shahar, I. *et al.* Effect of IL-6 on alveolar fibroblast proliferation in interstitial lung diseases. *Clinical immunology and immunopathology* **79,** 244–51 (1996).

148. Frevert, C. W., Huang, S., Danaee, H., Paulauskis, J. D. & Kobzik, L. Functional characterization of the rat chemokine KC and its importance in neutrophil recruitment in a rat model of pulmonary inflammation. *Journal of immunology (Baltimore, Md. : 1950)* **154,** 335–44 (1995).

149. Penttinen, R. P., Kobayashi, S. & Bornstein, P. Transforming growth factor beta increases mRNA for matrix proteins both in the presence and in the absence of changes in mRNA stability. *Proceedings of the National Academy of Sciences of the United States of America* **85,** 1105–8 (1988).

150. Ramirez, A. *et al.* Extracellular cysteine/cystine redox potential controls lung fibroblast proliferation and matrix expression through upregulation of transforming

growth factor-beta. *American journal of physiology. Lung cellular and molecular physiology* **293,** L972–81 (2007).

151. Baarsma, H. A. *et al.* Activation of WNT/β-catenin signaling in pulmonary fibroblasts by TGF-β_1 is increased in chronic obstructive pulmonary disease. *PloS one* **6,** e25450 (2011).

152. Balestrini, J. L., Chaudhry, S., Sarrazy, V., Koehler, A. & Hinz, B. The mechanical memory of lung myofibroblasts. *Integrative biology : quantitative biosciences from nano to macro* **4,** 410–21 (2012).

153. Liu, F. *et al.* Feedback amplification of fibrosis through matrix stiffening and COX-2 suppression. *The Journal of cell biology* **190,** 693–706 (2010).

154. Manali, E. D. *et al.* Static and dynamic mechanics of the murine lung after intratracheal bleomycin. *BMC pulmonary medicine* **11,** 33 (2011).

155. Kolb, M. *et al.* Differences in the fibrogenic response after transfer of active transforming growth factor-beta1 gene to lungs of "fibrosis-prone" and "fibrosis-resistant" mouse strains. *American journal of respiratory cell and molecular biology* **27,** 141–50 (2002).

156. Massagué, J. & Kelly, B. Internalization of transforming growth factor-beta and its receptor in BALB/c 3T3 fibroblasts. *Journal of cellular physiology* **128,** 216–22 (1986).

157. Alba, R., Bosch, A. & Chillon, M. Gutless adenovirus: last-generation adenovirus for gene therapy. *Gene therapy* **12 Suppl 1,** S18–27 (2005).

158. Botelho, F. M. *et al.* Pulmonary Expression of Oncostatin M (OSM) Promotes Inducible BALT Formation Independently of IL-6, Despite a Role for IL-6 in OSM-Driven Pulmonary Inflammation. *Journal of immunology (Baltimore, Md. : 1950)* **191,** 1453–64 (2013).

159. Zhao, J. *et al.* Smad3 deficiency attenuates bleomycin-induced pulmonary fibrosis in mice. *American journal of physiology. Lung cellular and molecular physiology* **282,** L585–93 (2002).

160. Bonniaud, P. *et al.* Smad3 null mice develop airspace enlargement and are resistant to TGF-beta-mediated pulmonary fibrosis. *Journal of immunology (Baltimore, Md. : 1950)* **173,** 2099–108 (2004).

161. Bonniaud, P. *et al.* TGF-beta and Smad3 signaling link inflammation to chronic fibrogenesis. *Journal of immunology (Baltimore, Md. : 1950)* **175,** 5390–5 (2005).

162. Takimoto, T. *et al.* Smad2 and Smad3 are redundantly essential for the TGF-beta-mediated regulation of regulatory T plasticity and Th1 development. *Journal of immunology (Baltimore, Md. : 1950)* **185,** 842–55 (2010).

163. O'Donoghue, R. J. J. *et al.* Genetic partitioning of interleukin-6 signalling in mice dissociates Stat3 from Smad3-mediated lung fibrosis. *EMBO molecular medicine* **4,** 939–51 (2012).

164. Nagahama, K. Y. *et al.* Oncostatin M Modulates Fibroblast Function via STAT3. *American journal of respiratory cell and molecular biology* (2013). doi:10.1165/rcmb.2012-0460OC

165. Kotaru, C. *et al.* Regional fibroblast heterogeneity in the lung: implications for remodeling. *American journal of respiratory and critical care medicine* **173,** 1208–15 (2006).

166. Prêle, C. M., Yao, E., O'Donoghue, R. J. J., Mutsaers, S. E. & Knight, D. A. STAT3: a central mediator of pulmonary fibrosis? *Proceedings of the American Thoracic Society* **9,** 177–82 (2012).

167. Simeone-Penney, M. C. *et al.* Airway epithelial STAT3 is required for allergic inflammation in a murine model of asthma. *Journal of immunology (Baltimore, Md. : 1950)* **178,** 6191–9 (2007).

168. Pegorier, S., Campbell, G. A., Kay, A. B. & Lloyd, C. M. Bone morphogenetic protein (BMP)-4 and BMP-7 regulate differentially transforming growth factor (TGF)-beta1 in normal human lung fibroblasts (NHLF). *Respir Res* **11,** 85 (2010).

169. Gao, X. *et al.* BMP2 inhibits TGF-β-induced pancreatic stellate cell activation and extracellular matrix formation. *American journal of physiology. Gastrointestinal and liver physiology* **304,** G804–13 (2013).

170. Zode, G. S., Clark, A. F. & Wordinger, R. J. Bone morphogenetic protein 4 inhibits TGF-beta2 stimulation of extracellular matrix proteins in optic nerve head cells: role of gremlin in ECM modulation. *Glia* **57,** 755–66 (2009).

171. Leppäranta, O., Tikkanen, J. M., Bespalov, M. M., Koli, K. & Myllärniemi, M. Bone morphogenetic protein-inducer tilorone identified by high-throughput screening is antifibrotic in vivo. *American journal of respiratory cell and molecular biology* **48,** 448–55 (2013).

172. Chen, D., Zhao, M. & Mundy, G. R. Bone morphogenetic proteins. *Growth factors (Chur, Switzerland)* **22,** 233–41 (2004).

173. Selman, M., Pardo, A. & Kaminski, N. Idiopathic pulmonary fibrosis: aberrant recapitulation of developmental programs? *PLoS medicine* **5,** e62 (2008).

174. Aumiller, V., Balsara, N., Wilhelm, J., Günther, A. & Königshoff, M. WNT/β-Catenin Signaling Induces IL-1β Expression by Alveolar Epithelial Cells in Pulmonary Fibrosis. *American journal of respiratory cell and molecular biology* **49,** 96–104 (2013).

175. Bolaños, A. L. *et al.* Role of Sonic Hedgehog in idiopathic pulmonary fibrosis. *American journal of physiology. Lung cellular and molecular physiology* **303,** L978–90 (2012).

176. Gomez-Arroyo, J. G. *et al.* The monocrotaline model of pulmonary hypertension in perspective. *American journal of physiology. Lung cellular and molecular physiology* **302,** L363–9 (2012).

177. Reynolds, A. M., Holmes, M. D., Danilov, S. M. & Reynolds, P. N. Targeted gene delivery of BMPR2 attenuates pulmonary hypertension. *The European respiratory journal : official journal of the European Society for Clinical Respiratory Physiology* **39,** 329–43 (2012).